



POLITECNICO
MILANO 1863

DEPARTMENT OF ENERGY
DOCTORAL PROGRAM IN ENERGY AND NUCLEAR SCIENCE AND TECHNOLOGY

**Fabrication and characterization
of carbon-atom wires
and wire-based nanocomposites**

Doctoral Dissertation of:
SONIA PEGGIANI

Advisor:

Prof. Carlo S. Casari

Tutor:

Prof. Matteo Passoni

The Chair of the Doctoral Program:

Prof. Vincenzo Dossena

Year 2020 – Cycle XXXIII

A nonna Lina.

“Non rimandare a domani quello che puoi fare oggi.”
“Don’t put off until tomorrow what you can do today.”
Benjamin Franklin

Abstract

Carbon-atoms wires (CAWs) are finite linear sp-carbon chains which exist in two different configurations: one based on alternated single and triple bonds (polyynes) and one composed of a sequence of double bonds (cumulenes). Their structure-dependent opto-electronic properties make CAWs appealing for different technological applications. However, these chains are highly reactive and spontaneously rearrange in more stable sp² structures by cross-linking reactions.

In this work, physical synthesis techniques as submerged arc discharge in liquid and pulsed laser ablation in liquid are first set up and then employed to synthesize CAWs in water and organic solvents. To increase the synthesis yield of polyynes in solution, the process parameters are optimized and, in the case of water as a solvent, a novel post-synthesis concentration method entirely based on high-performance liquid chromatography is developed. In this way, even the concentration of CAWs synthesized in water, which cannot furnish carbon atoms to form sp-carbon chains, results comparable to those reached in the case of organic solvents but avoiding the handling of toxic substances. Moreover, polyynes properties as size, termination, yield and stability are investigated as a function of the solvent by a multi-characterization technique. It is showed that surface-enhanced Raman spectroscopy is sensitive to CAWs termination and is exploited to understand the mechanism of formation of polyynes during the physical synthesis in water and in a polymeric solution. Furthermore, a new preparation method for CAWs-based nanocomposites is employed. The chains are produced by ablating graphite directly in a polymeric solution in a way that they can be encapsulated in polymeric matrices by a single-step procedure. Nanocomposites, obtained after solvent evaporation, are characterized by carbon atomic wires well blended with the polymer and detectable even after 11 months.

This thesis gives more insight on the properties of CAWs as single molecules and shows a novel and simple procedure to prepare polyynes-based materials where the chains are stabilized, thus paving the way to the creation of new functional materials for industrial applications.

Sommario

I Fili atomici di carbonio sono catene lineari finite di atomi di carbonio sp presenti in due diverse configurazioni: una basata su legami singoli e tripli alternati (poliine) e una su una sequenza di legami doppi (cumuleni). Le loro proprietà optoelettroniche dipendenti dalla struttura rendono le catene attraenti per diverse applicazioni tecnologiche. Tuttavia questi fili sono altamente reattivi e si riarrangiano spontaneamente tramite reazioni di reticolazione in strutture più stabili sp².

In questo lavoro, tecniche di sintesi fisica come la scarica ad arco sommersa in liquido e l'ablazione a laser pulsato in liquido sono dapprima installate e poi utilizzate per produrre i fili di carbonio in acqua e solventi organici. Per incrementare la resa di poliine in soluzione, si sono ottimizzati i parametri di processo e, in caso dell'acqua come solvente, si è sviluppato un nuovo metodo di concentrazione post-sintesi interamente basato sulla cromatografia liquida ad alta prestazione. In questo modo, anche la concentrazione dei fili atomici prodotti in acqua, la quale non può fornire atomi di carbonio per formare le catene lineari, risulta comparabile a quelle raggiunte con i solventi organici ma evitando la manipolazione di sostanze tossiche. Inoltre, le proprietà delle poliine come lunghezza, terminazione, resa e stabilità sono studiate in funzione del solvente con una tecnica di multicaratterizzazione. Si è dimostrato che la spettroscopia Raman amplificata da superfici è sensibile alla terminazione dei fili atomici ed è impiegata per comprendere il meccanismo di formazione delle catene durante la sintesi fisica in acqua e in una soluzione polimerica. In aggiunta, si è utilizzato un nuovo metodo per preparare nanocompositi a base di poliine. Le catene sono prodotte ablando la grafite direttamente in una soluzione polimerica così che possano essere incapsulate in matrici polimeriche tramite una procedura a singolo step. I nanocompositi, ottenuti dopo l'evaporazione del solvente, sono caratterizzati da catene ben miscelate con il polimero e ancora rilevabili dopo 11 mesi.

Questa tesi fornisce maggiori informazioni sulle proprietà delle catene lineari come molecole singole e mostra una nuova e semplice procedura per preparare materiali a base poliinica in cui i fili sono stabilizzati, aprendo così la strada alla creazione di nuovi materiali funzionali per applicazioni industriali.

Contents

Introduction	1
1 Carbon-atom wires	7
1.1 The "lacking" carbon allotrope	7
1.2 Structure, vibrational and electronic properties of carbon-atom wires	11
1.2.1 Ideal model of CAWs	11
1.2.2 Finite chain model	15
1.3 Applications of carbon-atom wires	18
1.4 Stability of carbon-atom wires	22
1.4.1 Stability issues	22
1.4.2 Stabilization strategies	23
2 Synthesis and characterization of carbon-atom wires	27
2.1 Synthesis techniques	27
2.1.1 Submerged arc discharge in liquid (SADL)	30
2.1.2 Pulsed laser ablation in liquid (PLAL)	38
2.2 Characterization techniques	47
2.2.1 Raman-based techniques	47
2.2.2 Liquid chromatography and UV-Vis spectroscopy	55
3 Thesis goals and methods	59
3.1 Specific goals of the thesis	59
3.2 Materials	63
3.2.1 Electrodes and Targets	63

3.2.2	Solvents and colloidal solutions	63
3.3	Synthesis methods	65
3.3.1	Submerged arc discharge in liquid apparatus	65
3.3.2	Pulsed laser ablation in liquid apparatus	66
3.4	Characterization methods	67
3.4.1	Raman spectrometers	67
3.4.2	High-performance liquid chromatograph and UV-Vis spectro- meter	69
3.4.3	Scanning electron microscopy	71
4	Carbon-atom wires by submerged arc discharge in liquid	73
4.1	Polyynes synthesized in water	74
4.1.1	Optimization of process parameters	74
4.1.2	Novel procedure to concentrate and separate polyynes	78
4.1.3	Size-separated polyynes	82
4.1.4	Polyynes stability	86
4.2	<i>In situ</i> SERS during SADL in water	90
4.3	Polyynes synthesized in mixed solution of water and organic solvents	92
4.4	Summary	94
5	Carbon-atom wires by pulsed laser ablation in liquid	97
5.1	Design and set-up of the apparatus	98
5.2	Methods for maximising polyynes yield	100
5.2.1	Optimization of process parameters	100
5.2.2	Concentration methods	104
5.3	Polyynes synthesized in different solvents	106
5.3.1	Solutions of polyynes mixture	106
5.3.2	HPLC and UV-Vis analysis of size and end-selected polyynes	109
5.3.3	SERS analysis of size and end-selected polyynes	112
5.3.4	Stability analysis	114
5.4	Summary	117
6	Wire-based nanocomposites	119
6.1	<i>In situ</i> synthesis of polyynes in PVA aqueous solution	120
6.2	UV-Vis spectroscopy of PVA/polyynes solutions	122
6.3	SERS measurements of PVA/Ag/polyynes solutions and nanocomposites	123

6.4	Stability of PVA/Ag/polyynes solutions and nanocomposites	129
6.5	PMMA/Ag/polyynes solutions and nanocomposites	131
6.6	Summary	137
7	Conclusions and perspectives	139
	Appendix	145
	List of Figures	147
	List of Tables	153
	Bibliography	155

Introduction

IN last years, the investigation of the third allotrope of carbon based on sp hybridization, the so-called carbyne, has revealed extraordinary theoretically predicted properties. The structure-dependent optoelectronic properties, the huge effective area ($\sim 13000 \text{ m}^2/\text{g}$), the high Young modulus ($\sim 32 \text{ TPa}$), the high electron mobility ($1.5 \times 10^5 \text{ cm}^2/\text{V}\cdot\text{s}$) and the high thermal conductivity ($148 \text{ kW}/\text{m}\cdot\text{K}$) are only some examples of the outstanding properties of carbyne. Those results raised up the interest of the scientific community on finite sp-carbon chains and their possible applications in different fields. These structures, also called carbon-atoms wires (CAWs), exist in two different configurations, one with alternated single and triple bonds (i.e. polyyne), and the other one with a sequence of double bonds (i.e. cumulene). They are naturally synthesized in interstellar and circumstellar medium, and can be indeed employed as active materials in electronic devices, for live-cell imaging, optical barcoding and, in particular, as materials for energy applications (e.g. photovoltaic, water splitting, hydrogen storage media). In that regard, an attractive possibility arises from a theoretical work published in 2011 by Sorokin et al., who, considering the high surface area of carbon-atom wires, have simulated their implementation as host material for metal atoms, as calcium, which are

good in absorbing hydrogen molecules at room temperature.

With the intention of fabricating sp-carbon chains and wire-based materials for technological purposes, it is important to exploit techniques that are cost-effective and scalable for mass production. From this perspective, physical methods are therefore more suitable than chemical ones. Submerged arc discharge in liquid (SADL) and pulsed laser ablation in liquid (PLAL) were first employed by Cataldo in 2003 and Tsuji in 2002, respectively, to produce polyynes of different length and termination in a liquid environment. The use of water as a solvent for SADL and PLAL is appealing for low cost and environment-friendly applications and need a further investigation because it has been reported only in few works of literature. Since water cannot contribute as carbon source during CAWs formation, the yield of polyynes in water is lower with regard to organic solvents, so concentrations methods are required to overcome this limit. Nevertheless, the study of the effect of different solvents during PLAL experiments on polyynes properties, e.g. yield, size, termination and stability, has never been performed so far. This could help in obtaining further insights on tuning the chain length and termination, so on the mechanism of polyynes formation. In this direction, *in situ* SERS measurements could be helpful in following the evolution of sp-carbon chains signals during their synthesis by SADL or PLAL in a SERS-active solution with Ag nanoparticles.

The major issue of polyynes concerns their poor stability under ambient conditions because they tend to spontaneously rearrange in more stable sp² structures. Consequently, to exploit a polyyne-based material for any application, it is necessary to find a good stabilization strategy. One approach consists of terminating the chains by bulky groups (e.g. sp² clusters, graphene edges and phenyl groups) which can keep distant the wires avoiding the cross-linking reactions. Another technique is to surround polyynes by rotaxane macrocycle or immersing them in a ionic liquid. Some papers, instead, have reported the encapsulation of the chains in a double- or multi-walled nanotube or in solid matrices as Ag or Au nanoparticles assemblies, SiO₂ dried gels and polymers, e.g. poly(vinyl alcohol) (PVA). PVA is commonly exploited to constitute nanocomposites because of its low-cost, chem-

ical stability, solubility in water and good filmability properties. Few studies have discussed the production of a nanocomposite by adding PVA to an organic solution of an already formed polyynes and metal nanoparticles. However, this procedure could prevent the complete blending between polyynes, metal nanoparticles and polymer. Furthermore, if PVA granules are directly added to a polyynes solution, a heating process is needed to dissolve the solid polymeric pellets and this could affect the chains integrity since they are susceptible to temperature rises. Conversely, if PVA is dissolved in a solvent and, then, added to the sample with sp-carbon chains, the chains concentration decreases reducing the signal intensity in optical and structural characterizations. Some critical issues in the preparation of polyynes-based nanocomposite need to be resolved and the polymer portfolio can be extended to satisfy different needs, e.g. poly(methyl methacrylate) (PMMA) for water resistant applications.

In this framework, this Ph.D. activity aims to give a contribution in handling some open issues of these promising 1D carbon-atom wires. The following thesis is divided in the chapters below:

Chapter 1 - Carbon-atom wires:

the history of the discovery of carbon-atom wires, their main properties and applications are here reported. In addition, stability issues and the strategies for stabilizing these structures are also discussed in the chapter.

Chapter 2 - Synthesis and characterization of carbon-atom wires:

the physical principles and state of art of the two synthesis methods and characterization techniques employed in this work are presented in the chapter.

Chapter 3 - Thesis goals and methods:

the specific goals of the thesis and the instrumentation adopted for the work are here illustrated.

Chapter 4 - Carbon-atom wires by submerged arc discharge in liquid:

the chapter deals with the low concentrated polyynes solutions obtained by SADL in water, showing how this problem is overcome and how competitive results are achieved. Moreover, the

in situ structural characterization of polyynes performed during their synthesis by arc discharge in aqueous solution with silver nanoparticles is also discussed together with the outcomes related to arc discharge in solution of water mixed with organic solvents.

Chapter 5 - Carbon-atom wires by pulsed laser ablation in liquid:

the chapter first illustrates all the steps taken to design and install PLAL. Then, the optimized process parameters and the remarks concerning the concentration by a standard method are displayed. Moreover, this chapter is also dedicated to the investigation of the role of the solvent during laser ablation in tuning yield, length, end-groups and stability of polyynes by employing a multi-characterization technique.

Chapter 6 - Wires-based nanocomposites:

the chapter describes the novel methodology developed to prepare polyynes-based nanocomposites, where polyynes can be stabilized and characterized in an extended film instead of as a single-wire level. The findings concerning the employment of PVA and PMMA as polymeric matrices are covered in this chapter.

Chapter 7 - Conclusions and perspectives:

the chapter traces the main outcomes of this Ph.D. thesis and shows some further research developments, which may be deepened in other on going/future studies.

The original outcomes of this Ph.D. thesis have led to the publication of the following papers:

- S. Peggiani, A. Senis, A. Facibeni, A. Milani, P. Serafini, G. Cer-rato, A. Lucotti, M. Tommsini, D. Fazzi, C. Castiglioni, V. Russo, A. Li Bassi, C. S. Casari, Size-selected polyynes synthesized by submerged arc discharge in water, *Chemical Physical Letters*, 740 (2020), 137054-137061. doi:10.1016/j.cplett.2019.137054
- A. Scaccabarozzi, A. Milani, S. Peggiani, S. Pecorario, B. Sun, R.R Tykwinski, M. Caironi, C.S. Casari, A Field-Effect Transistor Based on Cumulenic sp-Carbon Atomic Wires, *The Journal of*

Physical Chemistry Letters, 11(5), (2020) 1970-1974.
doi:10.1021/acs.jpcelett.0c00141

- S. Peggiani, A. Facibeni, A. Milani, C. Castiglioni, V. Russo, A. Li Bassi and C. S. Casari, *In situ* synthesis of polyynes in a polymer matrix by pulsed laser ablation in liquid, *Materials Advances*, 1(8), (2020), 2547–3074. Selected as a 2020 HOT Materials Advances article and front inside cover. doi:10.1039/D0MA00545B
- S. Peggiani, P. Marabotti, R.A. Lotti, A. Facibeni, P. Serafini, A. Milani, V. Russo, A. Li Bassi, C. S. Casari, “Solvent-dependent termination, size and stability in polyynes synthesis by laser ablation in liquids”, *Phys Chem Chem Phys* 22 (2020) 26312-26321. doi:10.1039/d0cp04132g

In addition, the results achieved in this thesis work were\will be also presented by myself in different international scientific conferences:

- “Applied Nanotechnology and Nanoscience International Conference”, ANNIC2018, October 2018, Berlin, Germany (oral contribution)
- Workshop at Politecnico di Milano on “Chemistry of graphene”, June 2019, Milan, Italy (participation only)
- “International Symposium on High-Performance Liquid Phase Separations Related Technique”, HPLC2019, June 2019, Milan, Italy (workshop and oral contribution)
- “The International Nanotech & Nanoscience Conference & Exhibition”, Nanotech France2019, June 2019, Paris, France (oral contribution)
- “International Conference on Diamond and Carbon Materials”, ICDCM2019, September 2019, Seville, Spain (oral and poster contributions, Silver Young Scholar Award)
- “International Polymer Characterization Forum”, POLY-CHAR 2020, postponed in April 2021, Venice, IT (workshop and oral contribution)

1

Carbon-atom wires

This chapter introduces carbon-atom wires (CAWs), linear chains based on covalently bonded sp-carbon atoms, which are appealing for the creation of new functional materials for future applications. The discovery of these nanostructures and the comparison to the other carbon allotropes is presented in Section 1.1. The structure, the vibrational and electronic properties of CAWs are defined in Section 1.2. Future applications of these carbon systems are discussed in Section 1.3. Finally, the stability issues of CAWs and the strategies to stabilize these structures are discussed in Section 1.4.

1.1 The "lacking" carbon allotrope

Carbon is the most appealing element for the creation of new innovative materials able to answer to the global technological challenges in fields such electronics, mechanics, medicine, photonics and energy. Indeed, carbon is versatile and can form various systems and nanostructures with different dimensionality and unique properties. To understand its peculiar chemical behaviour, the concept of hybridization must be considered. This phenomenon consists in the superposition of s and p atomic orbitals to generate new hybrid orbitals, i.e. sp, sp² and sp³, with different energies and shapes with respect to the unmodified ones. By the linear combination of atomic orbitals (LCAO) theory, it is possible to predict the structure of carbon molecules: linear (1-

dimensional), planar (2-dimensional) or tetrahedral (3-dimensional). Hybridization is favoured because the new hybrid orbitals are lower in energy compared to the unmodified counterparts and justifies the existence in nature of allotropic forms of pure carbon, as graphite and diamond, respectively based on sp^2 and sp^3 hybridization. Tennant experimentally demonstrated in 1797 that these two solid state forms have the same composition even if they display completely different properties [1].

Graphite is characterized by planar hexagonal layers kept together by van der Waals forces and formed by sp^2 carbon atoms linked by covalent σ bonds. Each carbon atom has also the $2p_z$ orbital orthogonal to the plane, which remains unhybridized and presents a delocalized electron. Because of this structure, graphite behaves differently within and between layers. It is a good thermal and electrical conductor through the plane and an insulator along the direction perpendicular to the plane. Moreover, it is a material with lubricant properties thanks to the weak van der Waals forces between its layers [2].

Diamond presents a tetrahedral structure where each carbon atom has four sp^3 -hybridized orbitals through which is covalently bonded to other four atoms. Thanks to its arrangement, diamond is the hardest material known, thus it is exploited in abrasive applications. It is an excellent thermal conductor because of the covalent bonds and low phonon scattering (thermal conductivity (λ) = 2200 W/m K). Furthermore, it has a bandgap of 5.5 eV, which means that it is an excellent electrical insulator. Diamond is not thermodynamically stable and tends to slowly transform into graphite [2].

The lacking third allotrope of carbon based on sp hybridization was never considered up to the end of the nineteenth's century when the first experiments on linear carbon synthesis were made. In particular, Glaser tried to fabricate linear sp -carbon chains in 1870 [3] while Baeyer postulated in 1885 the impossibility of producing this kind of structures since he did not succeed in isolating them because of their high instability [4]. This last statement braked the research on this topic for approximately forty years until the discovery of natural

compound of finite sp-carbon chains with alternating triple and single bonds, called polyynes, isolated from plants and fungi [5–9] and of a natural mineral present in carbon-rich aggregates in the Ries crater in Bavaria, called Chaoite or white carbon [10]. Thanks to the detailed optical studies on chaoite, El Goresy and Donnay confirmed that it was an allotrope of carbon because the primitive cell had a different size with respect to that of the graphite and other carbon-based materials [11]. Walton and coworkers addressed their activity to chemically prepared finite sp-carbon chains [12] and some others aimed to reproduce the physical conditions for the formation of the new mineral, as employing temperature of at least 2600 K [13, 14]. Kudryavtsev and coworkers registered the name “carbyne”, as the third (linear) allotropic form of carbon in USSR Committee of Inventions and Discoveries [15], after they claimed its synthesis employing oxidative coupling reactions. The existence of carbyne was strongly questioned by Smith and Buseck in the 80’s [16–19] and a discussion between opponents and defenders [20, 21] on the existence of carbyne occurred. A new optimism came from the work of Lagow and coworkers, who prepared sp-carbon linear chains with 28 carbon atoms and declared that wires longer than 300 atoms can be reached at high pressure [22]. Since carbynes were found as possible constituents of the interstellar dust [23], scientists conducted experiments to understand how sp carbon long-chain are formed in that environment [24, 25]. With this aim, Kroto, Smalley and Curl in 1985 ended up to synthesize a different carbon structure, a stable cluster of 60 carbon atoms with 12 pentagonal and 20 hexagonal faces, by irradiating graphite with a nanosecond laser [26]. The advent of nanotechnology and the discovery of this new carbon allotrope, the so-called fullerene, which earned them the Nobel Prize in Chemistry in 1996, marked the beginning of the synthetic carbon allotropes era [27], see Fig.1.1.

Indeed, this was followed by the discovery of carbon nanotubes, rolled up graphite sheets, synthesized by Iijima in 1991 [28] and graphene, one isolated sheet of graphite, thanks to the work of Geim and Novoselov in 2004 [29]. The great impact of these carbon nanostructures, which can be classified with respect to their hybridization as

sketched in Fig.1.2, induced to conceive other two- or three- dimensional new structures based on the combination of sp , sp^2 and sp^3 , such as graphynes and graphdiynes, first described by Baughman and Eckhardt in 1987 [30]. These 2D crystals are flat, one-atom-thin and consist of sp^2 carbon hexagons interconnected by means of sp carbon chains having 2 and 4 carbon atoms respectively [31].

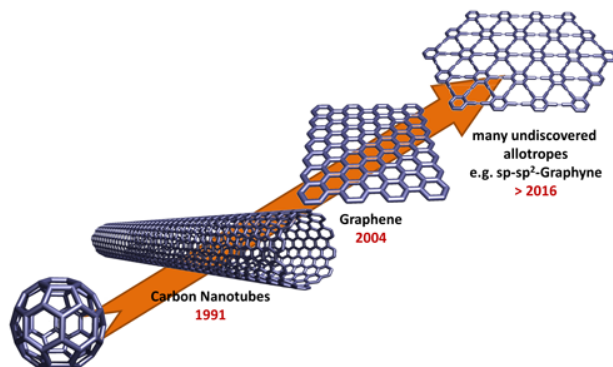


Figure 1.1: Significant achievements of the synthetic carbon allotropes era [27,32].

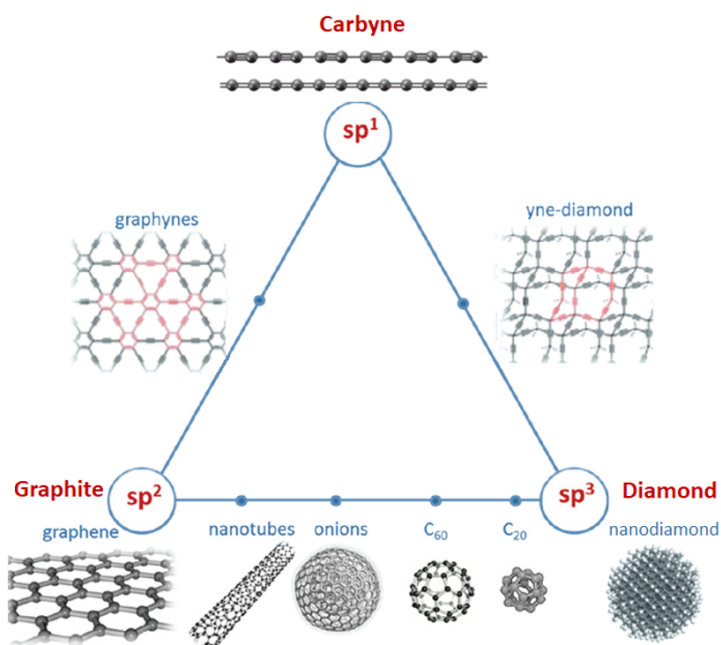


Figure 1.2: Ternary diagram depending on carbon hybridization state [33].

1.2. Structure, vibrational and electronic properties of carbon-atom wires

The possibility to combine carbon atoms with different hybridizations offers limitless structural possibilities. One-dimensional carbyne is the simplest example of synthetic carbon allotrope. Recently, the name *carbyne* has been adopted not to mean a solid form of sp carbon but a model system, consisting of infinite chains of sp-hybridized carbon atoms. Finite carbon systems with sp-carbon moieties are associated to the term *carbynoid structures*, whereas the isolated systems can be named as: *linear carbon chains* (LCCs), *carbon monatomic chains*, *carbon atomic chains* and *carbon-atom wires* (CAWs). This last term will be the one mainly used in this thesis as in the Ref. [34].

1.2 Structure, vibrational and electronic properties of carbon-atom wires

Carbon-atom wires (CAWs), due to their large π conjugation, have a strong structure-property relationship that makes these linear chains very appealing building blocks for advanced future applications. To interpret their structure and physical properties, it is convenient to start from the model of an infinite chain of carbon atoms (carbyne) following a solid state approach, as described in Section 1.2.1. The effect of the terminations can be considered relaxing this restrictive approximation, as showed in Section 1.2.2.

1.2.1 Ideal model of CAWs

Ideal infinite wires can be present in two different geometric configurations, one with equal double bonds, named cumulene, and the other one with alternated single and triple bonds, called polyynes (see Fig.1.3). Those structures can be considered as 1D crystals with a unit cell respectively composed of one and two atoms. Cumulene is characterized by a metallic behaviour because the conduction band is half filled. Indeed, every carbon atom has two 2p orbitals with an electron each [35]. Polyynes, instead, possesses semiconducting features. It has two atoms per unit cell, so its orbitals have two electrons each, filling completely the valence band. The latter is separated from the conduction band by an energy gap opened at the edge of the Brillouin zone, as depicted

in Fig.1.3 [36].

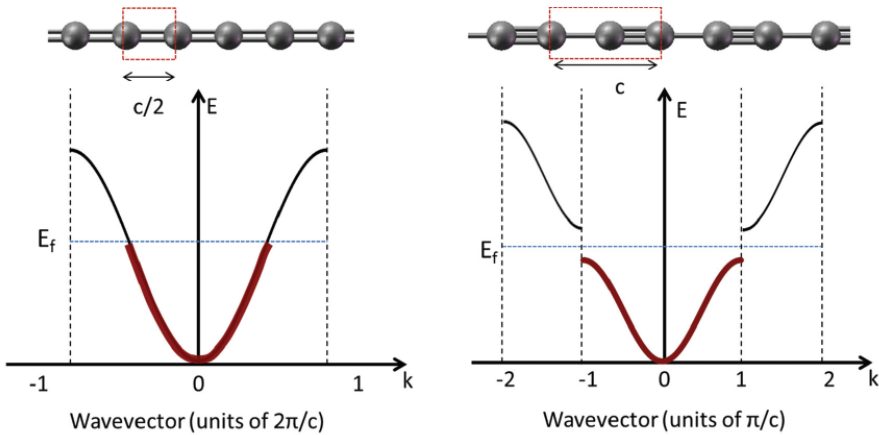


Figure 1.3: The band structure of the two possible arrangements of CAWs: the metallic cumulene on the left and the semiconducting polyynes on the right [33].

The origin of polyynes can be associated to a Peierls distortion of the cumulene structure. This happens due to the interaction between strongly delocalized π -electrons of metallic cumulene and longitudinal phonons, i.e. periodic lattice deformations. As a consequence, the lattice changes periodicity doubling the unit cell to obtain an energetically more favourable configuration [37, 38]. An important property of CAWs is the bond length alternation (BLA), i.e. the difference in length of two adjacent bonds. As reported in Fig.1.4a, infinite linear chains with BLA equal to zero correspond to cumulenes. Increasing BLA, the energy gap between the valence and the conduction band is higher and, in this way, the metallic cumulenes evolve towards semiconducting polyynes. Fig.1.4b indicates the specific BLA and band gap of sp-carbon chains. Quantum chemical calculations allowed the description of the potential energy curve as a function of BLA, as shown in Fig.1.4c [39]. The configuration at the minimum of energy is reached by polyynes with an optimized geometry, which provides a BLA of 0.038, as marked in Fig.1.4a [40].

For all polyconjugated systems, i.e. structures characterized by π -electron delocalization, the coupling between electronic states and nuclear vibrations is strong. This phenomenon, called electron–phonon

1.2. Structure, vibrational and electronic properties of carbon-atom wires

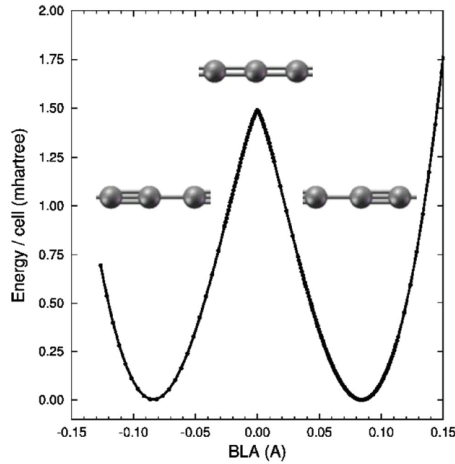
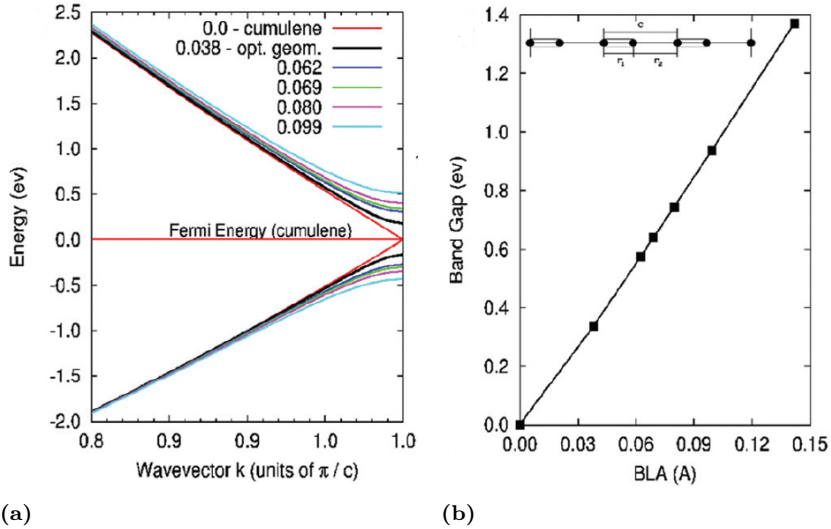
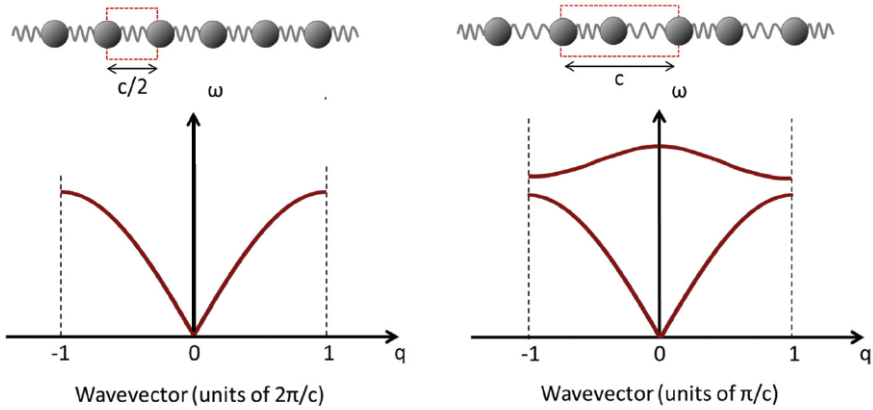


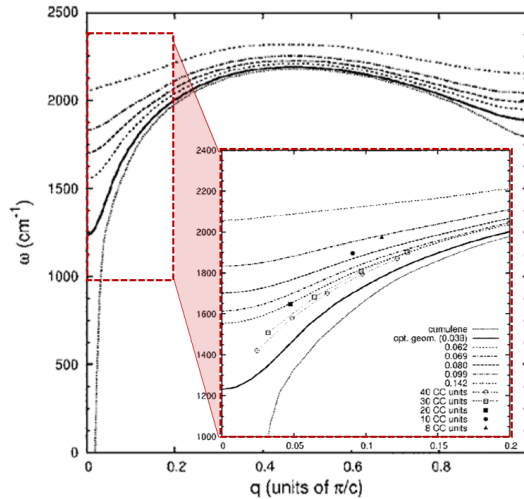
Figure 1.4: (a) Band structure of cumulene and polyene at different values of BLA in Å [33], (b) Band gap of sp -carbon chains as a function of BLA. At the top, the sp -chain structure and the definition of BLA [33], (c) Potential energy of infinite carbon atomic wires as a function of BLA showing the minimum potential energy for polyenic configuration [33].

interaction, is responsible for collective and long-range vibrations among all CC bonds of the chain and for the relaxation of nuclear geometry, which plays a fundamental role in determining the Raman active modes [41]. The number of optical phonon branches in a 3D solid lattice can be simply estimated by $3N-3$ formula, with N = number of atoms in unit cell. Cumulene has $N=1$, since it has a monoatomic unit cell. This means no optical phonons and only acoustic phonon branches, a longitudinal (LA) one and double degenerate transversal (TA) ones, so resulting without Raman active modes. This is true in the case of infinite chains [42], whereas, if it is terminated by endcapping group, the behaviour changes as explained in the next Section 1.2.2 [43]. Moving from cumulene ($BLA=0$) to polyynes ($BLA\neq 0$), each unit cell has 2 atoms and so it turns out to be characterized by 3 optical phonon branches, a longitudinal (LO) one and doubly degenerate transversal (TO) ones, together with the acoustic branches. Phonon dispersion branches of cumulene and polyynes are represented in Fig.1.5a. Looking only to longitudinal optical phonon curves in Fig.1.5b, the slope of the phonon curve related to cumulene ($BLA=0$) is almost a vertical tangent in correspondence to the phonon wave vector (\mathbf{q}) equal to zero, i.e. Kohn anomaly. This is associated to a strong electron-phonon coupling. The LO branches of polyynes with small band gap still suffer from Kohn anomaly in the vicinity of $\mathbf{q}=0$, showing a steep slope which decreases with largest BLA [40]. These outcomes were obtained by density functional theory (DFT), solving the vibrational dynamics of the chains at specific BLA, given by applying an external constant force [40]. To move on to the description of real systems, the effects of end-groups and charge transfer needed to be consider.

1.2. Structure, vibrational and electronic properties of carbon-atom wires



(a)



(b)

Figure 1.5: (a) Phonon dispersion branches of cumulene (left) and polyynes (right) [33], (b) Longitudinal optical phonon branches of cumulene and polyynes with different values of BLA. The region close to $q=0$ is zoomed. Modified picture from Ref. [40].

1.2.2 Finite chain model

Finite length CAWs can be interpreted by employing the model of an infinite chain at the same BLA. In this way, it is possible to describe the main trends concerning electronic and vibrational behaviours. How-

ever, to carefully discuss real finite wires, it is necessary to apply a relaxation of the infinite chain model assumption, taking into account the non-negligible effect of the end-groups on the overall configuration. Indeed, the energy gap and the frequency of nuclear displacement of CAWs are affected by the type of end-cap. The ability of changing electronic and vibrational properties in basis of the functionalization of the chain may allow the realization of new advanced materials, as theoretically showed in Ref. [35].

It is known that, keeping constant the termination and increasing the size of CAWS, π -conjugation increases and so, BLA decreases, as in every conjugated system [41]. However, there is an asymptotic lower limit for which is not possible to reach BLA=0 due to the switching on of the Peierls distortion [40, 43]. Efforts were made in understanding when Peierls distortions overcome the reduction of BLA induced by π -conjugation in finite real chains. A computational work of Yang *et al.* on long finite uncapped cumulenic chains proved that, only in wires longer than 52 atoms of carbon, Peierls distortion prevails over the BLA decrease by π -electron delocalization, imposing the more stable alternating configuration [44]. This result was supported by Innocenti *et al.*, who observed that the cumulenic structure is still maintained with 30 carbon atoms in the sp-chain and its bond lengths are distinctly different from H-capped polyynes with the same number of atoms, as shown in Fig.1.6 [43]. Chou *et al.* performed a geometry optimization for finite vinyl-capped cumulene and H-polyynes up to 300 atoms and noticed the influence at molecular level of Peierls distortion already in cumulene with more than 30 carbon atoms. This structure results in a polyynic configuration apart from the end of the chain, which is composed of sp²-hybridized carbon atoms of CH₂ groups [45].

These outcomes are in accordance with the fact that Peierls distortion can be strictly applied only for an infinite chain and not for short chains that are, instead, strongly influenced by end-capping, as showed by Milani and co-workers [46]. They reported DFT results on the bond length and BLA as a function of the number of carbon atoms for different finite end-capped chains, see Fig.1.7. The hydrogen- and phenyl-capping constrain the closest C-C bond to a triple bond and the

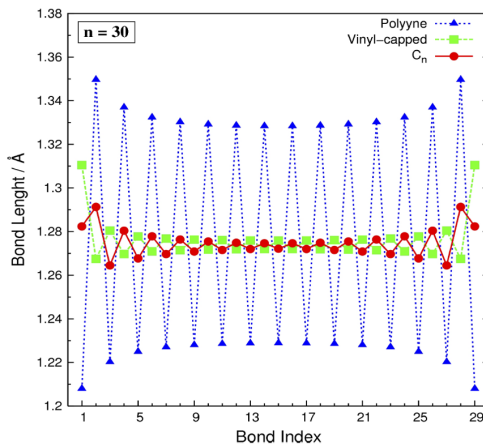


Figure 1.6: Comparison between calculated equilibrium bond lengths of hydrogen-capped polyynes, uncapped and vinyl-capped cumulene [43].

one right after as a single bond and so on, causing a polyynic configuration. Instead, a CH_2 termination induces a sequence of double bonds, obtaining a cumulene-like structure. The latter has a more equalized configuration than the hydrogen-capped chain with the same number of carbon atoms. This shows that the geometry is ruled not by Peierls distortion but by end-groups. The fact that, in finite cumulenes, BLA does not correspond exactly to 0, even if it is significantly smaller than that of polyynes [47, 48], as also showed in Fig. 1.7c, is another evidence of the importance of finite-size effects.

Increasing the chain length, not only the BLA value decreases but also the frequency of BLA oscillation, which causes the shift of the Raman signal to lower wavenumber. The collective BLA oscillation is associated to the out of phase stretching mode of single and triple CC bonds. It also called “R mode” or “ECC mode”, according to the effective conjugation coordinate (ECC) theory, which was developed to explain how the Raman lines of π -conjugated systems behaves [41, 49–52]. The collective C-C stretching mode of CAWs gives rise to Raman and IR signals in the range of $1800\text{--}2300\text{ cm}^{-1}$, whose positions depend on the length of the chain [53, 54]. Since Raman peaks of CAWs are located in a spectral region where no other carbon structures have characteristic signals, Raman spectroscopy turns out to be a very use-

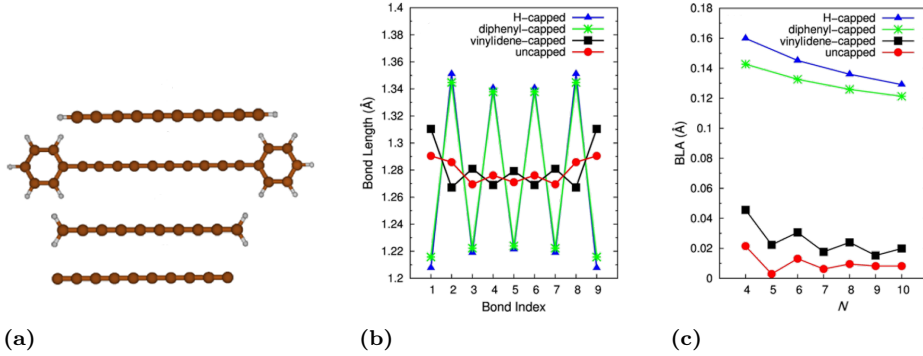


Figure 1.7: (a) Finite carbon-atom wires with different end-caps, i.e. hydrogen, phenyl-group, vinylidene-group and uncapped (from top to bottom), (b) the corresponding bond length in Å and (c) BLA as a function of carbon atoms of *sp*-chains bared or with different terminations [46].

ful technique to identify these systems and investigate their vibrational properties. Consequently, Raman spectroscopy was the characterization method mainly employed in this thesis and, so, the entire Section 2.2.1 is specifically dedicated to it, where physical principles and literature outcomes are discussed.

1.3 Applications of carbon-atom wires

The peculiar structure of CAWs implies an extraordinary high surface area and outstanding mechanical, electronic and optical properties, which were theoretically predicted simulating the ideal system of CAWs, i.e. carbyne. So far, only a few experimental works are reported on CAWs applications, due to their chemical reactivity, thus stability issues of the finite real chains.

The theoretical estimation of surface area of carbyne equal to 13.000 m²/g, which is larger than that of graphene, opened to the investigation of *sp*-carbon chains as a storage scaffold medium, being the appropriate host material for metal atoms, as calcium. Ca-decorated carbynes are good in absorbing up to six hydrogen molecules per atom at room temperature and their clustering is energetically unfavourable [55].

Employing first-principles calculations, the mechanical response of

carbyne under tension, bending and torsion were investigated. First of all, it is found that carbyne under tension has an extraordinarily high value of specific tensile stiffness equal to 10^9 Nm/Kg, which is twice in the case of nanotubes, graphene and diamond. This value is impressive considering that is comparable to that of double stranded DNA and it refers only to a single chain. So, to break a single atomic wire it needs 10 nN. Moreover, the torsional stiffness can be tuned with respect to the symmetry constraints imposed by chemical nature of terminal groups and an extreme mechanical performance is showed by reaching a nominal Young's modulus of 32.7 TPa in correspondence of an effective mechanical thickness of 0.772 Å [56]. These theoretical outstanding properties were found also in polyynic and cumulenic carbyne segments, i.e. C_8 , paving the way to possible mechanical applications as nanoropes or structural elements [57]. Some computational studies demonstrated a coupling between mechanical and electronic properties, indeed, both a strain and a twist can switch the carbyne from a cumulenic metal to a magnetic semiconductor. It is reported that a value of 10% strain causes a change in the band gap from 2.6 to 4.7 eV [56] while, with a 3% strain, Peierls dimerization increases inducing the transition from the metallic to the insulating state [58].

CAWs are expected to have intriguing electronic and phonon transport properties, useful for nanoelectronics applications. The expected theoretical maximum value of electrical conductance is of $2G_0$, where $G_0 = 2e^2/h$ is the quantum of conductance and is equal to 77 μ S, which corresponds to a resistance of 12.9 k Ω [59]. The study of Lang and Avouris concerns the conductance of carbon-atomic wires contacted by gold leads. It is noticed an oscillatory behaviour of density of states (DOS) depending on the number of carbon atoms present in the chain. Odd-numbered chains imply a fully occupied HOMO level and a constant value of conductance with the length, close to the maximum value, while even-numbered wires have a partially filled HOMO level and the conductance increases with the length. The charge transfer from the metal leads to the chains has an important effect on the conductance, resulting as a doping element for the chains, adding electrons to the electronic bands of π -conjugated systems [60]. The influence of

doping and strain on the conductance of an infinite cumulene was also investigated by Tongay *et al.*. In this study, heteroatoms, as C, O, N, modify the local electronic structures at the adsorption site while, under strain, the quantum ballistic transport with constant conductance of $2G_0$ of the wire evolves in an oscillatory behaviour [35]. Furthermore, it was studied that Cu-metalated carbyne preserves its metallic character because of the charge transfer between metallic Cu and the wire [61]. A system composed of an armchair and odd-numbered chain capped between two graphene nanoribbons, however, shows a net magnetization, regardless the magnetic state of the graphene contacts [62]. A very high value of electron mobility, i.e. $1.5 \times 10^5 \text{ cm}^2/\text{V}\cdot\text{s}$, was calculated for 1D extended graphdiyne nanowire and it decreases of one to two orders of magnitude in chemically functionalized nanowire with groups as OH, NH_2 , CH_3 , F, CN, NO_2 , and COOH [63]. Using molecular dynamics simulations, phonon transport in carbyne, i.e polyynes and cumulene, was predicted higher than graphene, which means that it exceeds 54 and 148 $\text{kW}/\text{m}\cdot\text{K}$, respectively. Acoustic phonons, whose mean free path allows the ballistic thermal transport up to micron-scale, dominate the thermal conductivity, which can be improved by tensile extensions in infinite polyynes [64].

Turning to experimental works, a paper reported the study of vibrational and electronic properties of disordered cumulenic species in a sp^2 -carbon matrix and showed that the presence of sp -component affects the conductivity of the whole configuration [65]. The measurement of the conduction of a single carbon atomic wire was first conducted by Wang *et al.* on chains capped by pyridyl-groups between two gold contacts, employing the scanning tunnelling microscopy (STM) tip [66]. Then, many other works [67–69] contributed to give more insight to this topic, as the one of Cretu and co-workers, where carbon atoms were breaking up from graphene nanoribbons by STM tip in order to form sp -carbon chains in between. They found out a drop in electrical conductivity of the single chain compared to the ideal one, which can be possibly due to the complex interaction between the wire terminations and the contact leads [67, 70]. Moreover, it was experimentally demonstrated that, under strain, CAWs are semicon-

ducting, whereas, unstrained, they are metallic with ohmic behaviour, as theoretically predicted in works mentioned before [71]. An interesting example of conductivity measurement of a carbon chain is given by Yuzvinsky et al., who obtained a sp-carbon chain by electron irradiation on carbon nanotube by means of transmission electron microscopy, inducing defects and heating and, thus, a shrinking effect. In correspondence of the carbon chain, a negative differential resistance was detected [72]. Recently, the first field-effect transistor (FET) based on cumulenic chains (i.e. [3]Ph) as a semiconductor material was fabricated (Fig.1.8). The bond length alternation, given by the terminations, ensures the semiconducting behaviour. This work, to which I contributed during my PhD, is an important milestone in solution-processed thin film electronics [73].

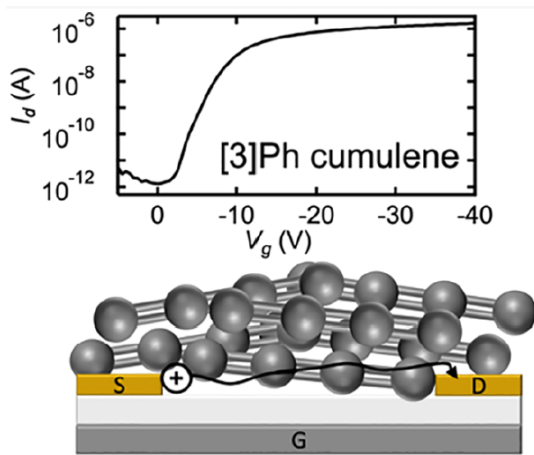


Figure 1.8: Transfer characteristic of a cumulenic [3]Ph microcrystal bottom-gate bottom-contact FET (top) and sketch of the cross section of FET device [73].

CAWs nonlinear optical properties, arising from the electron delocalization along the backbone chain, can be exploited in photonic devices, i.e. optical transistor or optical multiplexing. This last-mentioned technique allows the simultaneous measurement of different species in a non-destructive way, being suitable for biological and medical applications. Because of the broad linewidth or spectral overlap of the most common multiplexable optical materials, a limited num-

ber of spectral barcodes can be resolved. A recent work presented 20 chemically synthesized polyynes with distinct Raman signals, called *Carbow*, see Fig.1.9. It reached 30 resolvable colours, i.e. 30 parallel optical detections, also considering six signals from commercial dyes and four from fluorescent channels. In this work, *Carbow* was applied to optical barcoding, optical cell imaging, supermultiplexed imaging of organelles in living cells [74].

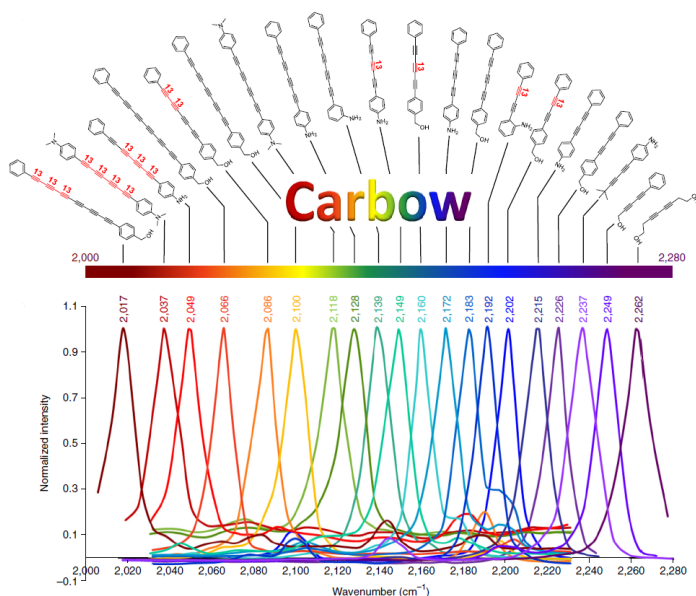


Figure 1.9: *Carbow*: chemical structures of 20 polyynes (top) and distinct Raman frequencies (bottom) [74].

All the theoretical and experimental studies showed in this section can give an idea on the huge impact that CAWs-based materials may have in technology because of their incredible variety of potential applications.

1.4 Stability of carbon-atom wires

1.4.1 Stability issues

The main issue that limits the use of carbon-atom wires in technological applications is their stability. CAWs are, in fact, very reactive and

sensitive to the surrounding environment, so they are easily subjected to degradation phenomena. One common decomposition process is the oxidation of the chains, which is promoted mainly by oxygen and ozone [75, 76] and the effect is even more enhanced at high temperature [77]. Cumulene is even less stable than polyynes if exposed to oxygen [78]. Another process is the crosslinking reaction: a spontaneous degradation mechanism due to interactions between chains. It can be accelerated by different factors, e.g. thermal gradients, high concentrated solutions and basic solvents, and leads to the formation of more stable sp^2 -based structures [78]. Moreover, hydrogenation is another detrimental process, for which polyynes tend to form bonds with H atoms losing sp -carbon atoms and resulting as partially-hydrogenated polyynes [79]. In addition, the photolysis induced by UV irradiation under inert atmosphere brings to polyynes fragmentation. It was observed that the kinetic rate constants of the chains under photolysis in inert environment are similar to those measured in different solvents and the presence of impurities in the polyynes solutions does not affect the photolysis rate, which instead depends on the light energy and the type of polyynes [75, 80]. These degradation mechanisms explain why the solid form of CAWs is so hard to obtain. Solutions of hydrogen-capped polyynes with a concentration less than 10^{-4} mol/L are stable for approximately 1 month, while cyanopolyynes are less stable because are more liable to oxidation. Usually, oxygen abstracts hydrogen atoms from the end of the wire, forming peroxides which further degrade the chain. In cyanopolyynes, one end-cap consists in CN-group, which is an electron-attractor, so it weakens the CH bond on the other side of the chain, facilitating the hydrogen abstraction [81]. For the same reason, longer chains are less stable than shorter ones. In fact, longer the chains, higher the π -conjugation is and weaker the CC bonds are [81].

1.4.2 Stabilization strategies

To avoid degradation of carbon-atom wires, different methods have been developed so far.

One strategy is to encapsulate long sp -carbon wires inside single-, double- or multi-walled carbon nanotubes [82–84]. In this way, Shi *et*

al. were able to observe linear sp-carbon chains up to 6000 carbon atoms [83] and half of the chains encapsulated in single-walled carbon nanotubes survives up to 673.1 K [77]. Other structures employed to surround polyynes were rotaxane macrocycle, which mechanically protect the carbon chains [85]. The decomposition of carbyne-rich nanostructured carbon thin film is inhibited if immersed in ionic liquid [86].

Another approach is having sterically bulky terminations on the chains, that act as spacers which avoid cross-linking reactions, e.g. sp² clusters [87], graphene edges [88] and phenyl or biphenyl groups [89–92]. In this way, it was possible to synthesize sp-carbon chains of 44 carbon atoms, stable even at temperature higher than the room condition [89]

Moreover, CAWs can be stabilized by embedding them in solid-state systems. Casari *et al.* observed that H-capped polyynes can be stabilized at ambient conditions for months by drying a mixed solution of sp-chains with silver colloids [93]. Matsutani and co-workers prepared a SiO₂ gel with H-polyynes by PLAL, still present after four months [94]. Another possible way to encapsulate sp-carbon chains is to exploit a polymeric matrix. In literature, there are some works based on poly(vinyl alcohol) (PVA) films with H-polyynes inserted [95–97]. Two works of literature present the preparation of polyynes in methanol, one by pulsed laser ablation in liquid [95] and one by submerged arc discharge in liquid [96]. PVA solid granules were added in the polyynes solutions and a heating treatment for dissolving the polymer was applied. In such a way, polyynes signals are detected after one month [95] and six months [96] respectively, showing that embedding polyynes in a polymeric matrix is a good stabilization strategy, which also allows the preparation of sp-carbon based materials for interesting applications.

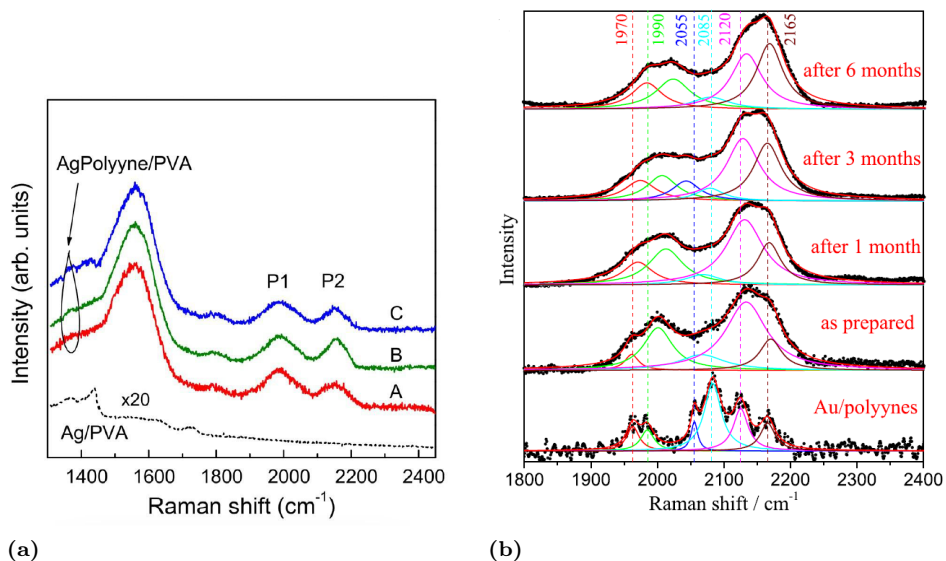


Figure 1.10: (a) Surface-enhanced Raman spectroscopy (SERS) spectra of polyynes and Ag nanoparticles in PVA films as prepared (A), after a week (B) and a month (C) with the two bands related to sp -carbon modes denoted by P1 and P2. The picture is adapted from Ref. [95], (b) time evolution of Lorentzian fitted SERS spectra of polyynes and Au nanoparticles in PVA film [96].

2

Synthesis and characterization of carbon-atom wires

This chapter introduces the techniques employed for the synthesis and characterization of carbon-atom wires (CAWs). The physical principles and the state of art related to the synthesis of polyynes by submerged arc discharge in liquid and pulsed laser ablation in liquid are presented in Section 2.1. Principles of function of Raman-based techniques, liquid chromatography and UV-Vis spectroscopy are described in Section 2.2, together with the corresponding main results present in literature on CAWs characterization.

2.1 Synthesis techniques

Carbon-atom wires can be synthesized by different techniques, each with advantages and drawbacks, and, depending on the purpose, it is possible to select the most convenient one. They are mainly based on a bottom up approach, excluding few cases such as the study employing the transmission electron microscopy, where sp-carbon chains are prepared by a top-down approach. The latter consists of removing carbon atoms from a graphene layer until a single atomic chain remains suspended between two graphene edges [98]. The bottom up syntheses are mainly divided in two categories: chemical methods and physical processes.

Chemical methods

Chemical techniques were mainly carried out in solution. The first polyynes synthesis dates back to 1869 and was based on the dimerization of ethynyl groups by means of copper salts by Glaser [3]. This technique is not selective since it gives products of all possible couplings, differently from Cadiot-Chodkiewicz reaction, which ensures only the coupling of alkyne to the haloalkyne [99]. However, the limit of both techniques concerns the isolation of a potential explosive copper acetylide. Since then, a variety of improvements were made on the metal-catalyzed homocoupling or heterocoupling method to be able to synthesize CAWs with a defined length and end-groups [12,91,100–102]. A noticeable result was achieved by Hirsch and coworkers, synthesizing model compounds for the hypothetical 1D carbon allotrope carbyne [103,104]. Another approach is based on polymerization reactions, exploiting polymers dehydrohalogenation and polycondensation of halides [105,106]. In doing so, polydisperse sp-chains can be obtained but, even changing the reaction parameters, it was not possible to obtain size-selected polyynes. The synthesis of cumulenes was less explored than that of polyynes because of their minor stability. Actually, the cumulene composed of three double bonds, which is the most stable cumulenic species, was synthesized by different methods, e.g. dimerization of carbenes or carbenoids, metal catalysed coupling of dihaloalkenes or terminal alkynes and dehalogenation [107]. Moreover, the typical route to synthesize cumulene with five double bonds is to first add metal-acetylide to a ketone, which defines the end groups. Then, the oxidative homocoupling of the terminal and the conversion to a dihalide are performed and finally, the reductive elimination with Zn or BuLi is undertaken [107].

Physical methods

Physical methods are based on the production of carbon vapour or plasma, which is rapidly quenched in order to reach the out-of-equilibrium sp-carbon species. The most-common ones are: pulsed microplasma cluster source, pulsed laser deposition, submerged arc discharge in liquid, pulsed laser ablation in liquid, all sketched in Fig.2.1.

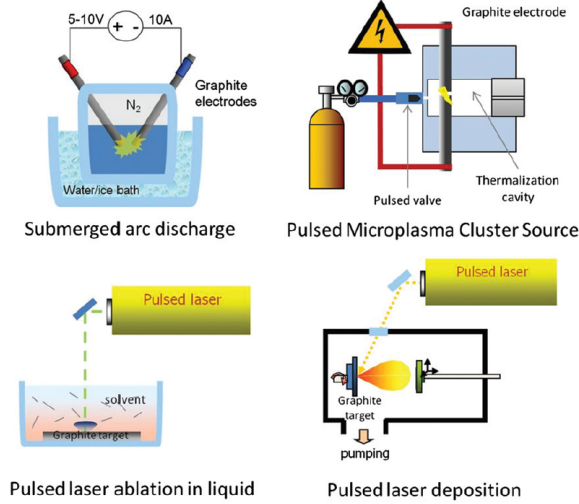


Figure 2.1: Sketches of four physical methods employed to synthesize carbon-atom wires [33].

The first method just mentioned is also called supersonic cluster beam deposition and it was developed by P. Milani and coworkers [108]. Carbon clusters are formed in the gas-phase and constitute a collimated molecular beam. Once the beam is intercepted by a substrate, nanostructured films rich of sp-carbon chains both polyynes and cumulenes start to grow [87]. Then, the pulsed laser deposition is based on the laser ablation of a target in ultra-high vacuum or in a background gas and on the consequent formation of a plasma region, which expands in a plasma plume. The ablated species reach a substrate where they condensate inducing nanostructures growth [109]. Submerged arc discharge in liquid is based on two electrodes immersed in a dielectric liquid, maintained in contact with an applied voltage. In this way, an arc discharge, which locally sputters the electrode material, is formed and a plasma region is originated, in which carbon-atom wires can be synthesized. The liquid rapidly quenches the plasma reaching the out-of-equilibrium condition where species can aggregate [110]. Pulsed laser ablation in liquid consists in laser ablation of a carbon-based target or powder in a solvent. Part of the ablated material is converted in plasma, which is confined by the liquid, so establishing the ideal

conditions of pressure and temperature to produce a mixture of poly-dispersed polyynes [111]. These two last mentioned techniques, which are described in details in the following sections, were chosen because they may be utilized for future mass production. They have a relatively low-cost, and are fast and scalable. The drawbacks of these techniques concern the low yield and the difficult control of the size and length of sp-carbon chains produced.

2.1.1 Submerged arc discharge in liquid (SADL)

In this section, a qualitative description of physical mechanisms and reactions involved during submerged arc discharge in liquid is first presented. Then, the state of art of this technique focusing on the synthesis of polyynes and silver nanoparticles, which are employed for structural characterization of sp-carbon chains, i.e. Raman-based technique, are also reported.

Physical principles

Discharges can be originated in liquids in different ways depending on the experimental parameters set on power supply (e.g. voltage, current, frequency) from which it is possible to obtain different plasma systems, as reported in the Fig. 2.1. The configuration employed in this work is the one inducing an arc discharge.

	Voltage (V)	Current (A)	Frequency (Hz)
Electron beam	100k–200 M	1 m–10(dc)	dc–10
Barrier discharge	5 k–20 k	1 m–10	10–100k
Pulsed corona	30 k–200 k	10 m–1 k	10–1 k
Flow stabilized corona	10 k–100 k	10 μ –100 m	dc
Arc discharge	0.1 k–0.5 k	10–100	dc
High frequency discharge	0.1 k–0.5 k	1 m–1 k	1 k–100 k
Microwave discharge	0.1 k–0.5 k	1 m–1 k	> 1 G

Table 2.1: *Characteristics of different discharges types [112].*

Arc discharges can be steady or showering¹ depending on the equivalent capacitance of the liquid. Liquids with high dielectric constant, as distilled water and methanol, present a showering arc [113]. Carter and Cambell performed the first detailed investigation of arc discharge in liquid in 1932, highlighting that the nature of discharge is a relevant influencing factor for the types of products and reactions involved [114]. Specifically, they considered a low voltage (e.g. 5-120 V) arc discharge² in distilled water, which should be free from electrolytes, that inhibit the discharge. The arcing between two graphite electrodes takes places when they are connected to a power supply, brought in contact and then, slightly separated, so a strong electric field in the liquid is triggered. To keep the arc with a tension in the 6-50 V range, since the arc is very short, it is necessary to maintain in contact the two electrodes, continuously adjusting their positions due to the material consumption. The lower the voltage, the higher are the number of adjustments required. When the arc is broken, electrolysis occurs giving products which are not associated to those obtained by arc. The arcing produces gas bubbles from the incandescent region of discharge. To cool down the liquid, a recirculating system is usually employed. This technique can be used to synthesize soluble and insoluble solid carbon compound, and gaseous products (e.g. O₂, H₂, CO, CO₂) [114].

Carter and Cambell gave a qualitative description of the reactions taking place during the discharge, investigating the effect of temperature of the arc and of the surrounding water, the arc pressure and the presence of water itself as a liquid media. Initially, when the electrodes are in contact, Joule effect is immediately induced from the great resistance of electrodes. Thus, the temperature increases (i.e. 3500 K) and steam is created. The arc takes place in the steam, which is maintained for longer time as much as the water is close to the boiling point. The highest pressure measured in the arc is of about 2330 kPa. Then, arc discharge causes thermal and electrical dissociation of steam, the latter leads to ions dissociation (i.e. H⁺ OH⁻), responsible of solid compounds, e.g. graphitic acid compounds. Furthermore, the

¹The case in which the arc may extinguish and reignite different times.

²The same condition exploited in this Ph.D. work.

discharge was accompanied by UV and visible radiations and photocatalytic reactions may be also provoked. In the work of Lange and coworkers, the spectroscopic features of the plasma emission during arc discharge between two electrodes of graphite in water were monitored [115]. The presence of C_2 radicals, carbon atoms, ions, atomic hydrogen and oxygen was identified and the average plasma temperature was estimated of about 4000-6500 K. This high value is associated to the presence of small bubbles which have high energy density and to the extremely exothermic reactions between carbon, oxygen and hydrogen. It was also observed that the density of C_2 radicals depends on the anode erosion rate and the diffusion process. In particular, water, which surrounds the plasma, limits the diffusion of the species, which are trapped within the bubbles, increasing the pressure inside [115].

As described in Xing *et al.*, the liquid during arc discharge has a twofold function: cooling down the electrodes and providing a gas bubble wall where nanomaterials can nucleate and grow [116]. Small bubbles near the bubble wall are characterized by high temperature gradient and high density of carbon species. In DC arc current, which is the condition employed in this work, the continuous flux of electrons emitted from the cathode reaches the anode, from which carbon ions and atoms are released, as visible in Fig.2.2a [117]. They move towards the cooling region near the bubble wall where a sufficient temperature gradient creates the suitable condition to form carbon structures, as shown in Fig. 2.2b [116].

In a work of Li and coworkers, the mechanism of plasma discharge was studied in tap water, gradually increasing the voltage of power supply from 30 to 130 V by bipolar pulsed power supply [118]. They individuated three stages for the formation of the discharge under water. The first is the pre-discharge, during which water is heating up by Joule effect for the small current present between electrodes, but, since water is conductive, no bubbles and spark³ were observed. The second is the initiation, where microbubbles are formed and high electric field is generated (10^5 V/m), so that micro-gap spark discharge is initiated

³Spark and arc are different only in terms of duration. Arc is a continuous discharge while spark is momentary.

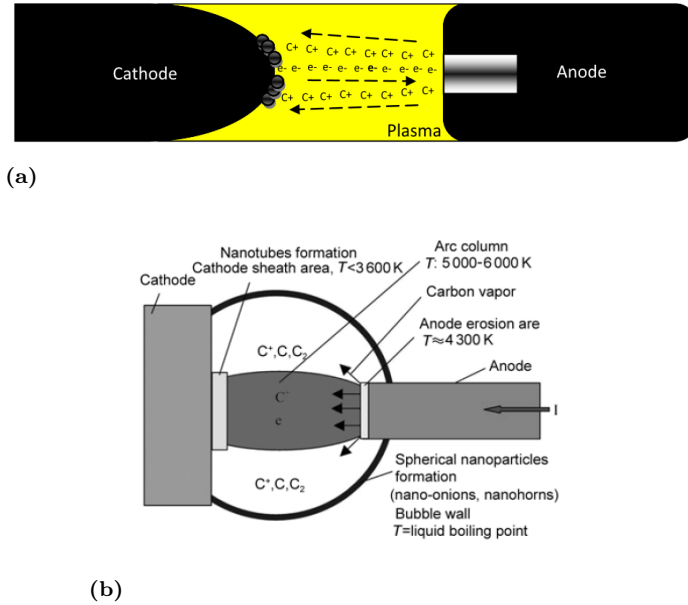


Figure 2.2: (a) Flux of electrons, carbon atoms and ions between two graphite electrodes at DC current [117], (b) Sketch of the physical model of the arc discharge in liquid [116].

at the edge of the electrodes. Finally, the third is the formation of water discharge, reached when the discharge voltage is 1 kV and the electric field is 10^7 V/m . In this way, the electrical breakdown of water is originated. The two micro-gap spark discharges started to grow from the two electrodes and then, they brought together allowing a high current flow, more than 10 A. From optical emission spectrum observed under plasma discharge in water, active species from water dissociation, as OH, H and O, were identified. If the discharge occurs in organic solvent as benzene, which is a non-conductive and non-polar solvent, only two stages were individuated: pre-discharge and formation of the discharge. To have the benzene breakdown, where the solvent becomes conductive allowing a current flow of 5 A, the electric field must be higher than benzene's dielectric constant, which is roughly 10^6 V/m . The optical emission spectrum demonstrates the presence of excited C, C_2 , CH, H radicals, obtained by multiple steps of dissociation and recombination [118].

The physical principles on which the technique of arc discharge in liquids is founded were here reported but the way the discharge interacts with the electrodes in liquid is complex and far to be clear, so it needs further and more detailed investigations.

Carbon-atom wires by SADL

The first work based on submerged arc discharge in liquid for the production of carbon-atom wires was carried out by Cataldo [110]. He took inspiration from some works of Tsujii, who synthesized polyynes by laser ablation of graphite or fullerene in a form of a solid target or powder suspension in organic solvents [111, 119]. The apparatus employed by Cataldo consists of two graphite rods with a diameter of 3 mm and 15 mm long, arranged in “V” configuration inside a glass cup, i.e. reactor, filled with 50 ml of solvent, as depicted in Fig.2.3a. They were connected to a power supply, setting a low voltage of 4-6 V and a DC current of 5 A. To ignite and sustain the arc discharge, the two electrodes were kept in contact maintaining a distance lower than 10^{-4} m. They are also slightly moved up and down to generate a very bright light. The liquid temperature during the discharge remains at ambient condition thanks to an external cooling bath. The solutions obtained in different solvents were analysed by high-performance liquid chromatography (HPLC) coupled to a diode-array detector (DAD), thanks to which hydrogen-capped polyynes of different length, $\text{H}(\text{C}\equiv\text{C})_m\text{H}$ with $m=2-8$, were detected in acetonitrile and decalin, see Fig.2.3b. Moreover, it was observed that the concentration of each component decreases with increasing the chain length. The shortest detected species, i.e. the one with $m=4$, has an estimated concentration in decalin of the order of 10^{-6} mol/L [110]. Cataldo investigated the role of solvents, e.g. acetonitrile, n-hexane, methanol, ethanol, water, liquid nitrogen, and the role of electrodes, e.g. graphite and titanium, in the synthesis of polyynes by arc discharge [79, 120–123].

Hydrogen-capped polyynes up to $m=9$ were noticed in acetonitrile at low temperature, i.e. 233.1 K, and polyynes up to $m=8$ were observed in methanol and hexane kept at room temperature. Moreover, the by-products formed in hexane during arc discharge could

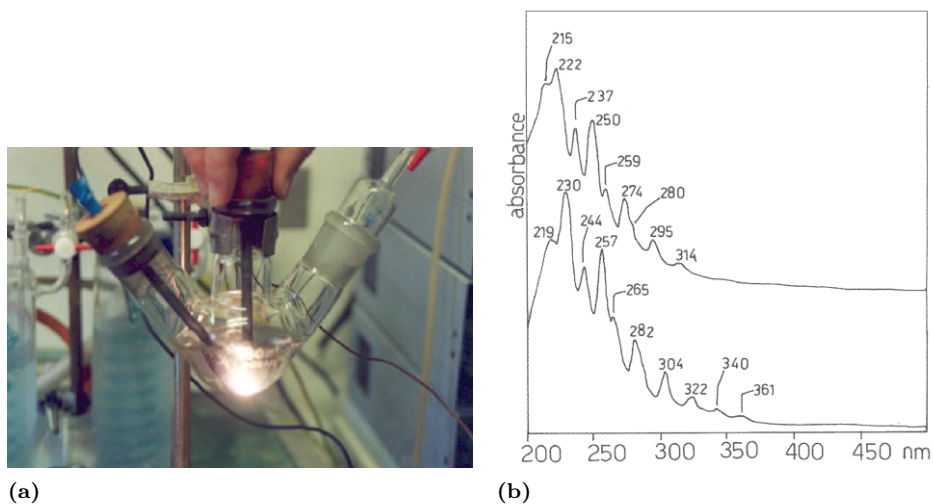


Figure 2.3: (a) Submerged arc discharge in liquid apparatus employed by Cataldo [110], (b) UV-Vis spectra of polyynes mixture after arc discharge in acetonitrile (at the top) and decalin (at the bottom) [110].

be partially hydrogenated polyynes. UV-Vis absorption spectra are, indeed, closed to those of ene-yne species and are eluted by HPLC at times similar to the species obtained after the hydrogenation of polyynes [79]. The experiment in distilled water resulted in the formation of hydrogen-capped polyynes, showing that hydrogen is coming from the plasmalysis of water, while carbon atoms from the vaporization of graphite electrodes. Arc discharge in liquid nitrogen produced cyanopolyynes, i.e. $\text{N}\equiv\text{C}-(\text{C}\equiv\text{C})_m-\text{C}\equiv\text{N}$ with $m=2,3,4$, and hydrogen-capped polyynes. Cyano termination is originated from the division of molecular nitrogen into atomic species, which can end the bare sp-chains, due to the high temperature of arc discharge. Hydrogen-termination can be caused by the humidity and traces of water in the liquid nitrogen and in the glass container [121]. Cataldo confirmed the identification of each type of polyynes by electronic absorption spectra, Fourier transform-infrared (FT-IR) spectra and by positive reactivity of polyynes mixture with a reagent specific for the detection of acetylene groups.

To better understand the mechanism of polyynes formation, Cataldo

Chapter 2. Synthesis and characterization of carbon-atom wires

Solvent	Hexane Graphite (% mol)	Hexane Titanium (% mol)	Benzene Graphite (% mol)	Benzene Titanium (% mol)	Methanol Graphite (% mol)	Methanol Titanium (% mol)	Ethanol Graphite (% mol)	Ethanol Titanium (% mol)
Polyyne C6	20.3	23.9	13.8	Detected	7.2	n.d.	8.9	n.d.
Polyyne C8	61.2	72.7	68.3	83	77.8	n.d.	73.5	n.d.
Polyyne C10	14.8	3.4	12.6	17	12.8	n.d.	12.3	n.d.
Polyyne C12	2.9	n.d.	3.2	Traces	2.2	n.d.	3.7	n.d.
Polyyne C14	0.63	n.d.	2.1	Traces	Detected	n.d.	1.5	n.d.
Polyyne C16	0.17	n.d.	Traces	n.d.	n.d.	n.d.	0.1	n.d.
Polyyne C18	n.d.	n.d.	n.d.	n.d.	n.d.	n.d.	n.d.	n.d.
Benzene	n.d.	Traces?			n.d.	Traces	n.d.	Traces
Indene	n.d.	Traces	n.d.	n.d.	n.d.	n.d.	n.d.	n.d.
Naphthalene	Traces	Traces	Detected	Detected	Traces	Traces	Traces	Traces
Acenaphthene	Traces	n.d.	Detected	n.d.	n.d.	Traces	n.d.	Traces
Acenaphthylene	Traces	Traces	Detected	Detected	n.d.	n.d.	n.d.	n.d.
Biphenyl	n.d.	n.d.	Detected	Detected	n.d.	Traces	n.d.	n.d.
Phenanthrene	n.d.	n.d.	Detected	Detected	n.d.	Traces	n.d.	n.d.
Anthracene	n.d.	n.d.	Detected	Detected	n.d.	Traces	n.d.	n.d.
Perylene	n.d.	n.d.	Detected	Detected	Traces	Traces	n.d.	n.d.
Pyrene	Traces	n.d.	Detected	n.d.	n.d.	n.d.	n.d.	n.d.
Crysen	Traces	n.d.	Detected	n.d.	n.d.	n.d.	n.d.	n.d.
Fluoranthene	n.d.	n.d.	Detected	Detected	n.d.	Traces	n.d.	n.d.
Benzo[b]fluoranthene	Traces	Traces?	Detected	Detected	Traces	n.d.	n.d.	n.d.
Benzo[b]naphto[2,1-cd]thiophene	n.d.	n.d.	Traces	Traces	n.d.	n.d.	n.d.	n.d.
Total polyynic conc. (mol/l)	4×10^{-4}	2×10^{-6}	5×10^{-4}	2×10^{-5}	5×10^{-4}	None	3×10^{-4}	None
Carbon black formation	Yes	Yes	Abundant	Abundant	Small	Small	Small	Small

n.d.=not detected.

Table 2.2: *Species produced by SADL in different solvents and with different electrodes [121].*

carried out also some experiments with titanium electrodes in different solvents. In the case of alcohols, e.g. methanol and ethanol, it was not possible to obtain polyynes, also because polycyclic aromatic hydrocarbons (PAHs) are hardly formed in alcohols even with graphite electrodes. Instead, in the case of titanium electrodes in n-hexane and benzene, polyynes were still detected but at two order of magnitude lower with respect to the case of graphite electrodes. These last-mentioned solvents are liable to form radicals, which can rearrange in PAHs and pyrocarbon, that can act as further sources of carbon atoms for sp- carbon chains. As a consequence, it was observed that the only possibility to have polyynes from arc discharge in alcohols is to employ electrodes of graphite, while for solvents as n-hexane and benzene, is enough the presence of PAHs generated from the solvent itself. Table 2.2 reports all the species obtained by arc discharge involving different solvents and electrodes [121].

In addition, polyynes were detected in a solution obtained by arcing two electrodes of graphite in CH_2Cl_2 while were not present after the discharge in other halogenated solvents as CCl_4 and CHCl_3 [124]. Recently, a paper of Wu et al. presented the results of arc discharge

between two electrodes of copper in alkanes, showing that the yield of polyynes is higher if the carbon-hydrogen ratio of alkane increases [125]. It was observed that alkanes decompose in C_2 and H radicals: the first helps in growing polyynes by coupling reactions and the second in terminating the chains [125]. Another possibility of analysing polyynes after arc discharge in liquid is to collect the gas generated by the arc in water and to cool it by cyclohexane. In this way, the gases emitted during the discharge can be eliminated, obtaining an environmental-friendly technique [126].

Relying on these literature outcomes, the choice of the appropriate solvent results fundamental to properly tune the length and termination of CAWs.

Silver nanoparticles by SADL

Arc discharge in liquid can be used also to synthesize metal nanoparticles necessary for the structural characterization of polyynes without employing chemical methods, as discussed later in the Section 4.2.

Tien *et al.* synthesized Au and Ag NPs by arc discharge in distilled water employing two electrodes of silver and gold, respectively [127]. Ag and Au nanoparticles are protected from agglomeration by repulsive electrostatic forces between nanoparticles due to the presence on their surfaces of atomic oxygen which forms hydrogen bond with water molecules, as shown in Fig.2.4 [127].

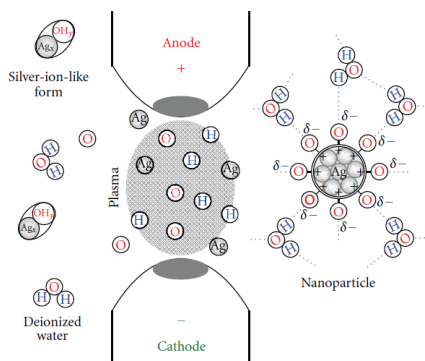


Figure 2.4: Mechanism of formation of Ag nanoparticles [127].

A similar work was carried out by Tseng and coworkers, who employed electrochemical discharge between silver electrodes in aqueous solution with sodium citrate by DC current. The role of sodium citrate is to reduce Ag ions into metallic silver but, if it is too much concentrated, the generated plasma becomes unstable, increasing the size of nanoparticles and their distribution [128].

2.1.2 Pulsed laser ablation in liquid (PLAL)

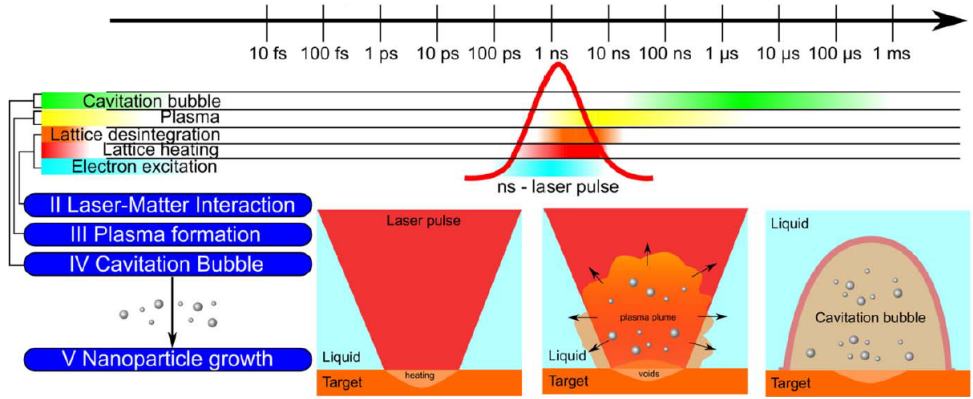
In this section, a qualitative description of physical mechanisms and reactions involved during pulsed laser in liquid is first given, then, the state of art of this technique focusing on the synthesis of polyynes and silver nanoparticles, which are employed for structural characterization of sp-carbon chains, is also reported.

Physical principles

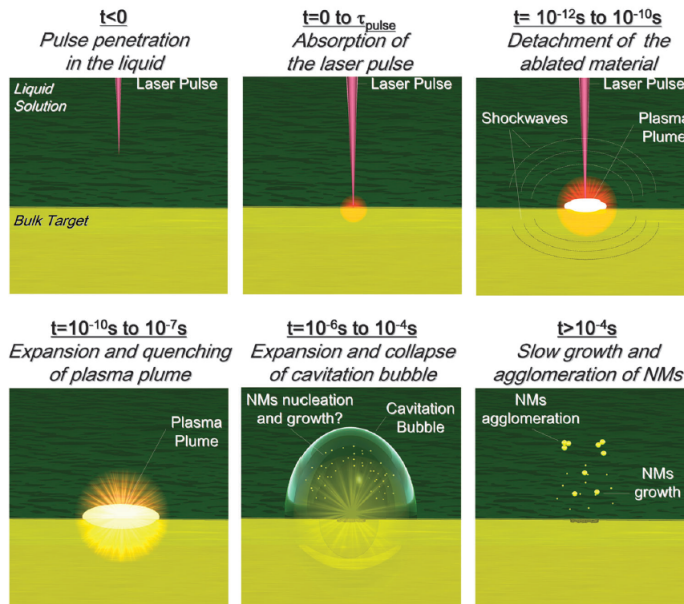
To study the mechanism of laser-matter interaction, it is necessary to differentiate between ultrashort pulsed laser ablation, ranging from femtosecond (fs) to picosecond (ps) laser pulses, and short pulsed laser ablation, ranging from hundreds of ps to nanosecond (ns) pulses. In this thesis work, a ns-laser is employed to ablate a graphite target immersed in a liquid. For ns-pulses, electronic excitation, heating and material erosion occur simultaneously, as sketched in Fig.2.5a. The study of the interaction between laser and plasma together with the understanding of the material removal in a reactive environment is still a topic under investigation. Moreover, the presence of the liquid, which mechanically confines and cools down the plasma region and chemically reacts with the ablated species, brings even more complexity to the description of the physical processes involved [129].

The main stages regarding the laser-matter interaction during PLAL can be summarized in Fig.2.5b and are discussed as follows.

Pulse penetration in the liquid. Intense laser pulses of megawatts power travel in the air and are focused by a lens through the liquid, which should be transparent to the radiation, so the light absorption



(a)



(b)

Figure 2.5: (a) Schematics of the ns laser ablation [129], (b) ns-laser ablation steps: from the pulse penetration in liquid to the growth of nanomaterials [130].

before reaching the target is negligible. In addition, the liquid environments are dielectrics, so they are considered as high-band gap semiconductors, where the plasma can be formed. The probability that non-linear optical processes occur in the liquid (e.g. self-focusing white light generation or filamentation of the beam [131]) during the crossing of ns-laser pulses is minor than in the case of ultrashort laser pulses. Liquid breakdown must be avoided for pulses longer than ps by working in defocusing conditions [130].

Absorption of the laser pulse and plasma ignition. The absorption of photons from a ns-pulse by a target immersed in the liquid is considered to happen simultaneously with the lattice heating and the material evaporation, thus generating a plasma. The material thickness, which absorbs the beam and where electric current flows, is called material skin depth [132]. In the case of ns-laser, in addition to photoionization, the material undergoes also thermal processes, e.g. thermoionic emission, vaporization, boiling and melting of the target, which affect a higher volume than that defined by skin depth [130].

Material detachment. Plasma is sustained by two types of mechanisms: particle-induced processes, consisting in excitation, ionization and de-excitation, and radiation-induced processes, as photoionization and radiative recombination by high energetic photons originated in the plasma region. In addition, the plasma, in the case of ns-pulses, can be further sustained at the plasma–liquid interface by the absorption of laser, which leads to a total plasma duration ranging from 200 ns to 1200 ns [129]. The plasma shape above the surface of the target results to be elliptical because of the external pressure of the liquid and is independent from the laser fluence. Free hot electrons from ionization of both target and solvent transfer their kinetics energy to the molecules in the plasma, increasing its temperature. The equilibrium between heating and cooling of hot electrons is reached during the ns-pulse duration. The liquid applies a certain pressure on the plasma, inducing pressure and temperature gradients higher than the case of gaseous plasmas. This helps in increasing the target etching by reactive species and so in improving the ablation rate. However, there is a limit in the plasma density, after which the laser beam cannot

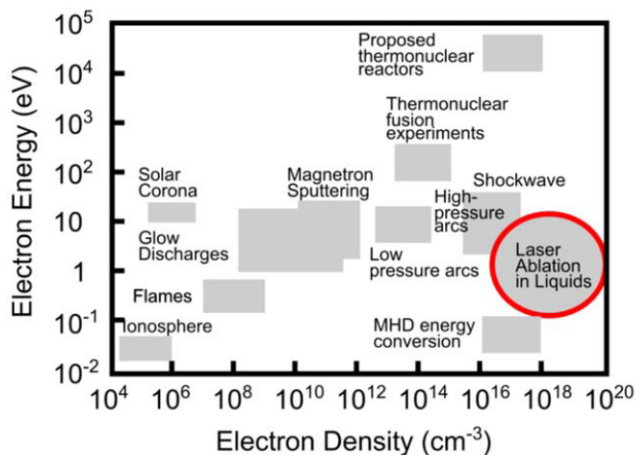


Figure 2.6: Classification of plasmas depending on electron energy and density [129].

penetrate anymore, and this shielding effect gives a decrease of efficiency [129]. The type of plasma can be classified in terms of electron density and temperature. In Fig.2.6, it is possible to compare the one originated from PLAL with other type of techniques.

Expansion and quenching of plasma plume. Plasma expands in the medium for several hundred of nanoseconds and a part of energy is transferred to the liquid environment. From one hand, the plasma is cooled down, from the other, the solvent is heated up to 10^3 K with its subsequent degradation, ionization and pyrolysis. The nucleation of nanomaterials starts in basis of the concentration, temperature and pressure conditions reached in the plasma plume but there is still no evidence if it occurs before or after the mixing of the species of the target with those of the solvent. Optical emission spectroscopy studies confirmed that these reactions take place in the plasma plume, even if quantitative analyses were not provided [133]. The nucleation and the growth of mixture of clusters and atomic precursors occur when the pressure of reactive species is higher that the vapour pressure at room temperature, i.e. in supersaturation conditions [130].

Expansion and collapse of cavitation bubble. A cavitation bubble is generated after 10^{-7} - 10^{-6} s from the energy transfer from the plasma

plume to the solvent. Some authors declared that the species are already formed in the plasma and then, they travel at the external limit of the bubble. Others claimed that the formation of nanomaterials takes place inside the bubble during its expansion. The temperature gradient at the interface between the bubble and liquid may indeed help in the nucleation and condensation of nanomaterials. So, this phenomenon cannot exclude the presence of nanostructures distributed elsewhere in the solvent. The bubble expands in the liquid with a time frame of 10^{-4} s decreasing its temperature and pressure, which results to be less than that of the exterior [130]. In this way, the bubble collapses and shockwaves are generated with a velocity close to the sound speed in that liquid. One shockwave is originated in the liquid, another one may be released from the target [129]. The emission of a shockwave causes a temperature and pressure increase at the collapse point, similar to the conditions found in the plasma plume (e.g. 10^3 K and 10^{10} Pa), inducing a phase transition in the new species formed [130]. For ns-pulses, the quantity of energy transferred in the formation of cavitation bubble and shockwave is higher than the case of fs-pulses, while the dynamics in the cavitation bubbles is instead independent from the laser pulse duration [129].

Slow growth and agglomeration of nanomaterials. After the generation of shockwaves from the collapse of cavitation bubbles, the system reaches a physical and chemical equilibrium. At this point, the synthesized species can slowly modify and grow. When the nanomaterials are not stable, they start to agglomerate, precipitating with time even longer than minutes [130].

Carbon-atom wires by PLAL

The first paper employing laser ablation in liquid as a synthesis technique for polyynes dates back to 2002 by Tsuji *et al.* [111]. The set-up of the technique consisted in a Nd:YAG ns-laser, which was directed to a cylindrical cell, where graphite powder is dispersed in organic solvent, as reported in Fig.2.7. Different wavelengths, i.e. 355, 532, 1064 nm, and solvents, i.e. benzene, toluene, hexane, were exploited for polyynes synthesis.

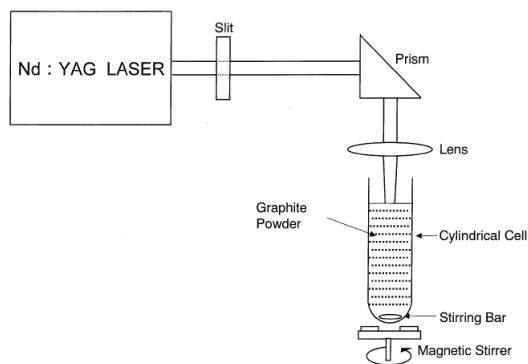


Figure 2.7: *Set-up of the PLAL technique employed by Tsuji [111].*

The carbon-atom wires detected by HPLC consisted of hydrogen-capped polyynes of different length. Specifically, the longest polyynes, i.e. up to 16 atoms of carbon, were obtained in benzene and toluene with 355 nm. It was claimed that the chain length is independent from the energy density of the radiation and that there is an optimum yield of polyynes in correspondence of a certain concentration of graphite powder in the solvent. If the graphite dispersed in the liquid is too high, it may cause the scattering of the laser and a decreasing in the efficiency of the process. Moreover, the formation of polyynes seemed to decrease with increasing the laser wavelength, even if the synthesis of polyynes was achieved in all the cases [111]. However, a work of Matsutani and collaborators declared the opposite, namely higher yield of polyynes in correspondence of higher laser wavelength. This can be explained considering the different type of target employed. In this last case, a solid pellet, located at the bottom of the cell, was used instead of graphite powder dispersed in the solvent, and so the laser beam, crossing the whole liquid volume, is scattered or absorbed from the by-products produced by the ablation. This effect is enhanced if the wavelength is short, i.e. 355 nm, which is closer to the absorption of impurities. As a consequence, employing a solid pellet, a minor yield of polyynes was obtained at shorter wavelength [134]. Tsuji and coworkers also described the mechanism of formation of polyynes as a chain reaction of carbon radicals, see Fig.2.8. The carbon radicals

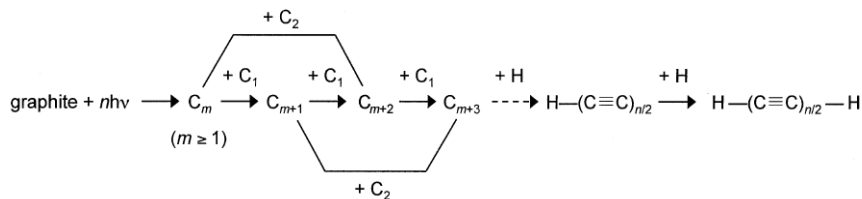


Figure 2.8: Scheme of the mechanism of polyynes formation [111].

from graphite particles, i.e. C_2 , react between themselves and with the radicals of the solvent, which mainly furnishes hydrogen atoms, that can terminate the sp-carbon chains [111, 119]. In such a way, it was stated that the hydrogenation and polymerization are two competing processes, and the degree of polymerization strongly depends on the solvent. An example is given from the fact that C_8H_2 was synthesized only in hexane and not in benzene and toluene, indicating that the polymerization in the last two mentioned solvents is faster than the hydrogenation in hexane [111]. These two mechanisms were also mentioned in the work of Compagnini *et al.* [135], who ablated graphite in water and acetonitrile.

Tsuji and collaborators prepared another work [119], which was based on the ablation of C_{60} particles instead of graphite powder. This experiment allowed the formation of hydrogen-capped polyynes and graphite-like carbon. It was found that polyynes concentration increases up to a certain value and then remains constant because, after that, the quantity of graphite-like carbon is so high that its laser absorption is not negligible. Moreover, it was also observed a different polyynes yield in basis of the hydrogen generation rate of the solvent employed during the ablation. Indeed, polyynes concentration in hexane is higher than that in methanol because of its faster H abstraction process linked to the smaller C-H bond dissociation energy [119]. Moreover, the ratio of hydrogen and carbon atoms in the solvent molecule seems to be the most crucial factor for the polyynes production in a work of Park *et al.*, where PLAL was performed in different alkanes (e.g. n-octane, n-hexane, n-heptane, and c-hexane) with ns-pulses at 1064 nm [136]. However, they observed that the effect of properties as

bond dissociation energy, total mass of hydrogen atoms per volume of solvent and thermal conductivity provided not a well-defined trend on polyynes yield [136].

Water as a solvent for PLAL was investigated in few works, which reported the preferential synthesis of short H-capped polyynes up to 12 atoms [135, 137, 138]. Matsutani *et al.* discussed the formation of hydrogen-capped polyynes up to 18 atoms after the ablation at 532 nm of perylene derivative, i.e. PCDTA, and graphite target in different alcohols (e.g. methanol, ethanol, 1-propanol, 1-butanol, t-butyl alcohol) [139]. Matsutani and coworkers also investigated the difference of ablating a graphite powder and a pellet in hexane at 532 nm, noticing that the C_2 radicals are produced in higher density on the pellet surface compared to powder, for which the diffusion rate of polyynes into the solvent is higher than their production rate [140]. The ablation in ethanol by ns-pulses at 532 nm was also reported by the group of Tabata, who deepened the spectroscopy studies on polyynes [53, 54, 141, 142]. Furthermore, Matsutani *et al.*, in another work, employed decalin as a solvent and 1064 nm as laser wavelength and they were able to reach the longest hydrogen-capped polyynes synthesized by PLAL so far [143, 144]. This achievement was justified considering that the density of C_2 radicals is increased in high viscous environments, as in the case of decalin. The carbon reactive species are, indeed, limited in their diffusion far away from the plasma region, allowing the polyynes to grow and become longer [143]. Besides hydrogen-capped polyynes, other types of polyynes were produced by PLAL. Specifically, cyanopolyynes, i.e. $H-C_n-CN$ ($n=6,8,10,12$) [145], or dicyanopolyynes, i.e. C_2N_2 ($n=6,8$) [138], were obtained after ablation in acetonitrile. Methyl-capped polyynes, i.e. $H-C_n-CH_3$ ($n=8,10,12$), were formed in hexane by ns-pulses [146] and in toluene by fs-pulses focused at the meniscus of the liquid [147].

A strong absorption background in the UV-Vis spectra of polyynes solutions after PLAL was observed by Compagnini *et al.* and it was associated to the by-products of the ablation, i.e. hydrocarbons. It was stated that, in the case of PLAL in acetonitrile, the unresolved UV-Vis background is higher than that of PLAL in water because carbon

contaminants can be also formed by the decomposition/carbonization of the solvent [135]. More recently, Taguchi *et al.*, who exploited ns- and fs- laser induced breakdown in a gas flow of hydrocarbons for polyynes synthesis, defined a new parameter to calculate the purity of polyynes solutions, called *index of purity* (χ_p). It is defined as the ratio between the area of hydrogen-capped polyynes absorption peaks to the area of the unresolved background related to hydrocarbons [148, 149]. In this way, it was observed that laser ablation in gas gives higher χ_p than the case of liquids. Looking at the yield of each species, it was suggested that the synthesis of polyynes occurs in a specific time window, that allows the cooling of the carbon radicals avoiding the degradation of sp-carbon chains [148].

Silver nanoparticles by PLAL

Pulsed laser ablation in liquid of a metallic target, as silver, can also be used to prepare silver nanoparticles, necessary for the structural characterization of polyynes without employing chemical methods, as discussed later in the Section 6.5.

Most of the synthesis of Ag nanoparticles by PLAL were performed in water [150–153]. Herbani *et al.* employed a ns-laser to ablate Au, Ag and Cu targets in water at different wavelength, i.e. 1064, 532, 355 nm, energy pulse and ablation time, in order to find the conditions at which the yield of nanoparticles is higher for each experiment [150].

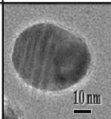
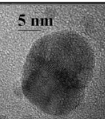
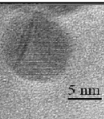
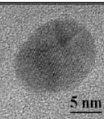
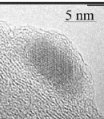
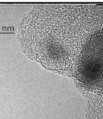
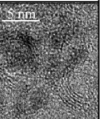
Target ↓	Solvent ↑	Water	Ethanol	Acetonitrile	Dimethyl- formamide	Tetra- hydrofuran	Dimethyl- sulfoxide	Toluene
		<chem>O</chem>	<chem>CCO</chem>	<chem>CC#N</chem>	<chem>CN(C)C=O</chem>	<chem>C1CCOC1</chem>	<chem>CSC(=O)C</chem>	<chem>Cc1ccccc1</chem>
Ag								
		Metal Ag/ Oxide AgO	Metal Ag	Metal Ag	Metal Ag	Metal Ag/ Carbon	Metal Ag/ Carbon	Metal Ag/ Graphite

Figure 2.9: Nanoparticles obtained by laser ablation of Ag in different solvents with 9 ns pulses at 1064 nm and 10 J/cm² [130].

Different optimized experimental parameters for obtaining the higher

concentration of nanoparticles were found in the work of Shukri *et al.* [152]. To stabilize silver colloids in water, cetyl trimethylammonium bromide (CTAB) surfactant was added to the solutions and, in this way, the nanoparticles were maintained for several weeks [152]. To estimate the concentration of silver nanoparticles capped by citrate, Paramelle and coworkers provided a table of the concentrations in function of the nanoparticles medium size [151]. Generally, nanoparticles are less stable and tend to coalesce more when organic solvents are used instead of water in the ablation of silver target [130]. This effect can be justified considering the lower dielectric constant of organic solvents and their degradation during the ablation. This causes the formation of different by-products, which may adsorb on the nanoparticles surface, thus inducing a lower Z-potential [130]. Nanoparticles obtained by laser ablation of Ag in different solvents with 9 ns pulses at 1064 nm and 10 J/cm² are reported in Fig.2.9.

2.2 Characterization techniques

Several methods are employed for carbon-atom wires characterization, e.g. transmission electron microscopy [71], scanning tunnelling and atomic force microscopies [154], IR and phosphorescence spectroscopies [155, 156], nuclear magnetic resonance spectroscopy [145, 157] and mass spectroscopy, to identify the exact carbon structure synthesized [158–160]. Among all the available techniques, the most common ones are: Raman-based techniques, liquid chromatography and UV-Vis spectroscopy. These last-mentioned methods are those exploited in this work and are presented in the following two sections.

2.2.1 Raman-based techniques

Raman spectroscopy is very sensitive to carbon-based structures and it is a suitable method to unambiguously detect carbon-atom wires, as already mentioned in Chapter 2. In this thesis, a Raman-based technique, called surface-enhanced Raman spectroscopy (SERS), was employed because it is useful for low concentrated polyynes solutions as those obtained by SADL and PLAL. First, the physical principles

of Raman spectroscopy are set out, then, Raman spectra of carbon-atom wires are described. Moreover, physical principles and polyynes spectra related to SERS measurements are also reported.

Physical principles of Raman spectroscopy

Raman spectroscopy is based on the Raman scattering, which consists of inelastic scattering of incident monochromatic radiation, discovered in 1928 by C.V.Raman [161]. The beam scattered from a sample illuminated by the monochromatic light is characterized by an elastic part, the so-called Rayleigh scattering, and an inelastic part, i.e. Raman scattering, for which the frequency (i.e. ω_L) shifts up or down with respect to the original incident beam. The elastic scattered radiation is filtered out by the Raman spectrometer, while the collected one is addressed to a detector and spectroscopically analysed. The shifts in frequency compared to that of the incident radiation provide the structural information of the sample. The Raman spectrum consists of the intensity of the inelastically scattered light as a function of the Raman shift expressed in cm^{-1} . The signals with frequency lower than the incident radiation are called Stokes peaks while those at higher frequency are called anti-Stokes peaks. Stokes peaks are the only acquired signals because they have higher intensity than the anti-Stokes ones [162]. The classical theory behind the Raman effect is based on an incident electromagnetic field, e.g. NIR, visible or UV laser, defined as $\vec{E} = \vec{E}_0 \cos \omega_L t$, which distorts the electronic distribution of the investigated material, inducing a time-dependent dipole moment ($\vec{M}(t)$). It is described by the following equation: $\vec{M} = \vec{\alpha} \vec{E}$, where $\vec{\alpha}$ is called polarizability and is a tensor representing the displacement of the electrical charges in the sample due to molecular vibrations. The material vibrating at specific frequency (ω_s) can be modelled as a harmonic oscillator and can be expressed in normal coordinate: $Q = Q_0 \cos(\omega_s t)$. If a small vibration of the nuclei is considered, the Taylor series can be applied to the dipole moment equation as follows:

$$\vec{M}(t) = \alpha_0 \vec{E}_0 \cos(\omega_L t) + \frac{1}{2} \left(\frac{\partial Q}{\partial \alpha} \right)_0 Q_0 \vec{E}_0 \{ \cos[(\omega_L - \omega_s)t] + \cos[(\omega_L + \omega_s)t] \} \quad (2.1)$$

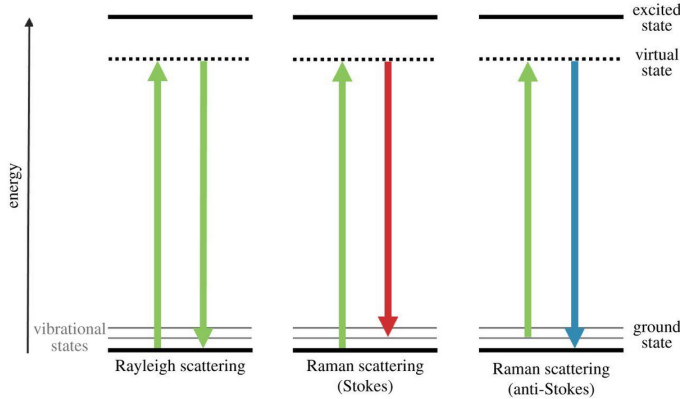


Figure 2.10: Sketch of Rayleigh scattering and Raman scattering (Stokes and anti-Stokes) [163].

As a consequence of the Eq.2.1, the condition to observe Raman effect is: $\frac{\partial Q}{\partial \alpha} \neq 0$. Calculating the intensity emitted per unit of solid angle as $I(t) = A |M(t)|^2$, where A is a constant, it was possible to properly foresee the presence of both Stokes and anti-Stokes signals, but not their correct relative intensities. Classical theory calculations, indeed, result in Stokes peaks less intense than anti-Stokes ones, which is not true from empirical observations [162]. The contradiction is resolved by employing the quantum theory, where photons are considered as particles which collide with lattice quantized modes of vibration, i.e. phonons, which uniformly oscillate at a certain frequency (ω_j). Therefore, the incident photons interact with the material, perturbing the electronic wave functions. In this way, the system can formally be considered as having obtained a non-stationary energy level of higher energy, which is associated to a virtual energy level. The latter has no finite lifetime, so the system simultaneously goes back to an allowed level and a photon can be re-emitted in three different ways, as represented in Fig.2.10. In Rayleigh process, the formation or annihilation of phonon is not observed, thus the crystal after the excitation goes back to the initial level. In Stokes process, a phonon is created, so the system arrives to an excited vibrational state. In anti-Stokes process, a phonon is annihilated, so the initial state of the lattice is in an excited state and the final one is at ground state.

From quantum theory, the intensity ratio between Stokes and anti-Stokes peaks results as the classical term multiplied by an occupation factor, related to the Bose-Einstein statistics, which considers that the population of the ground vibrational level is higher than that of the excited one, as shown in Eq.2.2.

$$\frac{I_{Stokes}}{I_{anti-Stokes}} = \left[\frac{\omega_L - \omega_j}{\omega_L + \omega_j} \right]^4 \exp \left[\frac{\hbar \omega_j}{k_B T} \right] \geq 1 \quad (2.2)$$

To observe the Raman effect, it is necessary to respect the conservation rule, which follows directly from the energy and momentum conservation between the initial and the final states. For crystals, the conservation rule states: $q \simeq 0$. This implies that only optical phonons at the centre of Brillouin zone can be excited in the first order of Raman scattering. In the case of molecules, Raman-active modes depend on the symmetries of the normal mode and of the equilibrium configuration, which can be verified by group theory. For amorphous or nanocrystalline materials, the fundamental selection rule is relaxed, so the Raman spectra typically show broad bands instead of well-defined peaks. However, further details on Raman scattering can be found in the following textbook [162].

Raman of carbon-atom wires

Raman signals of carbon-atom wires are located in the 1800-2300 cm^{-1} spectral region. As clearly evinced from Fig.2.11a, characteristic peaks of other carbon materials are not located in the sp-carbon fingerprint, in fact, sp² carbon falls between 1300-1600 cm^{-1} and 2700-3200 cm^{-1} , and diamond at 1332 cm^{-1} . This enables sp-carbon signal to be identified even in the case of sp-sp² carbon moieties [46].

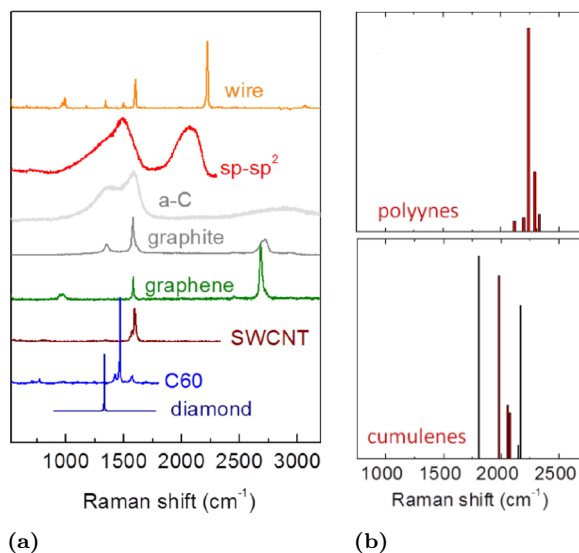


Figure 2.11: (a) Experimental Raman spectra of carbon solids and nanostructures, [46], (b) DFT simulations of Raman lines of polyynes and cumulene. Figure adapted from Ref. [46].

Raman peaks of sp-carbon chains are associated to CC stretching mode and their positions are different for polyynes and cumulenes. The vibrational modes of cumulenes have frequencies much lower than those associated to polyynes of the same length, as visible in Fig.2.11b [43]. Polyynes show very intense lines corresponding to the out-of-phase stretching of adjacent CC bonds, i.e. effective conjugation coordinate (ECC) mode or *R* mode, as in the case of polyenes [41] and are also known in literature as *alpha* lines [53]. These peaks shift to lower wavenumbers and have higher Raman cross section by increasing the chain length. A second less intense peak is named *beta* line and is particularly marked in short hydrogen-capped polyynes [53]. In fact, when end-groups enable the formation of really long chains, the ECC mode gets so intense that it covers all the other secondary peaks, making them barely invisible. Increasing the size of the chains, the position scheme of these lines becomes less and less regular. They can be located even at higher frequency than that of *alpha* peak. All these aspects related to sp-carbon Raman lines are depicted in Fig.2.12a.

Moreover, density functional theory simulations allow the assignation of *alpha* and *beta* peaks to specific collective stretching CC modes as reported in Fig.2.12b.

Raman spectroscopy is sensitive not only to the structural configuration and length of CAWs but also to the capping groups, as depicted in Fig. 2.13. In this picture, Raman spectra of polyynes with different length, termination and local order are shown. The phenyl-terminated polyynes can be recognized from the peak at around 1600 cm^{-1} related to the vibration of phenyl ring [90].

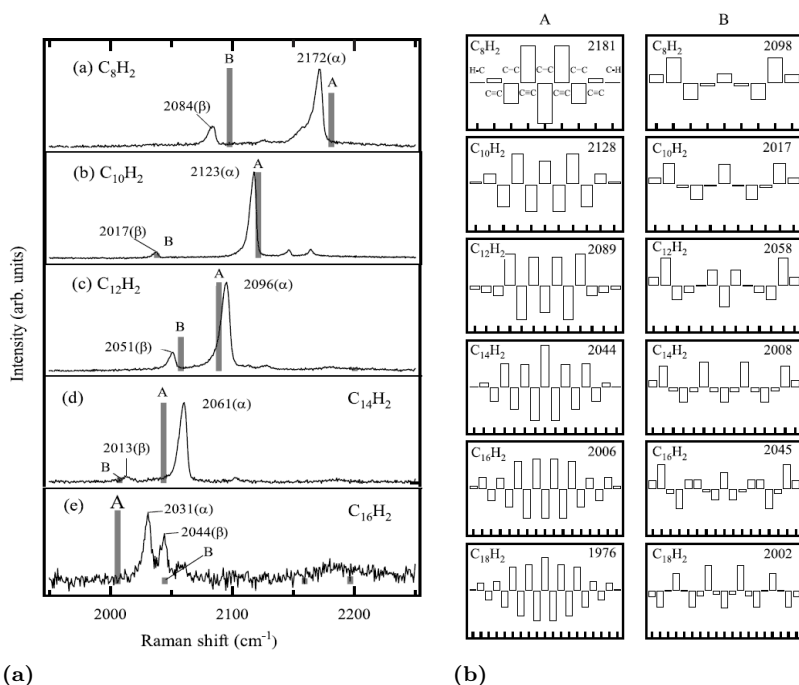


Figure 2.12: (a) Experimental Raman spectra of H-capped polyynes by PLAL with “alpha” and “beta” lines and the corresponding simulated peaks, marked by “A” and “B” [53], (b) Atomic displacements associated to CC stretching modes of H-capped polyynes at specific frequency, obtained by DFT calculations [53].

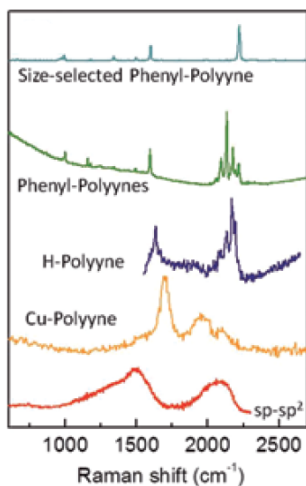


Figure 2.13: Raman spectra of different types of polyynes and $sp-sp^2$ moieties [164].

Physical principles of surface-enhanced Raman scattering (SERS)

Surface-enhanced Raman scattering (SERS) consists of the intensification of the Raman signal, observed for molecules close to metallic nanoparticles or to wrinkled metallic surface. This phenomenon involves two different intensification mechanisms: electromagnetic and chemical enhancement.

Electromagnetic enhancement. It is mediated by metal surface plasmons polaritons. The Raman scattered electromagnetic field can be intensified if the surface plasmons, i.e. collective electron oscillations at the metal surface, match the frequency of the incident wave. The electric field, in fact, can induce a dipole moment in the nanoparticle which sums to the electric field of the incident wave. The SERS effect is dependent on the position and width of plasmonic absorbance peak of metal nanoparticles, which, in turn, depends on their size and distribution. Small radii in particles lead to surface effects. The enhancement can be up to 10^{10} [165].

Chemical enhancement. It is caused by the charge transfer between the metal surface and the adsorbed molecule. This chemical effect is much weaker than the electromagnetic one, indeed, the enhancement factor is up to 10^2 . When molecules form a complex with metal nanoparti-

cles, a charge transfer is involved. In this way, it is possible to decrease the HOMO-LUMO gap of the isolated molecule, obtaining more easily the resonance with the NIR or visible lasers employed for Raman spectroscopy [166, 167].

SERS of carbon-atom wires

The first SERS spectra regarding sp carbon chains discussed in literature are reported in Fig. 2.14a and were obtained in two different ways: by mixing polyynes by arc discharge in methanol with chemically synthesized silver colloidal nanoparticles and by adsorbing polyynes by laser ablation in ethanol on a silver nanoisland film [168, 169].

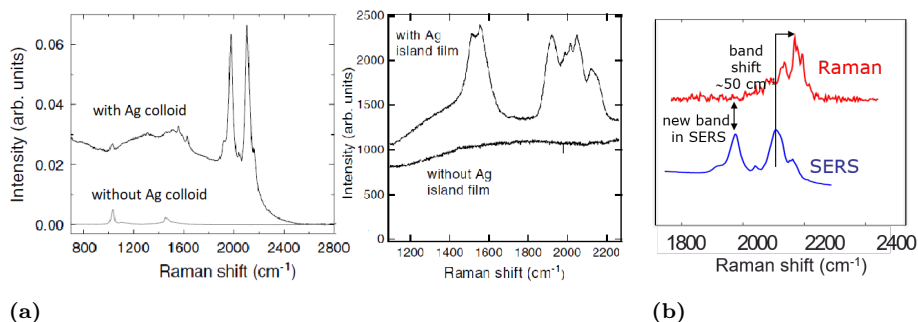


Figure 2.14: (a) On the left, Raman spectra related to polyynes by SADL in methanol with and without Ag colloids. On the right, Raman spectra of polyynes by PLAL in ethanol before and after deposition on a silver nanoisland film. Figure adapted from Ref. [168, 169]. (b) Comparison between Raman (up) and SERS (down) spectra. Figure adapted from Ref. [168].

In the work of Lucotti *et al.* [168], the enhancement of the Raman signal was of a factor of 10^6 . Besides the increment of the signal intensity, a SERS spectrum differs from a Raman one because of the red shift of the polyynes peaks and the appearance of a new band below 2000 cm^{-1} , as visible in Fig. 2.14b. This behaviour is due to the interaction of a strong polyynic chain with metal nanoparticles. The red shift, in fact, can be explained considering a possible charge transfer between the two, which, in turn, decreases the BLA of polyynes, so inducing a more equalized molecular structure, as the cumulene. Moreover, the

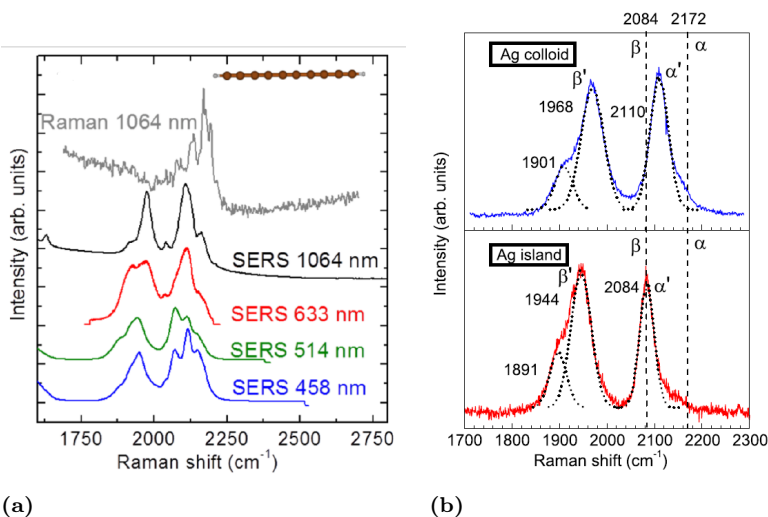


Figure 2.15: (a) Comparison between Raman spectrum and SERS spectra at different laser wavelength [46], (b) Comparison between SERS spectra obtained with two different SERS enhancers: Ag colloids and Ag islands [170].

origin of the band at lower wavenumber in SERS spectra can be related to the formation of cumulenenic complexes, thanks to the surface atoms of Ag nanoparticles, or to the creation of longer polyynes, assisted by the adsorption of shorter polyynes on the silver nanoparticle surface [168]. However, in the work of Tabata *et al.* [53], the bands in SERS spectra are considered as the SERS counterparts of the two *alpha* and *beta* Raman lines; for this reason, they are called α' and β' bands. Another important observation concerning SERS data is that the peaks seem to rely on the excitation light of the laser employed for the analysis [46] and the dimension of silver nanoparticles [170], as respectively represented in Fig.2.15a and in Fig.2.15b. The mechanisms involved in SERS measurements are complex and still under investigation because they depend on high number of factors.

2.2.2 Liquid chromatography and UV-Vis spectroscopy

It is known that to separate carbon-atoms wires in length and termination, high-performance liquid chromatography (HPLC) must be

employed. This technique is based on a mobile phase, which is generally composed of two different solvents and flows in the whole HPLC system. First, the sample is injected into the stationary phase, also called column, which is the core element of the apparatus. This element is crossed by all the species of the analysed solution and can retain the components for a certain time, i.e. retention time, depending on their structure. More the structure of the molecule is similar to the stationary phase, the longer will be the retention time. The mobile phase continuously flows during the entire analysis and each component will be gradually released by the column, flowing in the system and reaching a detector. In this way, a chromatogram can be recorded, where the intensity of the detector signals is plotted with time. After the detection, the separated species can be collected [171]. The sketch of HPLC apparatus is showed in Fig.2.16.

In the case of polyynes, which are non-polar molecules, the type of chromatography performed is called reversed-phase chromatography (aka hydrophobic chromatography). It is based on a hydrophobic stationary phase, instead of a hydrophilic stationary phase, which is referred to as normal-phase chromatography. The column, commonly employed for polyynes analysis, is composed of micrometric silica particles with alkyl ligand chains, while the mobile phase consists of a mixture of an organic solvent, e.g. acetonitrile and water [122]. With suitable methods, it is possible to separate polyynes in basis of the length and end-group. The longer the sp-carbon chains, the higher the retention time is, because the shorter chains are less retained on the column. Moreover, if the size is equal and the end-cap is different, two polyynes can be eluted in distinct times, thanks to the different polarity of the species, which depends on the termination. To detect polyynes, HPLC is commonly coupled to a UV-Vis spectrometer.

UV-Vis spectroscopy is a widely used technique to characterize electronic and optical properties of polyynes. It consists in measuring the absorption of the sample hit by an incident radiation with wavelength in the UV-Vis range (190-800 nm). The incident light is able to excite characteristic electronic transitions of the molecules. It is also possible to extrapolate quantitative information because of the linear relation-

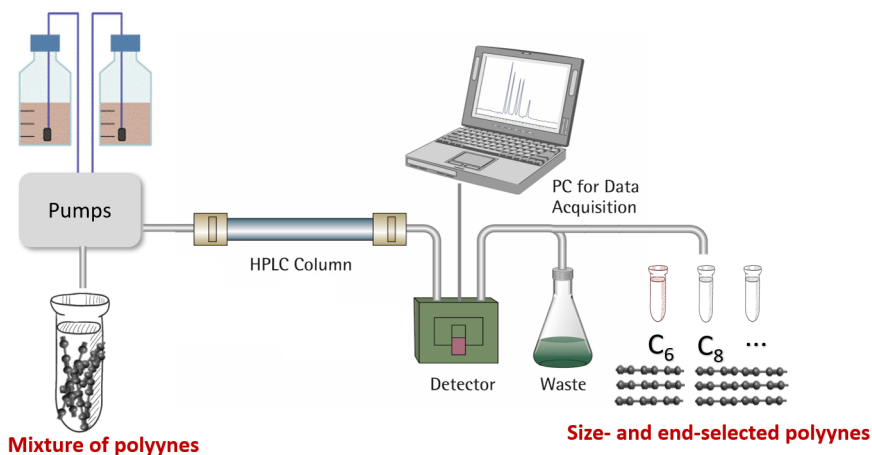


Figure 2.16: Main parts of the HPLC apparatus. Figure adapted from Ref. [172].

ship (i.e. Lambert-Beer law) between the intensity of the absorbed light and the concentration of the absorbing species of the sample. The absorbance is indicated with A , which is dimensionless and expressed in unit of absorbance (a.u.). It is equal to $\log_{10}(I_0/I)$, where I_0 and I are the intensity of the incident and transmitted light, respectively. The concentration of the absorbing sample is marked with c and defined in mol/L. These two terms are connected by the molar extinction coefficient, referred to as ϵ defined in L/cm·mol, which changes in basis of the solvent, and by the optical path in the sample, indicated with d , given in centimetres. In this way, the Lambert-Beer law can be defined as: $A = \epsilon c d$. This law is valid for samples, whose absorbance does not overcome one unit of absorbance and for incident light in UV-Vis-IR regions, which covers frequencies compatible to the electronic transitions of the molecules.

The absorption peaks of polyynes synthesized in this thesis fall in the UV range and are characterized by three main peaks at high intensity, in which the one at higher wavelength is the most intense one, and by secondary peaks at longer wavelengths with medium intensity, which are visible if the polyynes are enough concentrated [173]. In addition, from the UV-Vis spectrum, it is possible to understand how long the chains are. Polyynes, which are poly-conjugated systems, are

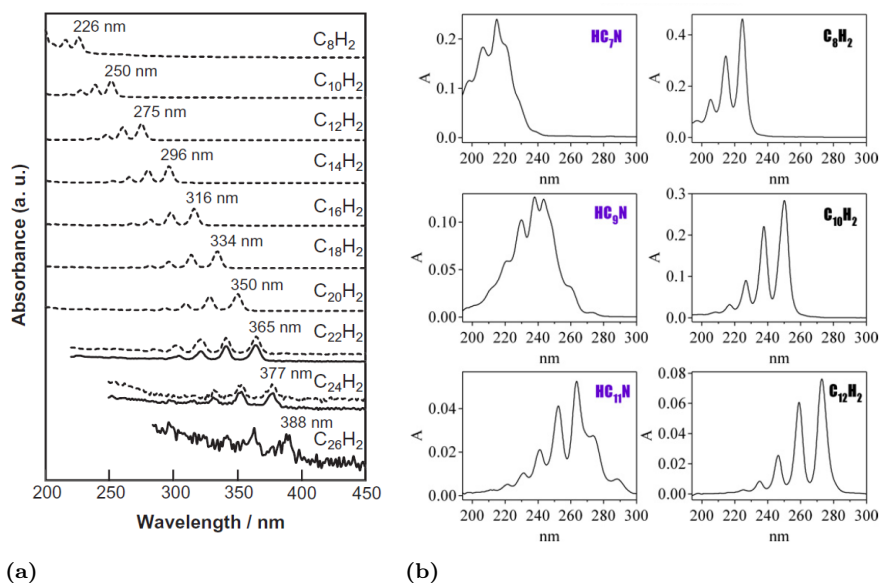


Figure 2.17: (a) UV-Vis spectra of hydrogen-capped polyynes at different length by PLAL in decalin [143], (b) UV-Vis spectra of cyanopolyynes (left) and hydrogen-capped polyynes (right) [145].

defined by a different conjugation in basis of the length, which induces a different HOMO-LUMO gap. Specifically, longer polyynes show higher conjugation with respect to the shorter ones, shifting the absorption peaks to higher wavelength, as clearly visible in Fig.2.17a. Indeed, longer polyynes have a higher number of 2p orbitals with electrons that can contribute to the π orbital [40].

The conjugation can change not only modifying the length but also the termination. Thus, by UV-Vis spectroscopy, it is possible to distinguish polyynes with different terminations thanks to the shifts and a different shape of the absorption peaks, as reported in Fig.2.17b, where cyanopolyynes spectra are compared to hydrogen-capped polyynes.

3

Thesis goals and methods

This chapter illustrates the specific goals of this research work and presents the materials, solvents and apparatus employed for the synthesis and characterization of isolated carbon-atom wires (CAWs) and CAWs-based nanocomposites. The objectives of the thesis are showed in Section 3.1. The materials employed during the experimental activity (e.g. electrodes, targets and solvents) are depicted in Section 3.2. Moreover, the synthesis methods, i.e. submerged arc discharge in liquid (SADL) and pulsed laser ablation in liquid (PLAL), are described in Section 3.3. Finally, the characterization instruments as Raman spectrometers, high-performance liquid chromatograph, UV-Vis spectrometer and scanning electron microscope are detailed in Section 3.4.

3.1 Specific goals of the thesis

This work aims to the fabrication and characterization of carbon-atom wires and wires-based nanocomposites with an application-oriented approach, by creating new functional materials that can be suitable for technological applications in the field of energy conversion devices (e.g. photovoltaics, water splitting, fuel cells). This research consists of an experimental activity, mostly conducted at Micro and Nanostructured Materials Laboratory (NanoLab) of Politecnico di Milano. It falls within an European Research Council (ERC) project, called

EspLORE (Grant N°724610) [174]. To fulfil the general aim, the main tasks pursued during my Ph.D. activity are listed in the following:

- a. design and installation of pulsed laser ablation in liquid (PLAL) technique, set-up of submerged arc discharge in liquid (SADL) apparatus and definition of methods for correct and safe sample analysis by high-performance liquid chromatography (HPLC);
- b. optimization of the synthesis process parameters and development of post-synthesis concentrations methods;
- c. synthesis and investigation of vibrational, optical and stability properties of polyynes with different length and end-groups;
- d. preparation and characterization of polyynes-based nanocomposites in view of creating new functional materials for future applications.

Since this research was a new activity for the laboratory, most of the instrumentation for the synthesis and characterization of carbon-atom wires needed to be arranged or developed from scratch. So, the task a. of the work is addressed to this. With the intention of fabricating polyynes-based materials feasible for many purposes, it is important to synthesize polyynes by techniques that are cost-effective and scalable for mass production, as SADL and PLAL, which were first exploited for this aim by Cataldo [110] and Tsuji [111], respectively. In particular, it is necessary to arrange SADL apparatus (see Section 3.3.1) and to design from scratch the PLAL set-up (see Section 5.1), considering the possibility of changing the direction, wavelength and the power of the laser beam so that the technique is enough versatile to fulfil the requirements of different experiments. Regarding the characterization procedures, it is necessary to define adequate high-performance liquid chromatography (HPLC) methods for separating polyynes in basis of the length and termination considering the theory mentioned in Section 2.2.2.

Task b. aims to achieve the highest possible concentration of sp-carbon chains by SADL and PLAL in a way that the characterization of size- and terminations- selected polyynes is improved. It is based on a two-fold action: the optimization of the synthesis parameters to reach

the highest possible yield and the application of post-synthesis concentration procedures. Thus, on one hand, a study of the correlation between the process parameters and the yield of polyynes is needed and, from the other, standard concentration post-synthesis methods, e.g. solid phase extraction (SPE) columns (Section 5.2.2), can be used. Moreover, a novel procedure entirely based on HPLC needs to be developed to automatize the concentration, separation and collection process of size-selected polyynes in water, see Section 4.1.1.

Task c. is carried out by employing SADL and PLAL in water and in organic solvents to study the effect of the liquid environment on the length, terminations, yield and stability of polyynes. Given the flammability problems of the arc discharge generated in low-boiling liquids at room temperature, only mixed solutions of different percentage of organic solvents and water can be exploited with SADL. Subsequently, the effect of different pure organic liquid environments on the yield, size, termination and stability of polyynes can be studied only employing PLAL. To analyse vibrational, optical and stability properties of CAWs, UV-Vis and surface-enhanced Raman spectroscopy (SERS) measurements are adopted. Thanks to high-performance liquid chromatography (HPLC), it is also possible to separate and, thus, characterize polyynes in basis of the length and termination, and to follow the evolution in time of each species. To better interpret the experimental data, the work takes also advantage from theoretical simulations of UV-Vis and Raman spectra by employing time-dependent density functional theory (TDDFT). All the corresponding outcomes concerning experiments by SADL in water are presented in Section 4.1 while those regarding mixed solutions of water and organic solvents are discussed in Section 4.3. The results relative to polyynes by PLAL are in Section 5.3 and in Ref. [175]. The two parallel activities were conducted working in collaboration with students, dealing with their Master thesis [176–178].

Task d. concerns the study of polyynes-based nanocomposites, which results the logical follow-up of the work done on polyynes at single wire level. The activity is driven by the need to stabilize sp-carbon

chains and to create new functional materials by a suitable method, which preserves the integrity of CAWs. Among all the possibilities discussed in literature, the stabilization of sp-carbon chains based on the encapsulation in solid polymeric matrices seems to be the most appealing one, also for obtaining new advanced nanocomposites, as explained in Section 1.4.2 specifically referring to Ref. [95, 96]. Those works involved the synthesis of polyynes in toxic solvents and a heating process to dissolve poly(vinyl alcohol) (PVA) pellets added to a solution of polyynes and metal nanoparticles, the latter are necessary for SERS studies. Hence, a novel methodology should be developed to overcome all the constraints related to the CAWs-based nanocomposites preparation and to understand the final degree of blending between polyynes, metal nanoparticles and polymer once the nanocomposite is formed. These new free-standing films are characterized by SERS measurements and scanning electron microscopy (SEM), which gives information on the morphology. The results concerning polyynes/PVA nanocomposites are shown from Section 6.1 to Section 6.4 and in Ref. [179]. Moreover, nanocomposites based on poly(methyl methacrylate)(PMMA) can be prepared to extend the study to other possible polymers which have never been employed in literature as matrices to encapsulate polyynes. This last activity was performed in collaboration with a student who wrote his Master thesis on this topic [180] and all the results are discussed in Section 6.5.

As previously mentioned, this Ph.D. thesis was totally conducted at Nanolab of Politecnico di Milano except for some *in situ* Raman measurements, which were performed in Chemical, Materials and Chemical Engineering Department "Giulio Natta". Since the first three tasks are considered for both the synthesis techniques employed in this study, i.e. submerged arc discharge in liquid (SADL) and pulsed laser ablation in liquid (PLAL), the whole results can be divided in the following three chapters: carbon-atom wires by submerged arc discharge in liquid (Chapter 4), carbon-atom wires by pulsed laser ablation in liquid (Chapter 5) and wires-based nanocomposites (Chapter 6). Materials and methods involved in this work are instead showed in next sections.

3.2 Materials

All the materials used in this thesis as target, electrodes and liquid environments are herein described.

3.2.1 Electrodes and Targets

Carbon-atom wires (CAWs) and Ag nanoparticles, exploited for surface-enhanced Raman spectroscopy (SERS), were physically synthesized by employing electrodes and targets made of graphite and silver with a purity of 99.99% (Testbourne Ltd), respectively. Electrodes for submerged arc discharge in liquid (SADL) were 200 mm long and 5 mm in diameter whereas targets for pulsed laser ablation in liquid (PLAL) were 2 mm thick and 8 mm in diameter. Those dimensions were chosen to properly fit with the whole set-up of the technique.

3.2.2 Solvents and colloidal solutions

Solvents

Different liquid media were used for arc discharge and laser ablation during this work, specifically: water (H₂O), acetonitrile (ACN), ethanol (EtOH), isopropanol (IPA), methanol (MeOH) and polymeric solutions of poly(vinyl alcohol) (PVA) in water and poly(methyl methacrylate) (PMMA) in acetone. Organic solvents, purchased by Sigma Aldrich, were characterized by a purity of $\geq 99\%$, ensuring the so-called HPLC grade, suitable for a correct liquid chromatography and for avoiding interference with solvent impurities during the polyynes growth. A summary of solvent properties relevant for the discussion of results is reported in Table 3.1.

Deionised water Milli-Q (0.055 μS) was employed for both techniques since it is cheap, easy to handle, non-toxic and non-flammable. Water can be used as a reference solvent for comparison with the results reached with the other liquids and is appealing for future mass production. Organic solvents, having flammability issues, were mixed in the case of arc discharge with at least 50% of water whereas pure ones were employed in the laser ablation with the foresight of employing an

external container of water for the cooling down during the synthesis. A criterion of solvent selection concerns the possibility to terminate the chains with endcaps different from hydrogen atoms as methyl or cyano groups. Moreover, the liquids need to be compatible with the peek tubing of the HPLC system and the mobile phase employed for the analysis.

Polymeric solutions of PVA were prepared dissolving polymer granules (Fluka, MW \sim 130 000, degree of polymerization $N \sim$ 2700) in water at 373.1 K with a magnetic stirrer, so achieving different concentrations, e.g. 0.03, 0.5, 1, 3, 10 wt.% of PVA in water. Polymeric solutions of PMMA were instead obtained dissolving PMMA pellets (Sigma Aldrich, MW \sim 350 000) in acetone at 333.1 K with a magnetic stirrer, reaching a solution of 2 wt.% of PMMA in acetone. Polymers were considered not only to obtain a higher concentration of CAWs but also to stabilize the sp-carbon chains during and right after the synthesis. In addition, the steps for the formation of a nanocomposite can be reduced.

Table 3.1: *Properties of the solvents selected for the experimental work [181].*

Solvent	Density (g/cm ³)	Boiling point (°C)	Refractive index	Polarity	Ostwald coefficient
Acetone	0.790	56	1.357	35.5	-
ACN	0.782	81.6	1.342	46	0.00083
EtOH	0.789	78	1.359	65.4	0.2417
IPA	0.786	82	1.375	54.6	0.2463
MeOH	0.792	64	1.326	76.2	0.2476
H ₂ O	1	100	1.333	100	0.031

Colloidal solutions

Silver colloids mixed to CAWs for SERS measurements were chemically synthesized following the Lee-Meisel procedure based on the chemical reduction of silver nitrate (AgNO₃) by means of sodium citrate Na₃C₆H₅O₇, which acts both as reducing agent and surfactant to prevent the coalescence of nanoparticles [182].

3.3 Synthesis methods

The apparatus of the two physical synthesis methods involved in this work are presented in the following part.

3.3.1 Submerged arc discharge in liquid apparatus

Submerged arc discharge in liquid (SADL) was the first method employed during this Ph.D. for the synthesis of polyynes. The technique was arranged following the set-up described in Ref. [110]. It consists of two electrodes placed in "V" geometry inserted in a three-necked flask of Pyrex glass, which is fixed by two pincers to a tripod support and has a maximum capacity of 500 ml. At one extremity, the electrodes are immersed in a solvent and, at the other, they are connected by two folding cables to the power supply (Electro-Automatik EA-PSI 9080-60 T). Two holed rubber stoppers surround the cables linked to the electrodes. The reactor presents a double wall, designed for the flowing of tap water between the two walls to cool down solvents during the arc discharge. There is a twist-off cap at the bottom of the flask to collect the solution after the synthesis once it is cooled. SADL experiments involved the use of direct current (DC) ranging from 5 A to 20 A and an applied maximum voltage of 25 V. It was necessary to consider that the cables connected to the electrodes support a maximum current of 50 A, while the maximum possible output voltage, current and power of the power supply is 80 V, 60 A and 1500 W, respectively. Volume at least of 75 ml was used to ensure a continuous and complete submersion of the electric arc during the whole synthesis, while a maximum volume of 100 ml was employed not to excessively dilute polyynes. Temperature during the synthesis was monitored by means of a thermocouple. SADL apparatus, shown in Fig.3.1, was positioned under a chemical hood to remove toxic gases that may be produced during the process by plasma-liquid interactions.

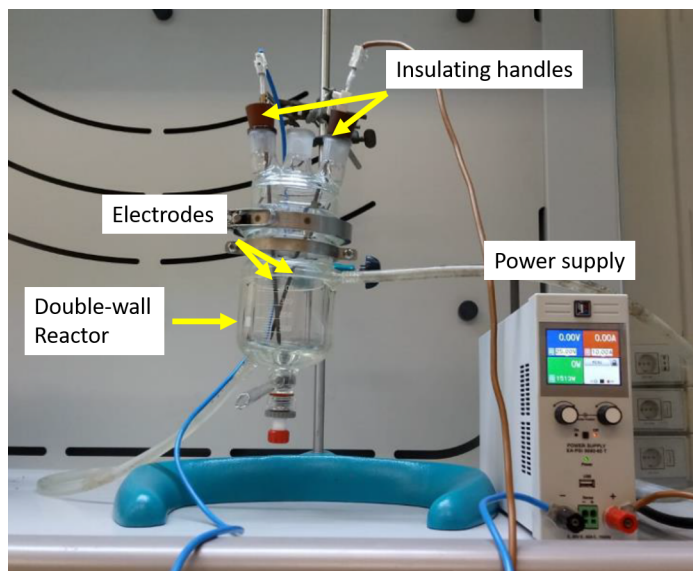


Figure 3.1: *Submerged arc discharge in liquid (SADL) apparatus.*

3.3.2 Pulsed laser ablation in liquid apparatus

Pulsed laser ablation in liquid (PLAL) apparatus was developed from scratch during the first year of Ph.D., designing and arranging all the components of the technique: laser support, optics and sample holder. For this reason, since it was a non-negligible part of the experimental work, the description of the apparatus and all the considered requirements are reported in Section 5.1 of the results chapter related to polyynes synthesized by PLAL. So, only the characteristics of the laser, which do not involve a personal contribute, are reported in this Section.

A compact Quantel Q-switched nanosecond Nd:YAG laser was employed for the polyynes synthesis. It has a repetition rate of 10 Hz and a maximum energy of 850 mJ at the fundamental harmonic of 1064 nm. It is also equipped with two single, compact and thermally regulated harmonics generator modules which include nonlinear crystals to ensure maximum conversion efficiency and stability. In addition, a removable component with a set of dichroic mirrors for wavelengths separation and a beam dump is connected to each module. The dou-

blers can be easily mounted to the laser head one after the other, as sketched in Fig. 3.2. In this way, it is possible to obtain the wavelength of 532 nm (the only one used in this work) at the highest energy of 430 mJ and that of 355 nm at 230 mJ. The pulse duration is of 5 ns at 1064 nm while for the other two wavelengths is of 6 ns. In this work, a beam attenuator module inserted between the laser head and the first mounted module for the 532 nm was used to gradually change the output laser energy, ranging from approximately zero to a maximum of 380 mJ.

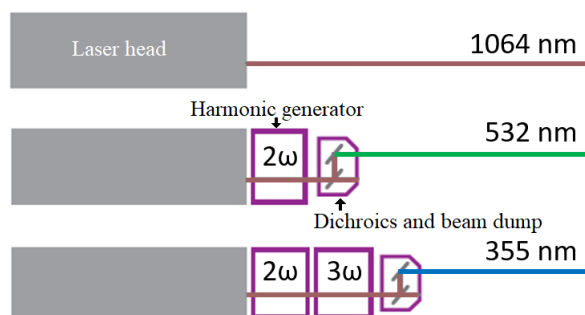


Figure 3.2: Sketch of the compact Nd:YAG laser head with the two modules for doubling and tripling the frequency.

3.4 Characterization methods

Polyynes-based solutions and nanocomposites of this work mainly underwent structural and optical characterizations. Morphology measurements were also carried out for samples with silver nanoparticles. All the information on the characterization instruments employed in this work are reported in the following paragraphs.

3.4.1 Raman spectrometers

As already discussed in Section 2.2.1, Raman spectroscopy is an important technique to characterize carbon-atom wires. The experimental apparatus of Raman spectrometers for *ex situ* and *in situ* structural

analysis are herein presented.

Ex situ analyses

All the ex-situ Raman measurements were performed by Renishaw InVia micro Raman spectrometers. One is composed of Ar⁺ laser with the possibility to choose two exciting radiations, the line at 514.5 nm (green) with the maximum power on sample of 10 mW and the one at 457 nm (blue) with the maximum power of 2 mW. Spectra were acquired by a 1800 greeds/mm grating with the green line. A super-notch filter (cut-off at 100 cm⁻¹) and a Peltier-cooled CCD camera allow a spectral resolution of about 3 cm⁻¹. The other Raman apparatus is provided by two diode-pumped solid-state lasers, one characterized by a λ equal to 532 nm and a maximum power of 70 mW and the other one has a λ equal to 660 nm and a maximum output power of 75 mW. It is also equipped with two fibre optic probes to execute long distance remote analyses and to automatically switch between laser and microscope, and an automatic x-y-z translator of micrometric resolution. Spectra were acquired by 1800 greeds/mm with the excitation line at 532 nm. All the laser powers set in these experiments did not cause any laser-induced degradation to the sample.

In situ analyses

In-situ analysis of polyynes-Ag nanoparticles solution by SADL was performed at the Department of Chemistry, Materials and Chemical Engineering "Giulio Natta" of Politecnico di Milano by a LabRam HR800 spectrometer, equipped with Olympus BX41 microscope. A diode laser with the excitement line at 785 nm was used for the experiment. The optical probe with conical tip is a silica core-silica cladding optical fibre. The silica inner core is of 200 μ n and a numerical aperture of 0.22. To produce the probe tip of the optical fibre, the first step was to remove the protective layer and immersed the probe tip of the fibre in a hydrofluoric acid (HF) solution covered by a layer of immiscible toluene. During the etching process, the evolution of the meniscus formed by the fibre crossing the HF solution/toluene interface drives the formation of a conical tip [183].

In-situ analyses of polyynes-Ag nanoparticles solutions by PLAL were performed directly in Nanolab by the second Raman spectrometer described in the previous paragraph. The excitation radiation of 532 nm was sent to the sample and an immersion optic with 10 mm of focal depth, mounted on the laser probe, was used to adequately approach the container with polyynes solution, as shown in Fig. 3.3.

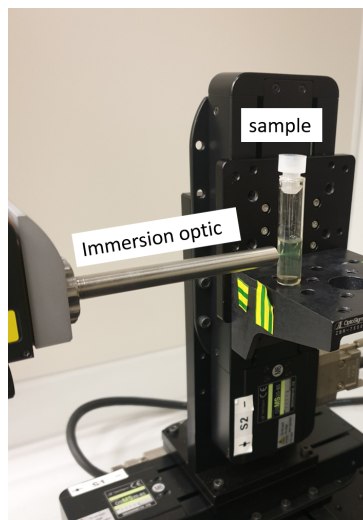


Figure 3.3: *The immersion optic connected to the laser probe approaching the sample.*

3.4.2 High-performance liquid chromatograph and UV-Vis spectrometer

Polyynes solutions were separated in basis of the length and termination by a Shimadzu high-performance liquid chromatography (HPLC) apparatus (see Fig.3.4). It is equipped with SIL-20A autosampler for the automatic injection of the sample in the system, a CTO-20A column oven to maintain constant the temperature during the analysis (in our case set at 313.1 K), two LC-20AT pumps, a SPD-M20 photodiode array UV-Vis spectrometer as a diode array detector (DAD), and a FRC-10A fraction collector to collect size- or terminations-selected polyynes. Two stationary phases, i.e. columns, were involved for polyynes solutions analyses: a Shimadzu Shim-pack GIST C8 column (250 mm of length (L) x 4.6 mm of internal diameter (I.D.)) made by

silica particles ($5\ \mu\text{m}$ size) linked to alkyl ligand chains of 8 carbon atoms and a Phenomenex Luna C18 column (150 mm L. x 4.6 mm I.D.) with silica particles of $5\ \mu\text{m}$ size connected to alkyl chains of 18 carbon atoms.

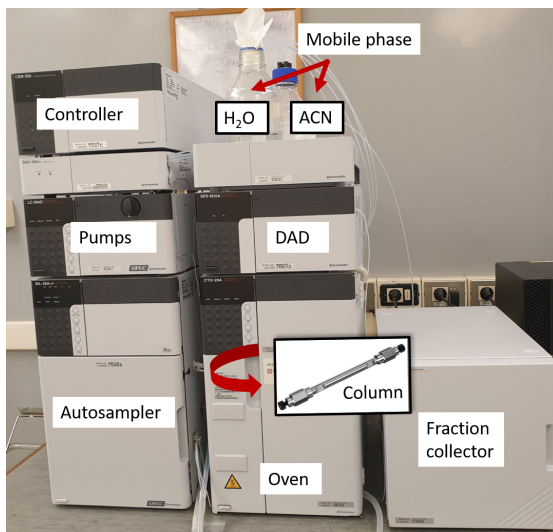


Figure 3.4: *High-Performance Liquid Chromatography apparatus (HPLC).*

The mobile phase, employed in the whole work, was composed of water and acetonitrile. HPLC methods were defined in two ways: the isocratic mode, where the composition of the mobile phase is kept constant during the whole HPLC analysis, and the gradient mode, where the composition of mobile phase changes in a way that acetonitrile increases with time while the water decreases. The flow rate of mobile phase was set from 0.5 to $1\ \text{mL min}^{-1}$ and the sample injection volume was selected from 1 to $100\ \mu\text{L}$. The total time necessary to complete the analyses ranged from 10 minutes up to 1 hour. It is important to note that because of the working principle of HPLC apparatus, the collected species were always diluted with the mobile phase. Apart from UV-Vis spectrometer coupled to HPLC (DAD), a stand-alone Shimadzu UV-1800 spectrophotometer was exploited to estimate the concentration of the species and for quick analyses, since it could take just few minutes to give a spectrum. Both the UV-Vis spectrometers are provided by a tungsten and a deuterium lamps, which test the ab-

sorption of the sample in 190-800 nm range, in the case of DAD, and in 190-1100 nm range, for the stand-alone apparatus.

Spectra from stand-alone spectrometer were generally acquired in the UV region, i.e. from 190 to 350-400 nm, where polyynes here synthesized absorb. The solutions were measured in a quartz cuvette with an optical path of 10 mm. Quartz is the right material for cuvettes when samples absorb in the UV region, in contrast to glass, which absorbs in the range of polyynes thus covering their signals. Another factor that can hinder the polyynes UV-Vis spectrum is the solvent cut-off, i.e. the wavelength below which the solvent itself absorbs the total light. Most of the organic solvents employed in the thesis have a cut-off between 200 nm and 210 nm except for acetone, PVA and PMMA solutions, which are not transparent in the polyynes region.

3.4.3 Scanning electron microscopy

The morphology of silver nanoparticles produced by SADL and PLAL and of samples with silver nanoparticles were investigated by scanning electron microscope (SEM). However, the resolution of this instrument is not enough high to observe polyynes. The instrument details of SEM employed in this thesis are reported.

Instrument

High resolution Field Emission-SEM Zeiss Supra 40 was the scanning electron microscope model exploited in this work. It is based on Gemini column, equipped with Everhart-Thornley secondary electrons detector, high-efficiency In-Lens and back-scattered electron detectors, and Oxford EDXS spectrometer. The accelerating voltage ranges from 1 kV up to 30 kV (1-20 kV in this work). The sample holder is connected to five different motors (x, y, z, rotation and tilt). SEM images shown in the following chapters were obtained by In-lens and Everhart-Thornley secondary electrons detectors. The former gives high contrast images while the second gives topographic information.

4

Carbon-atom wires by submerged arc discharge in liquid

This chapter concerns the synthesis and characterization of CAWs by submerged arc discharge in liquid (SADL). The main part of this chapter is dedicated to the results regarding the use of water as a solvent for SADL, because it is cheap and environmental-friendly and so appealing for mass production. The results related to the formation of hydrogen-capped polyynes ($\text{H-C}_n\text{-H}$), that, for simplicity, will be indicated by C_n , are presented in Section 4.1. Then, SERS *in situ* measurements were set up to study the evolution of polyynes during the discharge and the results are reported in Section 4.2. Organic solvents were also mixed to water in order to increase the concentration of polyynes during the synthesis process. The corresponding achievements are illustrated in Section 4.3. Finally, a summary of the main remarks obtained with these experiments is provided in Section 4.4. My personal contribution consisted in the whole experimental activity here presented. Specifically, some measurements of Section 4.1.1, 4.1.4, 4.2 and 4.3 were performed in collaboration with two Master students [176,177]. The original results presented in Section 4.1 led to a publication that I first-authored [184].

4.1 Polyynes synthesized in water

Distilled water was first selected just as a solvent to test SADL since it is low-cost and non-toxic. However, these properties are appealing for future mass production by SADL, as mentioned in Section 3.1, so many efforts were made in order to optimize the formation of polyynes in water. Moreover, there was the need to extend the knowledge on the synthesis of CAWs by arc discharge in water since only a first attempt was present in literature [121]. After the discharge between two electrodes of graphite, solutions with visible carbon particulate were obtained, as the one reported in Fig.4.1. So, the solutions after SADL need to be filtered before any characterization measurement to facilitate the detection of polyynes. After this step, a clear solution without precipitated species at the bottom of the vial was noticed.

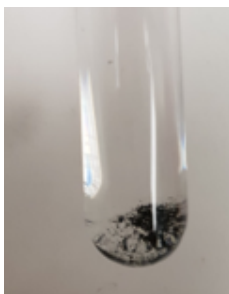


Figure 4.1: *Water after 15 minutes of arc discharge between two electrodes of graphite.*

4.1.1 Optimization of process parameters

To better investigate polyynes properties and to make functional materials suitable for many applications, there is the need to reach the highest yield of polyynes. So, the first task was to find the best condition at which operate the arc discharge. Different experiments were performed changing the process parameters once at time. UV-Vis spectroscopy was employed to extrapolate, from the polyynes UV absorptions, the maximum concentration reached in all the cases. In particular, the intensity of UV-Vis peaks was estimated by the peak-valley difference in absorbance, the considered valley is the one which precedes the peak.

Looking at Fig.4.2, it is possible to see UV-Vis spectra of samples prepared at different currents, depths under the water level at which the electrodes form the arc discharge and time. The peaks at 199, 206, 215, 225 nm can be found in all the pictures, indicating the synthesis of hydrogen-capped polyynes long 6 atoms of carbon (C_6), which refers to the peak at 199 nm, and 8 atoms (C_8), which relates to the other three peaks marked in Fig.4.2a. Longer polyynes are barely detectable in all the cases because of their low concentration.

The effect of increasing the current was observed in Fig.4.2a. The considered maximum currents were the following: 10 A, 15 A and 20 A. The output voltage of the power supply was set at 25 V while the arcing time and the depth at which electrodes form the arc under water were fixed at 10 minutes and 3 cm, respectively. It was noticed that increasing the current, the intensity of polyynes absorption peaks is lower. In the case of 10 A, the peak-valley difference at 199 nm is 24% and 87% higher than that at 15 A and 20 A, respectively. In addition, the peak-valley difference at 225 nm is larger of about 32% and 78% than that of 15 A and 20 A, respectively. During the arc discharge, the formation and the degradation of polyynes, which is due to cross-linking reactions and photodegradation, are two coexisting phenomena. Thus, to optimize the synthesis yield, it is needed to find the condition at which the formation is predominant. At 15 A and 20 A with the same voltage of 25 V, the reached power may be so high that induces a temperature increase, which affects the integrity of polyynes more than the case at 10 A.

Then, the depth at which the electrodes form the arc discharge under the solvent surface was changed, the case at 3 cm and at 2 cm of depth are reported in Fig.4.2b. It is noticed that higher depth corresponds to larger absorption. A reason of this behaviour may be related to the fact that plasma at 2 cm under the liquid level is not well confined by the liquid, causing an instability and a consequent increase of bubbles. Moreover, a plasma region very close to the liquid superficial level can limit the diffusion of polyynes, constraining them to remain where they are more affected by UV radiation and heat. In this SADL apparatus described in Section 3.3.1, 3 cm of depth can be

obtained filling the flask with 100 ml of water.

In Fig.4.2c, it can be seen a non trivial behaviour of polyynes concentration as a function of arcing times, i.e. 10, 20 and 40 minutes. It was reported in literature that up to 150s, a continuous increment of polyynes signal was registered [79]. Extending the time to tens of minutes, it was observed that there is a signal growth up to 10 minutes, then a decrease until 20 minutes, and finally a further rise till 40 minutes. This phenomenon is clearly evinced from the inset of Fig.4.2c, where the valleys of the peaks at 199 nm were matched. A possible explanation is related to the prevalence of the detrimental effect of the discharge between 10 and 20 minutes over the polyynes formation. However, exceeding 20 minutes, the concentration of polyynes compensates the degradation processes and results higher than after the initial 10 minutes. It was also analysed the solution after 20 minutes of total arcing, subject to a break of 5 minutes after the first 10 minutes of synthesis. During the break, the solution cools down from 320.1 K to 296.1 K, so polyynes can be more preserved and can also diffuse in water far away from the discharge point. This is showed by the higher intensity of the spectrum indicated with “10 + 10” in Fig.4.2c with respect to the one at 20 minutes without break.

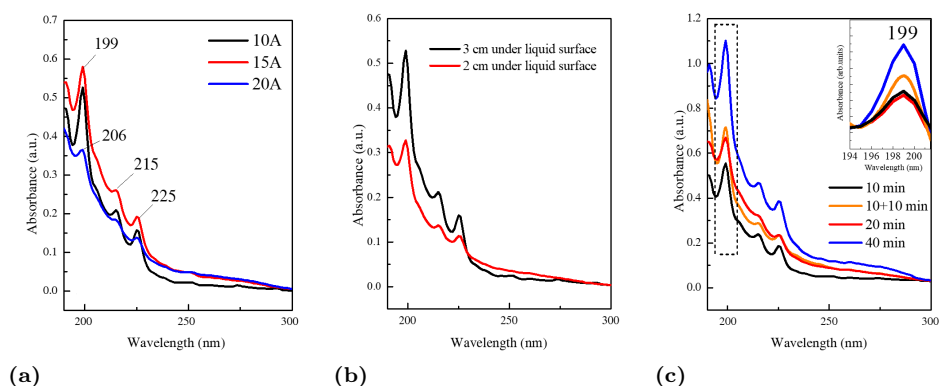


Figure 4.2: UV-Vis spectra of polyynes solutions by arc discharge in water: (a) changing the current, (b) changing the depth at which the discharge is generated and (c) changing the time of discharge.

All these remarks ended in the selection of the optimal process parameters for arc discharge in water as: 10 A, 25 V in 100 ml. Since the concentration of polyynes does not increase linearly with time, arcing 40 minutes gave not enough polyynes to overcome the time consuming aspect. So, the arcing time was fixed at 10 min.

Four tests were carried out at the optimal process parameters just stated to evaluate how the number and duration of breaks can affect the polyynes yield. UV-Vis spectra of the solutions resulting from these experiments are represented in Fig.4.3. Two tests were performed with four breaks: in one case, with the break duration of 2 minutes and, in the other one, of 5 minutes. The other two tests were done with only one break: in one experiment, 2 minutes long and, in the other one, 5 minutes long. In all the cases, the total arcing time was set at 10 minutes. The temperature of the solution measured by a thermocouple kept close to the wall of the flask was checked: before starting arcing, after each arcing step and after each break. All the collected temperature data are reported in Table 4.1. Looking at the peak-valley difference at 199 nm, it can be deduced that the condition at which the surrounded water is maintained at the lowest temperature allows the formation of more polyynes. Then, the duration of break is more effective than the number of breaks carried out in terms of polyynes yield. Moreover, it should be noted from temperature values given in Table 4.1, that the tap water, flowing between the two walls of the reactor and necessary to cool down the solvent during the arcing, is evidently really important but not enough to keep the solution at room temperature. A possible drawback of employing breaks refers to the higher time-consumption and to the incremented air exposure, which could enhance the oxidation of the chains.

As already said, it is a matter of finding the best balance among the formation and the diffusion of polyynes far from the plasma region, and their decomposition.

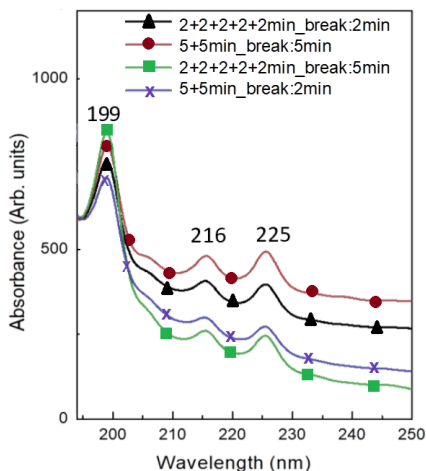


Figure 4.3: UV-Vis spectra of the solutions after arc discharge in water carrying out breaks of 2 or 5 minutes every 2 or 5 minutes of arcing.

t Arcing time	T ₀ Before arcing	T After arcing	T ₀ After break	
			Break time 2min	Break time 5min
10min	295.1 K	320.1 K		296.1 K
5 min		314.1 K	305.1 K	297.6 K
2 min		306.1 K	302.1 K	296.1 K

Table 4.1: Temperature measured by a thermocouple, before and after arc discharge at different arcing and break times.

4.1.2 Novel procedure to concentrate and separate polyynes

It was observed that, even optimizing the experimental synthesis parameters, the only two types of polyynes clearly detectable at UV-Vis spectrometer were C₆ and C₈. The solutions were also analysed by HPLC to identify all the components present in the liquid samples, even those that in the UV-Vis spectra of a mixture are covered by the background signal due to hydrocarbons impurities. Indeed, it was possible by HPLC to even observe the peak of C₁₀. Each polyyne in the sample can be revealed by extrapolating the chromatogram at the wavelength at which that specific chain has its highest absorption peak, as shown in Fig.4.4. Moreover, from the chromatogram, it is

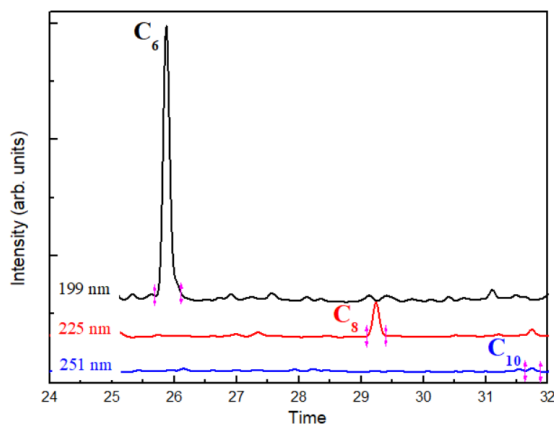


Figure 4.4: Chromatogram extracted at 199, 225 and 251 nm to visualize the peak of C_6 , C_8 and C_{10} , respectively.

also possible to deduce the relative fraction of polyynes in a solution, thanks to the ratio between the chromatographic areas of each peak. Specifically, it results that C_6 has a relative molar ratio of 93.2%, C_8 of 6.4% while C_{10} of 0.4%. The order of magnitude of the concentration of C_8 has an estimated value of 10^{-7} M, considering the Lambert-Beer law and the molar extinction coefficient related to the peak at 225 nm, which is found in literature [12, 173]. As a consequence, the molarity of C_6 and C_{10} is 10^{-6} M and 10^{-8} M, respectively, which were derived from the relative fractions obtained from HPLC analysis.

To see longer polyynes and improve the concentration of all the CAWs synthesized in water, it was necessary to adopt a concentration method after synthesis. In particular, it was developed a procedure entirely based on HPLC, which automatizes not only the concentration process but also the separation and the collection steps. The batch-loading on-column concentration, aka on-column focusing, was performed involving a C8 column (column properties are presented in Section 3.4.2) and adapted to aqueous solutions of polyynes. First, eight vials with at least 1 ml of polyynes solutions were inserted in the HPLC autosampler. Second, 10 consecutive injections of $100\mu\text{l}$ from each vial were programmed, for a total of 80 ml of solution introduced in the system. In order to effectively accumulate the sp-carbon chains

Chapter 4. Carbon-atom wires by submerged arc discharge in liquid

INSERTION of 8 vials with solutions of polyynes in water



SEPARATION by gradient mode and **COLLECTION** of size-selected polyynes
flow: 1 ml/min
gradient slope: 3%/min

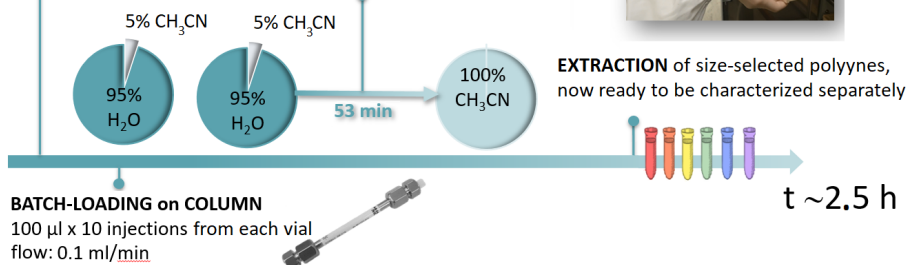


Figure 4.5: Sketch of the HPLC procedure for automatizing the concentration and separation of aqueous polyynes solutions.

on the top of the column without losses, the chromatograph during the injections was held in the ready-to-run conditions at reduced flow rate, i.e. mobile phase of acetonitrile/water 5/95 %v/v and flow rate of 0.1 ml/min. After sample loading, the flow rate was set to the normal value of 1 ml/min and, then, a method to separate and collect polyynes was adopted. It consists of a gradient program with an initial mobile phase of acetonitrile/water 5/95 %v/v for the first 3 minutes, then, a linear gradient from 3 to 33 minutes, which reaches a final mobile phase composed of acetonitrile 100%. This mobile phase was kept for other 20 minutes to remove any possible species still retained on the column, for a total time of 53 minutes. After, size-selected polyynes were extracted from the HPLC fraction collector and were ready to be characterized separately. All the steps of this procedure are summarized in Fig.4.5 and took around 2 hours and a half.

Thanks to this methodology developed for concentrating aqueous solutions, hydrogen-capped polyynes up to C₁₆ were detected. The concentration of polyynes longer than C₁₀ was estimated to be less than 10⁻⁹M. These results proved that it is possible to obtain the same types of polyynes as in the case of arc discharge in organic solvents [121] but avoiding the toxicity issues related to these liquids.

The chromatographic peaks related to the detected hydrogen-capped polyynes are presented in Fig.4.6 before and after concentration, shown at the wavelength at which their absorption peak is higher. Moreover, it was also defined, where possible, the concentration factor of size-selected polyynes (G_{BL}), which is the ratio between the area of the chromatographic peak before and after concentration ($G_{BL} = A_{after_conc}/A_{before_conc}$). The concentration process is more efficient for longer polyynes, as demonstrated from the values of G_{BL} . In the case of C_{10} , G_{BL} is equal to 281, presenting an increment of more than two hundred times than the case of C_6 , for which its value is of 24.3, and the case of C_8 , for which G_{BL} is equal to 60. However, the shorter chains still remain overall much more concentrated.

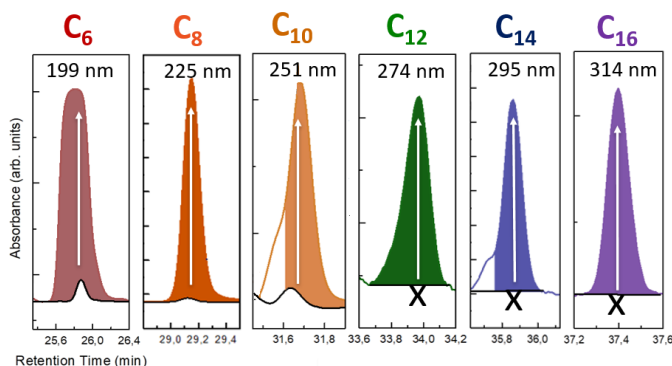


Figure 4.6: Sections of chromatograms relative to each detected hydrogen-capped polyyn, before and after the concentration. Chromatograms are observed at the wavelength at which each size-selected polyyn has his maximum absorption.

After the automatized concentration, separation and collection procedure, the most concentrated size-selected polyynes, i.e. C_6 , C_8 , C_{10} , were characterized separately by HPLC, UV-Vis and SERS spectroscopy. The red regions of the chromatograms in Fig.4.7 show the peak of C_8 before and after (in the inset) the HPLC collection. The latter chromatogram testifies that C_8 is effectively collected and isolated from the initial mixture of polyynes, since it is the only species found during the HPLC analysis.

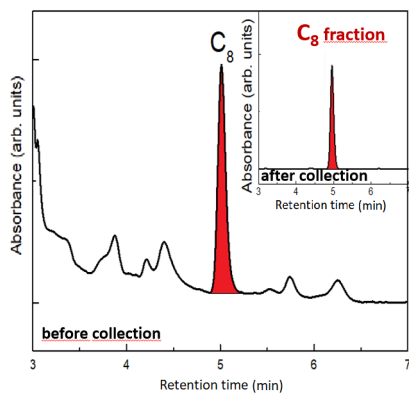


Figure 4.7: Chromatograms observed at 225 nm before and after (in the inset) the collection of C₈.

4.1.3 Size-separated polyynes

UV-Vis spectra of the separated hydrogen-capped polyynes from 6 to 16 atoms of carbon were identified thanks to the DAD coupled to HPLC, and are reported in Fig.4.8. Spectra were normalized for a better view, in fact longer polyynes are present in a concentration of three order of magnitude lower than C₆ or C₈. Absorption bands are connected to the in-phase C≡C/C-C stretching/shrinking mode, which is also related to the most intense Raman mode. As expected from literature (see Sections 1.2.2, 2.2.1 and 2.2.2), increasing the length of sp-carbon chains, the absorption peaks shift to larger wavelengths, corresponding to a polyyne with smaller band gap and a lower frequency of the CC mode. The electronic structure is, in fact, influenced by BLA, which decreases with increasing the length. Moreover, the distance between two consecutive main absorption peaks is not constant but decreases by increasing the chain length until it becomes independent from size effect, e.g. the main absorption peaks of C₆ (at 199 nm) and C₈ (at 225 nm) are distant 26 nm while, in the case of C₁₄ (at 295 nm) and C₁₆ (at 314 nm), the distance is reduced to 19 nm. It was experimentally demonstrated that the minimum length of sp-carbon chain at which optoelectronic properties are independent of the chain length but just affected by the environment is of 230 carbon atoms.

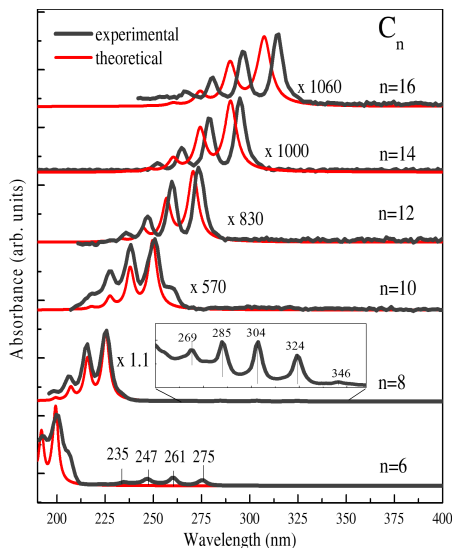


Figure 4.8: Normalized UV-Vis spectra of size-selected hydrogen-capped polyynes from 6 up to 16 atoms of carbon. In black, experimental data, in red, simulated UV-Vis spectra obtained by DFT calculations. The inset shows the magnification of low intensity peaks of C_8 .

Below this length, the spatial resolution of the instrument does not allow any further experimental investigation [185].

Since the cut-off of the UV-Vis spectrometer is at 190 nm, only the intense peak of C_6 at 199 nm is present. Low intensity peaks were also identified in the case of the two most concentrated species, i.e. C_6 and C_8 . These peaks are located at 235, 247, 261, 275 nm in the case of C_6 [79] and correspond to forbidden transitions as discussed in Ref. [149, 186] while, in the case of C_8 , the low intensity peaks are detected at 269, 285, 304, 324, 346 nm. The latter are slightly different with respect to the Ref. [173], due to the different environments where polyynes were synthesized. The experimental data were well described by simulations based on time-dependent density functional theory (TD-DFT), see Appendix, thanks to which vibronic spectra were computed and presented in red line in Fig.4.8. The calculated spectra underwent a rigid shift of 19.5 nm to perfectly match the experimental spectrum of C_8 . This species is indeed the most studied polyynes and its spectrum was reported in different works [53, 111, 170, 187] and,

differently to C_6 , is completely detectable in the experimental range. For these reasons, it can be considered a reliable reference system to determine the shifting factor for the computed spectra. After the application of the scaling value, only little discrepancies remain between experimental and simulated data. These effects can be ascribed to an energy overestimation of the theoretical spectra, due to the fact that the partial multireference feature of the excited polyynes is not considered by TD-DFT.

The origin of the SERS bands of aqueous solutions of polyynes mixture can be assigned thanks to the comparison with SERS spectra of isolated fractions, i.e. C_6 , C_8 and C_{10} . To do this, each sample was mixed to Ag colloids, whose plasmonic peak is centred at 410 nm, as reported in the UV-Vis spectrum of Fig.4.9a. The morphology of silver nanoparticles was studied by scanning electron microscopy (SEM), as reported in the inset of Fig.4.9a. Ag nanoparticles tend to aggregate in presence of polyynes, as shown by the appearance of a right shoulder on the plasmonic peak, which enlarges the absorption region (see Fig.4.9a). In this way, the laser wavelength (i.e. 514.5 nm) employed for Raman characterization can be absorbed allowing the SERS enhancement, as demonstrated in previous papers [92, 168, 170, 188]. In all the cases, the sp^2 band was negligible, so only the sp region between 1800–2200 cm^{-1} is reported in Fig.4.9b. Moreover, two different main bands are evident in all the spectra as also found in other works [90, 168]: one above 2000 cm^{-1} , attributed to the Raman effective conjugation coordinate (ECC) band, and one at lower frequency, whose origin is discussed in Section 2.2.1. The band above 2000 cm^{-1} of polyynes mixture results in a superposition of C_6 and C_8 features, while the one of C_{10} is not corresponding to any noticeable band of the mixture. It must be considered that size-selected polyynes have concentrations and Raman cross sections, which change in basis of the chain length [53]. The Raman cross section of C_{10} , which is higher than one order of magnitude with respect to that of C_8 [53], does not compensate the lower concentration, explaining why in the spectrum of the mixture there is no the band related to C_{10} but just an incremented baseline. Furthermore, the band below 2000 cm^{-1} of polyynes

mixture is the convolution of all the bands of size-selected polyynes, i.e. C_6 , C_8 , C_{10} .

Data here presented seem to confirm the observation of Hanamura and co-workers [170], which noticed a red shift of the positions of sp-carbon SERS signals with the decrease of Ag nanoparticles size. Specifically, SERS features found in this work, which correspond to Ag nanoparticles of 60-80 nm, are centred at positions which are in between the case of silver nanoparticles with a diameter smaller than 20 nm [170] and silver nanoislands of several hundreds of nanometres size [53]. Further studies should be performed to deepen the dependence of SERS bands positions with the size and shape of Ag nanoparticles.

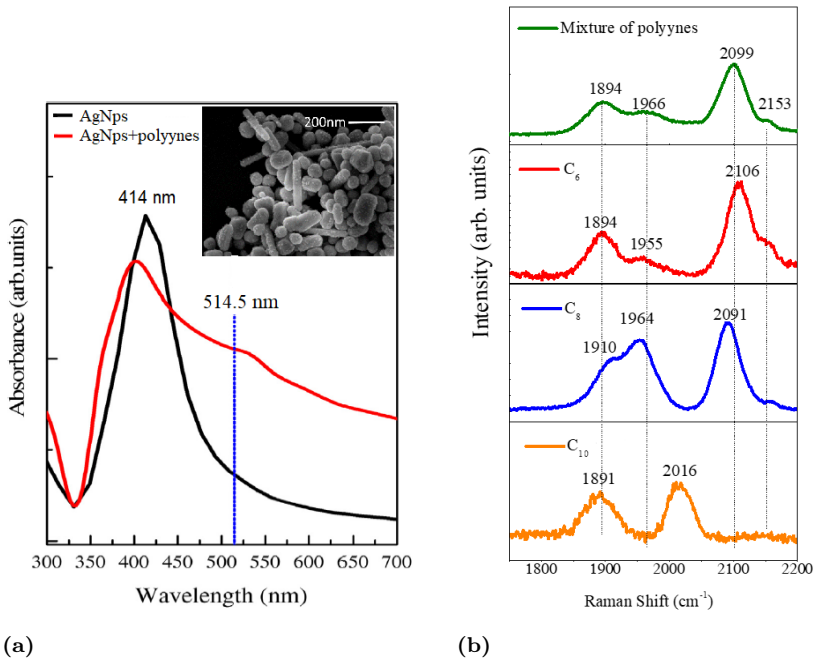


Figure 4.9: (a) Absorption spectra of chemically synthesized Ag colloids (in black) and Ag colloids mixed with solution of polyynes mixture in water (in red). Dotted line (in blue) indicates the wavelength (λ) at 514.5 nm of the Raman laser employed. Inset: SEM image of Ag colloids (detector: InLens, accelerating voltage: 10 kV, magnification: 150000, working distance: 4.4 mm). (b) From the top to the bottom, SERS spectra (excitation line at 514.5 nm) of: polyynes mixtures in water, C_6 , C_8 , C_{10} .

4.1.4 Polyynes stability

The evolution in time of H-capped polyynes was investigated at different experimental conditions to find possible stabilization strategies.

The solutions of polyynes mixture were subjected to different exposures of one hour each, as: solar light, temperature higher than room temperature, i.e. 323.1 K, and air flow. All the solutions were analysed by HPLC, so UV-Vis spectra related to C_8 extracted from DAD are reported in Fig.4.10. As discussed in Section 1.4.1, these agents, in particular the air flow, can boost the oxidation and cross-linking reactions between the chains. This is the reason why all the samples studied in this work were always kept in closed vials.

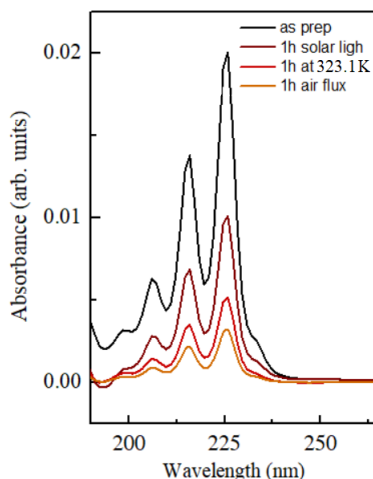


Figure 4.10: UV-Vis spectra of polyynes mixture as prepared and after different exposures of one hour to: solar light, 323.1 K and air flow.

Then to test if the effect of an organic solvent could help in preventing the polyynes decomposition, filtered aqueous solution of polyynes mixture was divided in two parts. One was diluted by 1/5 %v/v of water and the other one by 1/5 %v/v of acetonitrile. These solutions were studied by consecutive UV-Vis spectroscopy measurements, reported in Fig.4.11a and Fig.4.11b, keeping the samples in close test tube between each analysis. After two weeks, the polyynes signal is decreased in both samples but with two different rates: polyynes peaks are better

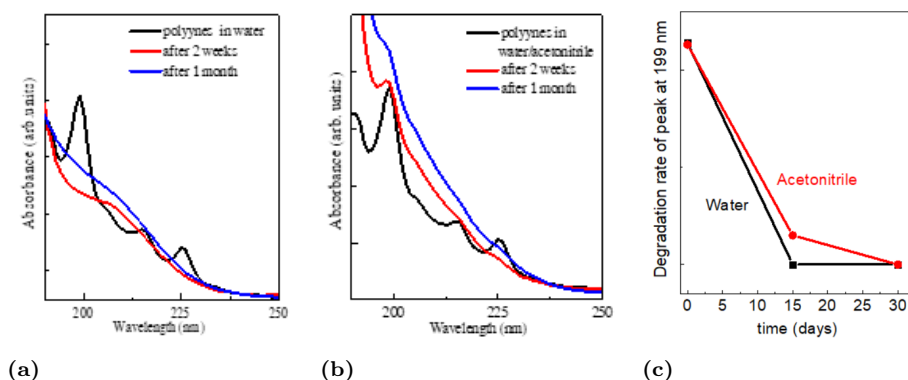


Figure 4.11: (a) UV-Vis spectra of polyynes mixture in time after dilution with 20% in volume of water, (b) UV-Vis spectra of polyynes mixture in time after dilution with 20% in volume of acetonitrile, (c) degradation rate of peak at 199 nm in the two cases.

defined in the case of acetonitrile dilution. After 1 month, some features of polyynes are, in fact, still present only in the sample diluted by acetonitrile. The degradation rate of the peak at 199 nm related to C_6 is represented in Fig.4.11c as a function of time. The fact that acetonitrile has a beneficial effect on polyynes stability was already observed by Cataldo [81]. Indeed, the higher solubility of polyynes in acetonitrile compared to water decreases the polyynes aggregation and the consequent cross-linking reactions. In addition, the lower quantity of oxygen dissolved in acetonitrile with respect to water can slow down the oxidation process of polyynes [189]. However, in the case of polyynes in water solution, no precipitated products were found at the bottom of the vial indicating a possible solvation of CAWs in water if they are low concentrated, as also mentioned in Ref. [137, 158].

The stability study of size-selected polyynes was carried out by periodic HPLC analyses looking at the UV-Vis spectrum of the species. Fig.4.12a shows the UV-Vis spectra of isolated C_8 in water and acetonitrile. This liquid environment comes from the composition of HPLC mobile phase during the collection of the species, which consists of acetonitrile/water 87/23 %v/v. The signal remains almost unchanged

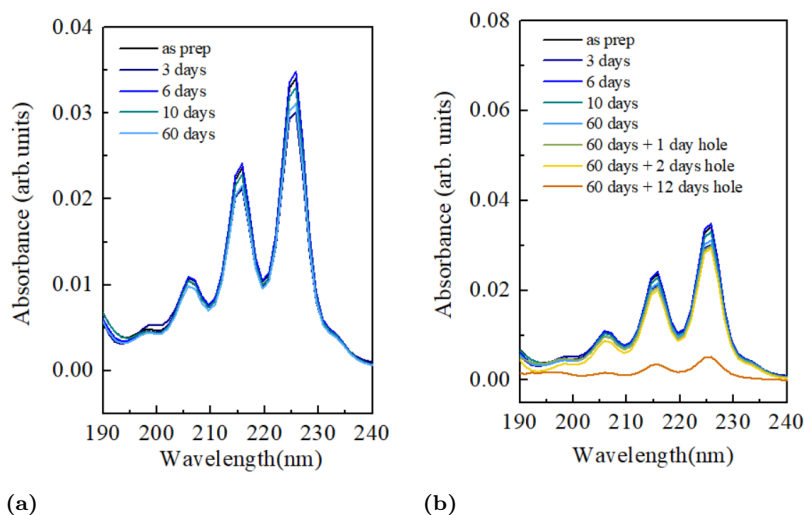


Figure 4.12: UV-Vis spectra of C₈ polyynes at different ageing time: (a) sample kept in closed vial, (b) effect of a hole in the tap of the vial.

for 2 months, probably due to the presence of the high quantity of acetonitrile, which helps in preventing degradation of polyynes compared to water, as just mentioned in the previous paragraph. Another reason, which explains the stability of isolated C₈, can be related to the process of separation itself. Indeed, by selecting the species, the concentration of polyynes is strongly lowered, as well as the probability of interactions and cross-linking reactions [120]. In addition, C₈ was maintained in a closed vial, where the quantity of air is only that entering during tap closure. If UV-Vis spectra of this sample are carried out after undertaking a hole in the cap, it is possible to observe a quick decrease of the signal, which is lowered of about six times in twelve days, see Fig.4.12b.

An improved stability with respect to polyynes mixture in water was also observed in solid Ag nanoparticles and polyynes assemblies deposited on a substrate. SERS spectra were performed on these samples as prepared, after 2 weeks and 1 month and are reported in Fig.4.13. The signals are characterized by the presence of two main bands peaked at 1978 cm⁻¹ and 2110 cm⁻¹ with a shape different from the spectrum

of liquid polyynes mixture reported in Fig4.9b. This behaviour testified that SERS effect strongly depends on the type of interaction between the analyte and SERS enhancers, distinguishing between solid and liquid systems [93, 96, 188]. In a liquid, the species are free to move and polyynes can be more adsorbed on Ag nanoparticles, while, in a solid, the species are immobilized in a way, which depends on the relative quantity of polyynes and silver nanoparticles and on the adopted deposition technique. Here, the sample was obtained by the drop casting of the sample on a silicon substrate at room temperature. The signal of polyynes does not change for one month, in agreement with a previous work [93]. This method allows the stabilization of hydrogen-capped polyynes thanks to a twofold role of Ag nanoparticles in preventing the cross-linking interactions: on one hand, Ag colloids can act as spacers and, on the other, they strongly interact with sp chains stabilizing the electronic configuration, as demonstrated from the Ag nanoparticles aggregation when mixed with polyynes.

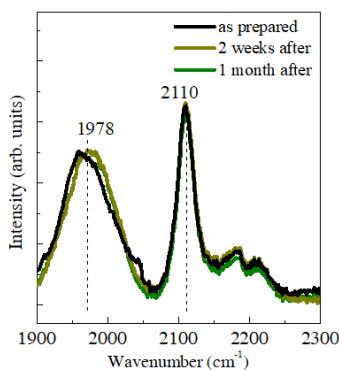


Figure 4.13: SERS spectra (excitation line: 514.5 nm) at different ageing time of polyynes mixture mixed with Ag colloids dried on a substrate.

In this Section, stability studies were performed for polyynes solutions by SADL but the same considerations can be applied to polyynes synthesized by PLAL. Indeed, solutions obtained by the two techniques in the same solvent are different in terms of polyynes and by-products concentration.

4.2 *In situ* SERS during SADL in water

To investigate the formation process of polynes, *in situ* SERS measurements were performed for 40 minutes during the arc discharge in water.

First, a SERS-active solution was prepared by arcing two electrodes of silver in 100 ml of distilled water at 20 V and 5 A for 7 minutes in order to form Ag nanoparticles, whose plasmonic peak is centred at 403 nm (see inset of Fig.4.14a). The process parameters were defined thanks to the experiments performed in collaboration with a student during his Master thesis work [176]. The excitation line of the laser exploited in this study, i.e. 785 nm, was selected because it allows a low luminescence background in SERS spectra.

At this point, an etched fiber-optic with a conical tip, whose fabrication is described in Section 3.4.1, is connected to the Raman spectrometer and placed in the solution with the noble metal nanoparticles just prepared. Then, silver electrodes were replaced with graphite ones. The local enhancement and the collection volume very close to the fiber allowed a continuous acquisition of spectra during the synthesis without stopping the arc discharge. The presence of silver nanoparticles is able to screen the light produced by the discharge significantly reducing the amount of light entering in the spectrometer. A selection of the spectra collected every three minutes during the 40 minutes of arcing was reported in Fig.4.14a, after the normalization to the signal of the fiber. In Fig.4.14b, the zoom of the spectra in the sp^2 and sp range was showed after the subtraction of the signal of the fiber (i.e. the spectrum at 0 minutes measured before starting the arcing). After 3 minutes of arcing, a small sp -carbon band above 2000 cm^{-1} started to grow, indicating the formation of sp -carbon wires. After 9 minutes, two broad bands clearly appear at about 1960 cm^{-1} and $2100\text{--}2120\text{ cm}^{-1}$. These two features increase until 29 minutes, after that, they display a decrease in the intensity, mostly for the band at higher wavenumber, as observed after the end of the arcing process, depicted by the red curves of Fig.4.14. A possible explanation for the decrease of SERS bands intensities can be associated to the continuous

precipitation of silver nanoparticles at the bottom of the beaker. Such phenomenon may reduce the effective concentration of Ag nanoparticles in solution leading to the decrease of SERS effect and to an increase of the background signal, which is due to the vanishing screening effect of Ag nanoparticles from the plasma emission. Other reasons can be related to the saturation of SERS active sites in Ag nanoparticles or to polyynes degradation. The latter may be associated to the detrimental effect of the discharge on CAWs or for exceeding their saturation limit in water, so inducing sp^2 structures. However, sp^2 signal decreases together with the sp band, so the conversion of sp -carbon chains to sp^2 -based structures does not seem to be the main process.

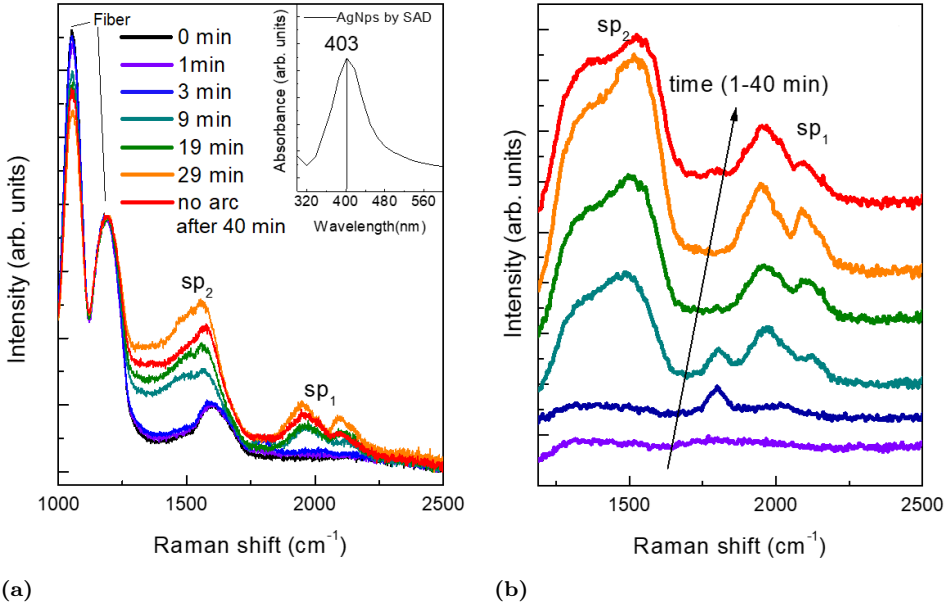


Figure 4.14: Evolution of SERS spectra (excitation line: 785 nm) during 40 minutes of arc discharge. (a) Data normalized with respect to the signal of the fiber. Inset: Ag nanoparticles (AgNps) synthesized by arc discharge between two silver electrodes in water. (b) Smoothed and vertically shifted data after the subtraction of the spectrum at 0 minutes.

The SERS spectrum at the end of the process presents some differences with respect to the one reported in Fig.4.9b although both

refer to aqueous solutions of polyynes mixture by SADL. One reason is related to the use of different silver nanoparticles. In this case, Ag nanoparticles were freshly made by arc discharge in water instead of chemical method, which involves the use of citrate, and are characterized by a shift of 10 nm in the plasmonic peak with respect to chemically-made nanoparticles. Moreover, Ag nanoparticles were not added at the end of the synthesis process but they were already present in the arcing solution, thus interacting with polyynes from the beginning of their formation. Finally, the solution was not filtered before SERS measurements, so carbon particulates were not removed. This may explain the occurrence of strong Raman sp^2 signal, which increases with arcing time. Indeed, after 9 minutes, a large band at about 1500 cm^{-1} appears. It can be attributed to the sp^2 amorphous carbon formed during the arcing. This is in line with the observation of particulate suspended on the liquid surface at the end of the synthesis process. In addition, a peak centred at 1797 cm^{-1} appears after 3 minutes of continuous arcing and disappears after 19 minutes. It may be related to the C=O stretching mode of by-products, induced by the presence of an oxygen source during the formation of polyynes in water, stabilized and enhanced by silver nanoparticles. In a previous work by Lucotti *et al.*, *in situ* SERS measurements of polyynes were carried out by using an optical fiber as SERS active probe [190]. In that study, the fiber needed to be coated by silver nanoparticles, which were chemically immobilized on its surface. Conversely, the method adopted in this thesis does not need any chemical modification of the fiber, opening, in this way, to an easy and fast *in situ* investigation of polyynes formation mechanisms.

4.3 Polyynes synthesized in mixed solution of water and organic solvents

To obtain longer hydrogen-capped polyynes and/or sp -carbon chains terminated by different end-caps, preliminary experiments were performed in mixed solutions of acetonitrile and water as well as in solutions of isopropanol and water, employing the optimized parameters

4.3. Polyynes synthesized in mixed solution of water and organic solvents

discussed in Section 4.1.1. These data were collected in collaboration with a student during his Master thesis activity [177]. To operate in safe conditions and avoid possible flammability issues, less than half of the entire liquid volume, i.e. 100 ml, was composed by organic solvents. UV-Vis spectra of Fig. 4.15a indicate that by increasing the quantity of acetonitrile with respect to water, i.e. 10%, 20%, 40%, the absorption peaks of C_6 , i.e. 199 nm, and C_8 , i.e. 216 nm and 225 nm, increment in intensity until even the peak of C_{10} , marked by 251 nm, is well evident. Similar results can be also obtained when a mixed solution of 40% of isopropanol and 60% of water is employed, as depicted in Fig. 4.15b. The higher polyynes concentration achieved when acetonitrile or isopropanol are added to water and used as solvents for SADL shows that polyynes are more soluble in organic liquids than pure water. In addition, these solvents could also furnish carbon atoms during the synthesis process contributing in the sp-carbon chains growth.

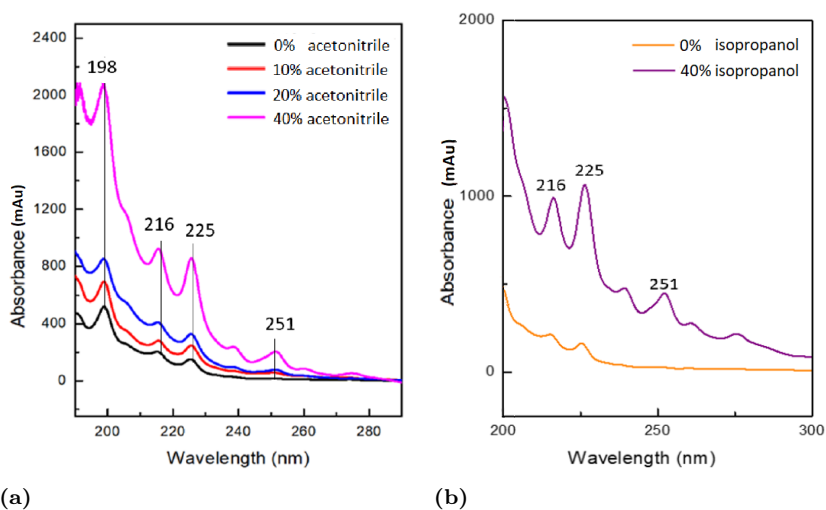


Figure 4.15: UV-Vis spectra of polyynes in solutions of: (a) water and different percentage of acetonitrile, (b) water and different percentage of isopropanol.

The solutions prepared by arc discharge in mixtures of water and organic solvents were characterized by HPLC. Looking at the chromatograms, others types of polyynes were detected compared to those

found in water. All the corresponding UV-Vis spectra extracted from DAD are presented in Fig.4.16. For both the mixtures, hydrogen-capped polyynes (C_n) with $n=6-18$ and methylpolyynes (HC_nCH_3) with $n=8-12$ were identified. Cyanopolyynes (HC_nCN) with $n=6-10$ were also revealed only in the case of arc discharge in acetonitrile-based mixture. The data were confirmed by the comparison with literature [79,145–147] and by TD-DFT simulations (see Appendix).

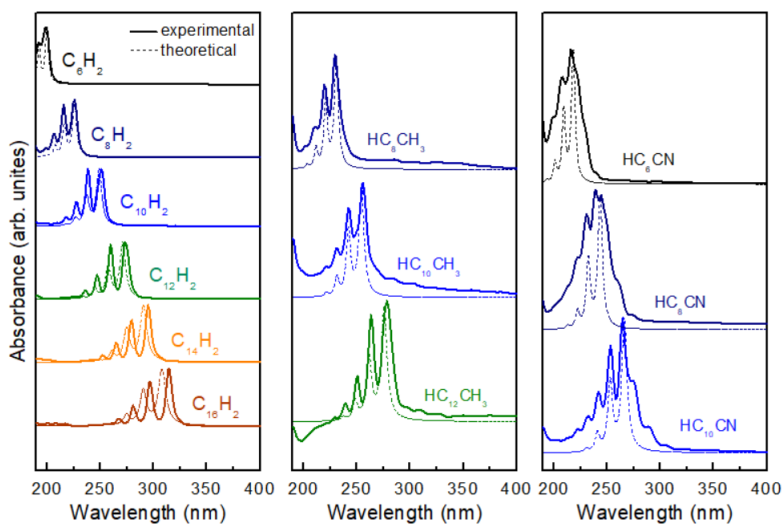


Figure 4.16: Simulated (dashed lines) and experimental (solid lines) normalized absorption spectra of H-capped polyynes (C_n) with $n=6-18$, methylpolyynes (HC_nCH_3) with $n=8-12$, and cyanopolyynes (HC_nCN) with $n=6-10$.

4.4 Summary

This chapter mainly concerned the achievements obtained by arc discharge in water, which is an appealing solvent for future CAWs mass production due to its low cost and non-toxicity. Then, *in situ* SERS experiments performed during SADL and preliminary results carried out in mixed solution of water/organic solvent were also discussed.

After the optimization of the process parameters, an automatic procedure to concentrate, separate and collect polyynes in aqueous solutions was successfully developed. In this way, arc discharge in water

turned out to give the same kind of polyynes that can be obtained with organic solvents but without toxicity and flammability issues. The most concentrated species, i.e. C₆, C₈, C₁₀, were collected and analysed by SERS. This study allowed the identification of the origin of sp-carbon bands in SERS spectrum of polyynes mixture. Moreover, it was noticed that acetonitrile helps in preventing the degradation of polyynes and that dried solutions of Ag colloids and polyynes mixture are stable for at least one month. The latter can be explained considering silver nanoparticles acting as spacers between the chains and strongly binding to polyynes, thus avoiding their degradation.

The evolution of polyynes during the synthesis by SADL was investigated by *in situ* SERS. First, a SERS-active solution of Ag nanoparticles was prepared by arc discharge in water between two electrodes of silver. Then, an optic fiber connected to a Raman spectrometer was inserted in the solution. At this point, SERS measurements were carried out during 40 minutes of arc discharge between two electrodes of graphite. In this way, it was possible to notice the sp-carbon signal growth up to 29 minutes and its decrease until the end of discharge, i.e. 40 minutes. This signal degradation can be due to the precipitation of both Ag colloids and polyynes, being degraded by the continuous arcing.

Finally, the arc discharge in mixture of water/organic solvent led to obtain longer and higher concentrated H-polyynes with respect to the synthesis in 100% water. In addition, the identification of methyl-capped and cyano-capped polyynes shows the possibility of tuning CAWs termination in basis of the solvent employed in SADL.

5

Carbon-atom wires by pulsed laser ablation in liquid

This chapter presents the results of the synthesis and characterization of CAWs by pulsed laser ablation in liquid (PLAL). The technique was developed from scratch, starting by defining the basic requirements and then, carrying out its design and set-up; the details are showed in Section 5.1. The polyynes yield was improved by acting in two ways: optimizing the process parameters and concentrating polyynes solutions after the synthesis, see Section 5.2. Moreover, the effect of different solvents (e.g. water, methanol, ethanol, isopropanol and acetonitrile) in polyynes synthesis was investigated by a multi-technique characterization; all the results are illustrated in Section 5.3. Finally, all the achievements were briefly recalled in Section 5.4. My personal contribution consisted in the whole experimental activity here presented. Some measurements of Section 5.2.1 and Section 5.3 were performed in collaboration with one Master student [178] and a Ph.D. student. I also reported the new outcomes presented in Section 5.3 in a published paper [175].

5.1 Design and set-up of the apparatus

At the beginning of this Ph.D. work, pulsed laser ablation in liquid (PLAL) was designed after the identification of main requirements: option of varying direction, wavelength and energy of the laser beam, possibility to focus the laser on the target and to homogeneously ablate the solid target surface. Accordingly, the technique apparatus needs the appropriate laser support, optics and optics holders, and sample holder. As SADL, even PLAL must be utilized under a chemical hood for safety issues.

Laser support

The optical path employed during the whole research activity is such as to ensure the ablation of the target from the top of the vial. So, the laser support has to be elevated with respect to the sample. However, the overhead position of the laser does not prevent to work in a different configuration where, for example, the ablation of the target takes place laterally through the vial thickness. In that case, only few components need to be changed. Moreover, the laser support requires to be long and resistant enough to sustain all the modules that can be added to the laser head to change wavelength and energy, i.e. harmonic generators of 532 nm and 355 nm and beam attenuator.

Optics and optics holders

Optics necessary for the synthesis of polyynes by PLAL were selected to be resistant to the power and wavelength employed in this work. They consist of two main components: the mirror rotated by 45° , which deviates the beam of 90° from the horizontal direction to the vertical one towards the sample, and the focalising lens, characterized by a specific focal length, which is used to adapt the dimension of beam spot on the target. Recently, further components were implemented to the apparatus to easily measure the energy of the laser before and after each ablation. Specifically, a mirror at 45° is inserted in an optics holder right after the laser head, so it deviates the beam to

5.1. Design and set-up of the apparatus

the power meter sensor. The last mentioned components can be easily added or removed depending on the need.

Sample holder

The sample holder was mounted on x-y-z translator stages, which can be controlled by a Matlab[®] code custom developed. Z-translator defines the position of the sample with respect to the focalising lens, setting the focal spot of the laser. X-Y stages move the sample in a spiral way to homogeneously ablate the surface target, so preventing its ageing.

The initial sketch of PLAL apparatus is presented in Fig.5.1, while the technique, once it was set-up under chemical hood in Nanolab of Politecnico di Milano, is represented in Fig.5.2.

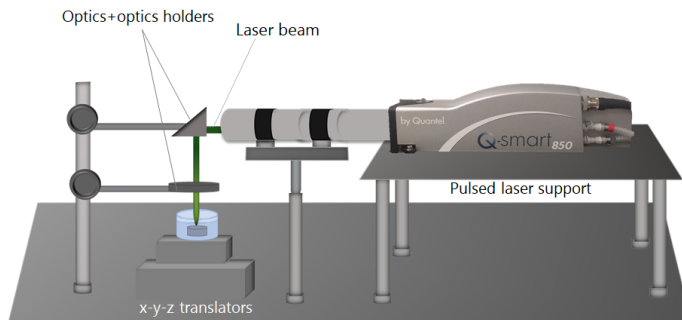


Figure 5.1: Design of PLAL technique.

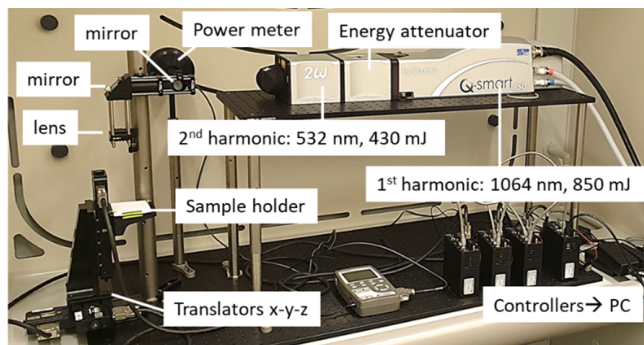


Figure 5.2: PLAL apparatus under chemical hood at Nanolab.

5.2 Methods for maximising polyynes yield

As already said in Section 4.1.1 for the case of SADL, it is necessary to improve the concentration of CAWs solutions by PLAL to allow more and improved characterizations of polyynes mixture and isolated size-selected polyynes. Consequently, it is possible to give further insights on CAWs properties in view of new functional materials. The two ways to reach this aim are presented in Section 5.2.1 and Section 5.2.2, respectively.

5.2.1 Optimization of process parameters

The optimization of process parameters is one strategy to improve the polyynes yield by PLAL. Formation and degradation of polyynes are two competing mechanisms when physical methods are exploited, hence, it is not simple to find the proper process parameters which allow the highest attainable yield. The laser wavelength at 532 nm, which was the most used ones in literature as discussed in Section 2.1.2, was selected for all the experiments reported in this work.

Ablation time and volume

Concerning the results found in literature on the ablation time, it emerges that the irradiation time, at which polyynes yield is higher, strongly depends on the target [54, 139]. Moreover, it was showed that polyynes absorptions were already well visible after 5 minutes of ablation of graphite pellet in distilled water by employing different laser wavelengths, i.e. 1064, 532, 355, 266 nm [191]. The same experiment was repeated in this work by choosing the laser wavelength of 532 nm and characterizing the polyynes solution by UV-Vis spectroscopy. Then, other spectra were collected every 10 minutes until a whole irradiation time of 35 minutes was reached, as reported in Fig.5.3a. In this configuration, the absorption of peaks associated to hydrogen-capped polyynes long 8 atoms of carbon, i.e. C_8 , increases with the irradiation time while those related to C_{10} are more defined at 15 minutes. Thus, from now on, the described experiments refer to 15 minutes of irradiation time. In addition, UV-Vis spectra of ablations

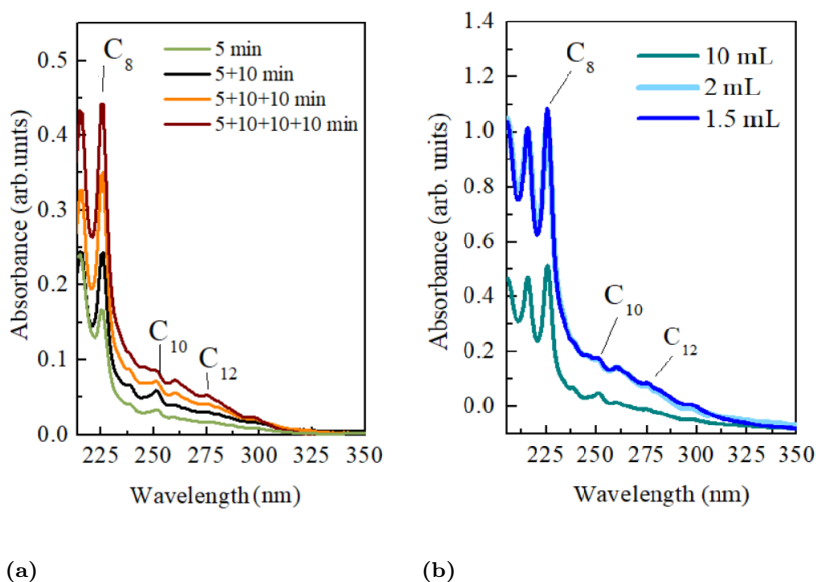


Figure 5.3: UV-Vis spectra of polyynes mixtures with main UV-Vis peaks of C_8 , C_{10} and C_{12} marked: (a) after different irradiation time of graphite pellet in distilled water, (b) after ablation of graphite pellet in 1.5 ml, 2 ml and 10 ml of distilled water.

performed by changing the volume of the solvent, i.e. distilled water, from 10 ml to 2 ml and 1.5 ml are represented in Fig.5.3b. The absorption of polyynes peaks is effectively increased in the cases of reduced volumes but a saturation limit seems to be reached: the peaks do not increase anymore under a volume of 2 ml.

Fluence

Another significant process parameter to play with is the fluence, which is defined as the ratio between the energy per pulse, that can be selected by the beam attenuator in a range between 0 mJ and 380 mJ for the case of 532 nm, and spot area, determined by the distance (h) between the target and the focalising lens. To calculate the correct value of fluence, it is necessary to compute the right laser spot area, so the radius on the target (r_F). The focalisation of the lens, whose radius is indicated by r_L , is affected by the effect of the refraction of the

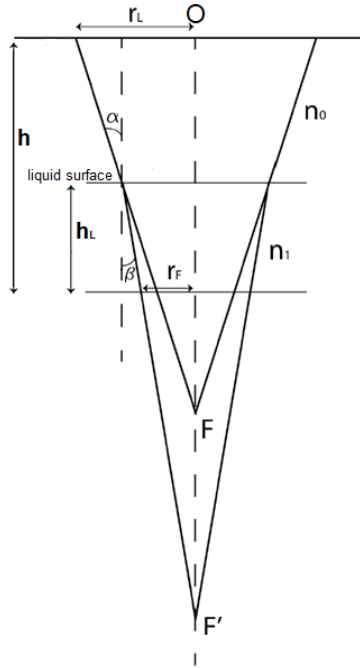


Figure 5.4: Refraction effect on the focal length due to the ablation in liquid environment.

liquid layer, whose thickness is denoted by h_L . In fact, the solvent with a refraction index (n_1) higher than that of air (n_0) induces a further focalisation, as represented in Fig.5.4. The real focal distance ($\overline{OF'}$) is higher than the lens focal length in air (\overline{OF}). With the approximation of geometrical optics, r_F can be computed from the Eq.5.1 knowing all the other parameters, where n is defined as the ratio between n_1 and n_0 .

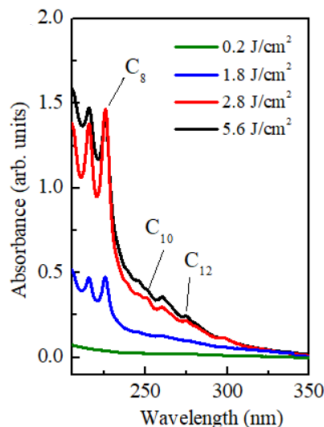
$$r_F = r_L - (h - h_L) \frac{r_L}{OF} - h_L \tan \left[\arcsin \left(\frac{r_L}{n \sqrt{r_L^2 + OF^2}} \right) \right] \quad (5.1)$$

Moreover, the laser radiation can be considered as a gaussian beam, thus, when it is focalised, it has a finite spot size instead of a point. Since this phenomenon is not taken into consideration in the geometrical optics, the calculations discussed by Menéndez and coworkers in Ref. [192] were employed to extrapolate the ($\overline{FF'}$), from which the r_F

can be computed.

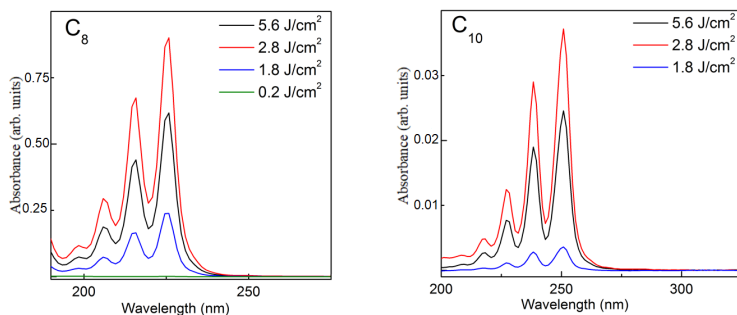
The next set of experiments were intended to optimize the fluence by ablating graphite pellet immersed in 2 ml of water for 15 minutes. Each selected fluence did not generate splashes during the ablation, otherwise it would have been reduced by increasing the spot area or by decreasing the energy per pulse. The fluence was varied increasing the energy per pulse from 10 mJ to 300 mJ and keeping constant the spot size on the target at 5.35 mm^2 . Polyynes were not synthesized at fluence of 0.2 J/cm^2 and energy per pulse of 10 mJ while polyynes signals are well detectable already at fluence of 1.8 J/cm^2 and energy of 96 mJ, as shown in Fig.5.5a. The optimum value of absorbance was reached at fluence of 2.8 J/cm^2 and energy of 150 mJ, looking at the peak-valley difference of the absorption peaks of polyynes mixtures while the signals are slightly less intense at fluence of 5.6 J/cm^2 and energy of 300 mJ. These results were also confirmed from UV-Vis spectra extracted from HPLC separation of C_8 and C_{10} reported in Fig.5.6a and Fig.5.6b, respectively. Previous studies reported the identification of an ablation threshold, at which the laser fluence induces enough instabilities in the target lattice to remove a monolayer of material [193]. In the case of graphite ablated by a ns-laser at 1064 nm in vacuum, the ablation threshold value was found at a fluence of 2.4 J/cm^2 [194], while, at 532 nm, the ablation threshold was individuated at 1.5 J/cm^2 [195]. In the work of Zhu and coworkers [196], the ablation rate by a ns-laser in water was often found higher than in air, because of the liquid confinement effect which increases the plasma pressure on the target [129]. In this work, since the ablation of graphite was carried out not in vacuum conditions but in liquid, the threshold ablation fluence is expected to be lower than the case of vacuum, in particular, lower than 1.5 J/cm^2 but higher than 0.2 J/cm^2 , the experimental lower limit just mentioned. Furthermore, the fact that UV-Vis signals started to decrease at fluence of 5.6 J/cm^2 may be explained considering that the critical electron density in the plasma reached a limit, which shields the laser. So, the laser cannot anymore reach the graphite but may only degrades the already formed polyynes in the liquid, leading to a decrease in the ablation efficiency [129]. Further experiments are

currently performed in the lab to deepen the effect of the fluence on polyynes yield by varying the energy per pulse or the spot size.



(a)

Figure 5.5: UV-Vis spectra of polyynes mixtures after the ablation of a graphite pellet in water at different fluences, obtained varying the energy per pulse from 10 mJ to 300 mJ and keeping fixed the spot size at 5.35 mm². The main absorption peaks of C₈, C₁₀, C₁₂ are marked in the picture.



(a)

(b)

Figure 5.6: DAD-absorption spectra of size-selected hydrogen-capped polyynes obtained from HPLC separation of polyynes mixtures synthesized at different fluences: (a) C₈, (b) C₁₀.

5.2.2 Concentration methods

To concentrate aqueous polyynes solutions, in addition to the batch-loading on column method, already presented in Section 4.1.2, a com-

mon technique is based on solid-phase extraction (SPE) cartridge, whose results are next reported.

In this work, Supelco SPE LC-8 cartridge with a maximum quantity of analyte equal to 500 mg and a volume of 3 ml was employed to concentrate aqueous solutions of polyynes. These columns are composed of the same stationary phase of the C8 HPLC column, so they will retain nonpolar molecules, as polyynes, in polar solvent, as water. The SPE-based sample concentration, herein adopted, consisted of loading 10 ml of aqueous solution of polyynes onto a preliminary washed and conditioned column. These millilitres of solution were obtained after five ablation of graphite in 2 ml of water. Then, 4 ml of acetonitrile were used to elute polyynes retained on the cartridge, so concentrating them of 2.5 times. These 4 ml were collected in 4 different vials, 1 ml each, to understand where polyynes were most concentrated. It resulted that 2 ml of elution are enough to dilute sp-carbon chains, as shown in Fig. 5.7, where the chromatographic peak areas of C_6 and C_8 are reported as a function of each millimetre of the eluting solvent. In this way, it is possible to concentrate by SPE cartridges 10 ml of aqueous polyynes solution up to 5 times eluting with just 2 ml of acetonitrile.

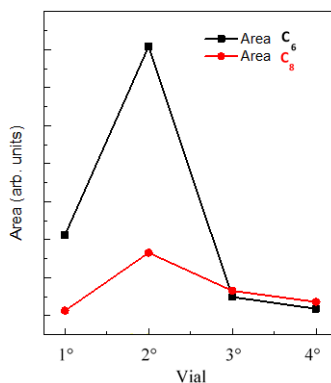


Figure 5.7: Chromatographic peak area of C_6 and C_8 from each millimetre of eluting solvent, i.e. acetonitrile.

Another well-known method to concentrate liquid solutions is the rotary evaporator, already exploited from previous papers to increase

the concentration of polyynes in ethanol [53]. Only preliminary experiments were performed close to the end of the Ph.D. activity, showing promising results not only to concentrate polyynes in organic solvents but also in water. To properly analysed high concentrated solutions of polyynes obtained from rotary evaporator, an upgrade of the actual HPLC system is required, switching from an analytical loop to a semi-preparative one.

5.3 Polyynes synthesized in different solvents

The effect of different solvents during PLAL on polyynes properties, e.g. yield, size, terminations and stability, was deeply investigated and the corresponding results are reported in this Section. All the syntheses were performed keeping constant the experimental parameters mentioned in the previous paragraph (i.e. wavelength, ablation time, volume, fluence). The selected solvents, characterized by different polarity and transparency to the laser wavelength of 532 nm, were the following: water (H_2O), methanol (MeOH), ethanol (EtOH), isopropanol (IPA) and acetonitrile (ACN). After the ablation in these liquids, polyynes solutions did not present any visible carbon particulate as in the case of SADL, as demonstrated in Fig.5.8. However, the solutions were filtered before any characterization and showed a different colour varying from the brown yellow of acetonitrile-based sample to the transparency of water-based sample.

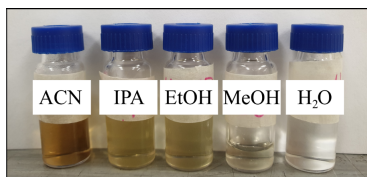


Figure 5.8: *Polyynes solutions after ablation in different solvents.*

5.3.1 Solutions of polyynes mixture

To evaluate the solvent role in the formation of polyynes, UV-Vis spectra of all the solutions were carried out and are illustrated in Fig.5.9a. Each curve shows several peaks assigned to hydrogen-capped polyynes

5.3. Polyynes synthesized in different solvents

of different length, from 8 to 16 atoms, whose main peaks are marked on the picture. Moreover, it is possible to notice a correlation between UV-Vis absorption of the spectra in Fig.5.9a and the colour intensity of each solution of Fig.5.8, e.g. acetonitrile-based sample has the highest polyynes UV absorptions and corresponds to the solution with the most intense colour. These colours may be associated to the quantity of by-products formed in each synthesis, affecting the spectra by an unresolved background of absorption. To evaluate the polyynes yield with respect to the amount of by-products in each solvent, the so-called index of purity indicated by χ_p , was computed [148, 149]. χ_p is defined as the ratio between the sum of all the areas of main peaks¹ related to H-polyynes, fitted with gaussian curves, and the area of hydrocarbons, fitted with a decreasing exponential. Spectra after subtraction of backgrounds are reported in Fig.5.9b together with the curve fitting of polyynes peaks and background (in the inset of Fig.5.9b).

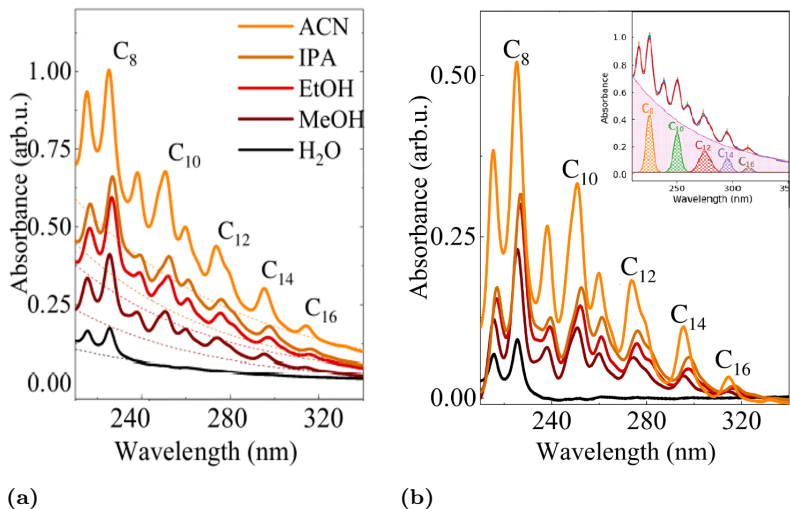


Figure 5.9: UV-Vis spectra of filtered solutions of polyynes in acetonitrile (ACN), isopropanol (IPA), methanol (MeOH), ethanol (EtOH) and water (H_2O) after laser ablation (a) before background (dotted lines) subtraction and (b) after. The curve fitting performed on the background and on the main absorption peaks of hydrogen-capped polyynes were highlighted in the inset.

¹The 0-0 bands of the ${}^1\Sigma_u^+ \leftarrow X^1\Sigma_g^+$

The lowest χ_p and polyynes concentration were found in the case of PLAL in water, as depicted in Fig.5.10. One reason may be connected to the slightest hydrogen generation rate in water. Hydrogen, indeed, is necessary to terminate the sp-carbon chains and the energy to break H–OH bond is equal to 4.8 eV, which is higher than the energy to break C–H bonds of the organic liquids, i.e. 4.3 eV [129, 197]. Furthermore, water cannot contribute to the chain growth because it has no carbon atoms in its structure.

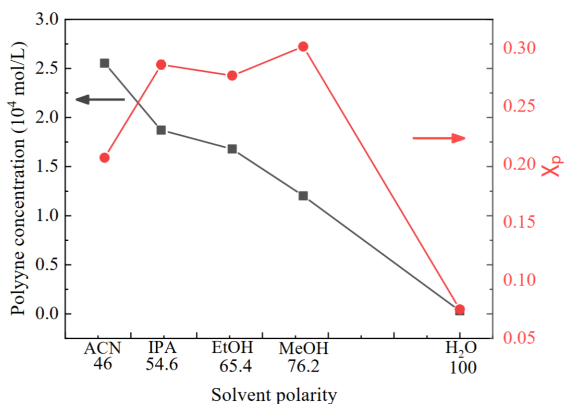


Figure 5.10: Polyynes concentration (mol/L) (in black) and χ_p (in red) as a function of solvent polarity.

Among the organic solvents, the lowest χ_p is associated to acetonitrile because it is more liable to decomposition compared to alcohols [121]. The highest degradation of acetonitrile, from one side, gives more by-products, explaining its lowest index of purity, from the other, it can furnish more carbon atoms for polyynes synthesis, justifying the highest value of concentration highlighted in Fig.5.9b. In addition, acetonitrile has the slightest value of oxygen dissolved and the lowest polarity, see Table 5.1. It was, indeed, observed that the polyynes concentration decreases by increasing the solvent polarity. In general, solvents with low polarity and low quantity of oxygen dissolved help in preserving polyynes, which are non polar molecules and are likely to oxidise in presence of oxygen, as already discussed in the previous chapter. Concentrations of each size-selected polyynes and χ_p values are indicated for each solvent in Table 5.1.

5.3. Polyynes synthesized in different solvents

Table 5.1: Polarity (p), Ostwald coefficient (l), polyynes concentration (c [mol/L]) and χ_p for all the solvents.

	ACN	IPA	EtOH	MeOH	H ₂ O
p [197]	46	54.6	65.4	76.2	100
l	0.00083 [189]	0.2463 [198]	0.2417 [198]	0.2476 [198]	0.031 [199]
C ₈ (cx10 ⁻⁴)	1.42±0.07	1.09±0.02	1.07±0.01	0.750±0.005	0.0313±0.0002
C ₁₀ (cx10 ⁻⁵)	7.3±0.4	4.57±0.08	4.07±0.06	2.72±0.03	0
C ₁₂ (cx10 ⁻⁵)	2.6±0.1	1.8±0.1	0.93±0.06	1.17±0.02	0
C ₁₄ (cx10 ⁻⁶)	7.8±0.4	11±4	8.0±0.3	4.6±0.2	0
C ₁₆ (cx10 ⁻⁶)	6.5±0.3	3.4±0.1	3.0±0.1	1.6±0.1	0
tot	6.80 x10 ⁻⁴	4.27x10 ⁻⁴	3.70x10 ⁻⁴	2.48x10 ⁻⁴	6.65x10 ⁻⁶
χ_p	0.2057±0.0005	0.2860±0.0043	0.2766±0.0035	0.3015±0.0003	0.0749±0.0001

5.3.2 HPLC and UV-Vis analysis of size and end-selected polyynes

After the UV-Vis characterization of polyynes mixture, HPLC analysis was carried out for each sample to separate polyynes depending on length and termination. Except for water, it was possible to identify hydrogen-capped polyynes ranging from 6 to 22 carbon atoms and methyl-capped polyynes with chain length spanning from 6 to 18 carbon atoms in all the organic solvents. In particular, as far as we know, it was the first time that C₂₂ was detected in acetonitrile and isopropanol, and that methyl-capped polyyne long 18 carbon atoms was noticed in any solvent. Even in water, one type of methylpolyynes was individuated, i.e. HC₈CH₃. Moreover, also cyanopolyynes were detected in acetonitrile from short (i.e HC₆CN) to mid chain lengths (i.e HC₁₂CN). UV-Vis spectra from HPLC DAD of all the mentioned size- and end-selected species are reported in Fig.5.11, which refers to acetonitrile-based solution.

Most of the polyynes assignments were confirmed by comparing the UV-Vis spectra of Fig.5.11 to those present in literature [143–147]. Theoretical TD-DFT simulations (see Appendix), represented in thin lines in Fig.5.11, were necessary to support the identification of all the species, in particular for those whose UV-Vis spectrum was not present in literature. The positions of polyynes UV absorption peaks extracted from experiments, simulations and literature are presented in Table 5.2.

Another important factor, which helps in discriminating polyynes, is the time at which each species is detected by HPLC. With our HPLC

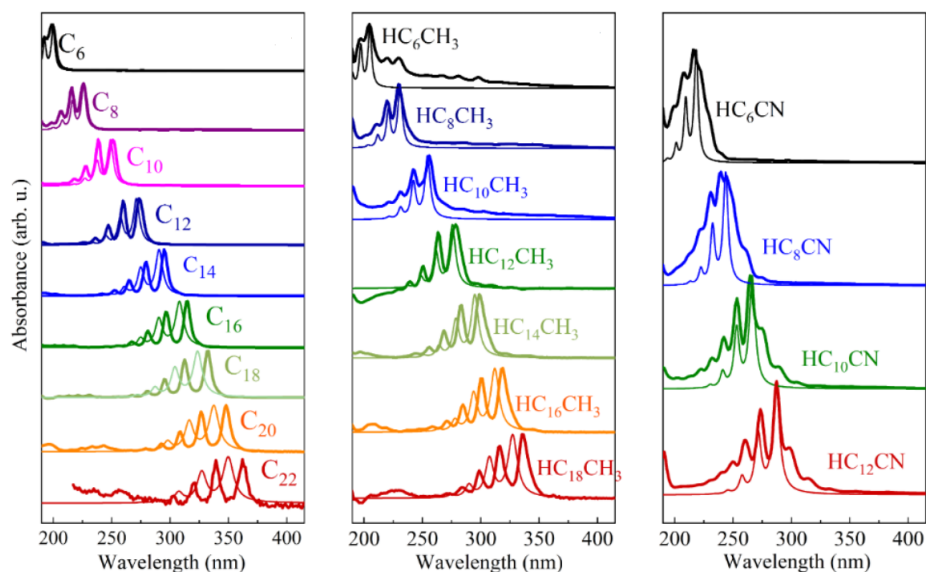


Figure 5.11: HPLC analysis of polyynes solution in acetonitrile: normalized experimental (thick lines) and simulated (thin lines) UV-Vis spectra of H-polyynes (left), CH_3 -polyynes (centre) and CN-polyynes (right).

Table 5.2: Polyynes after ablation of graphite in acetonitrile with the corresponding times on chromatogram and positions of experimental, simulated and literature UV-Vis absorption peaks.

n. of C atoms (end-cap)	t_R (min)	Wavelength(nm)		
		Experimental	Simulated	Literature
6(H)	9.919	198	200	199 ¹⁷⁹
6(CN)	11.484	216 208 200	218 209 201	215.6 207.2 198.9 ¹⁴²
6(CH_3)	11.98	205 197	205	/
8(H)	14.149	226 216 207	226 216 208	226 216 206 ¹⁴¹
8(CN)	15.323	239/244.5 231 222	244 232 222	239/244 231 222 ¹⁴²
8(CH_3)	16.058	230 220 211	231 221 212	/
10(H)	17.89	251 238 228	249 237 227	251 239 227 ¹⁴¹
10(CN)	18.627	265 253 242	266 253 241	264.5 253.3 242.0 ¹⁴²
10(CH_3)	19.623	256 242 231	254 242 231	257 243 232 ¹⁴³
12(H)	21.092	273 260 247	271 257 245	275 260 247 ¹⁴¹
12(CN)	21.468	287 273 261	287 271 258	287.4 273.7 261.1 ¹⁴²
12(CH_3)	22.64	278 263 251	276 261 249	279 264 251 ¹⁴⁴
14(H)	23.777	295 280 265	291 275 261	296 280 267 ¹⁴¹
14(CH_3)	25.120	299 283 268	295 279 264	302 285 269 ¹⁴⁴
16(H)	26.004	315 296 281	308 290 275	316 298 281 ¹⁴¹
16(CH_3)	27.251	319 301 285	312 294 278	/
18(H)	28.045	333 313 295	324 304 287	334 314 295 ¹⁴¹
18(CH_3)	29.691	335 316 299	327 307 290	/
20(H)	30.795	348 326 309	337 316 298	350 328 310 ¹⁴¹
22(H)	34.288	362 339 321	350 327 308	364 341 321 ¹⁴¹

5.3. Polyynes synthesized in different solvents

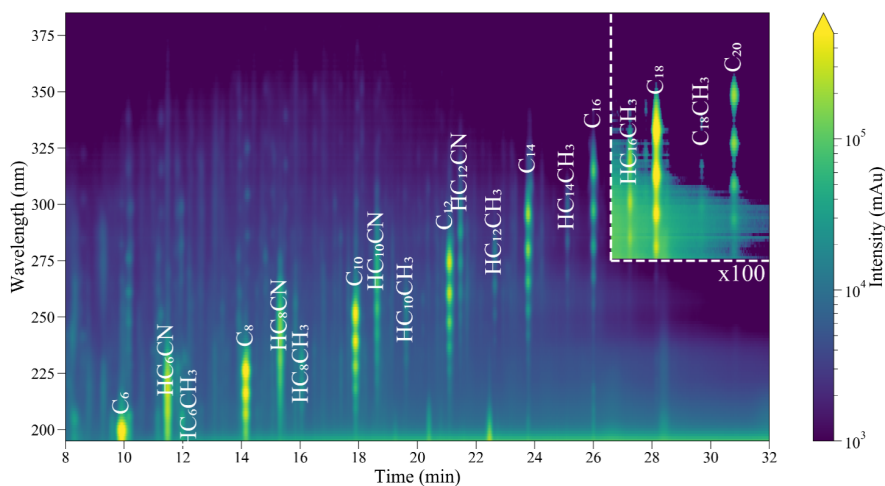


Figure 5.12: HPLC analysis of polyynes solution in acetonitrile: absorbance as a function of the wavelength and time extracted from DAD coupled with HPLC, with all the types of polyynes marked.

method, shortest and more polar molecules will be eluted first [171]. Considering the same termination, shortest polyynes will exit before, while, at same size, chains ended by cyano-group, which is more polar than methyl group, will be identified before, as demonstrated in Table 5.2, whose times are extracted from Fig.5.12. The latter shows the absorption of each polyynes obtained by PLAL in acetonitrile as a function of wavelength and elution time, displaying the expected sequence of detection.

These results revealed that solvents have a crucial role in the formation of polyynes during PLAL, as already noticed also in the case of SADL (see Section 4.3). They can furnish carbon atoms to grow the chain but also terminations to end the polyyne [129, 145]. The first effect is demonstrated by the larger concentration of polyynes obtained in organic solvents compared to water. The second one is displayed by the types of polyynes terminations detected in basis of the functional groups of the solvent, e.g. cyanopolyynes were found only in acetonitrile, whose structure is $\text{CH}_3\text{-CN}$. In addition, the detection of methylpolyynes in water, which is not composed of methyl-groups, shows the possibility to form this kind of termination from the bind-

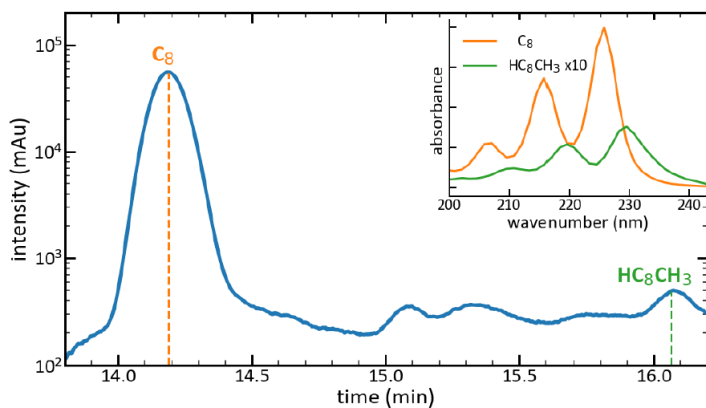


Figure 5.13: HPLC chromatogram of polyynes solution in water, extracted at 225 nm, with the chromatographic peaks of C_8 and HC_8CH_3 . The corresponding UV-Vis spectra are reported in the inset.

ing of three hydrogen atoms, even if it is a very unlikely process, as derived from the absorbance of hydrogen-capped polyynes compared to the one of methyl-capped polyynes in Fig.5.13.

5.3.3 SERS analysis of size and end-selected polyynes

To strengthen the capping assignation of the species previously discussed, three types of polyynes with the same chain length, but different capping, i.e. hydrogen, methyl- and cyano- group, were separated and collected by HPLC system. Surface-enhanced Raman spectroscopy was performed on each sample after the addition of Ag colloids because polyynes concentrations were too low to observe Raman signals (see Table 5.1). SERS spectra of the three samples have two main bands, as shown in Fig.5.14. The one over 2000 cm^{-1} is associated to polyynes ECC Raman band while the origin of the band below 2000 cm^{-1} , which appears in all the polyynes SERS spectra [53, 168, 200], is still object of investigation as addressed in Section 2.2.1. For this reason, the band corresponding to Raman ECC peak is the one considered in the following discussion. Since it is known that the interaction between polyynes and Ag nanoparticles is preferentially localized at the edge of the chain [168], SERS is expected to discriminate between different terminations.

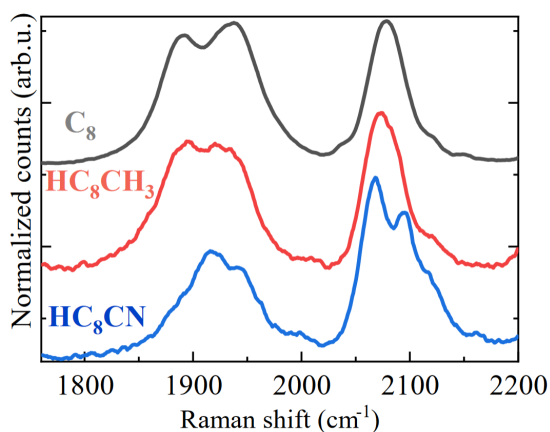


Figure 5.14: Normalized experimental SERS spectra (excitation line: 532 nm) of solutions of size-selected polyynes with four triple bonds and different endcap (from the top): C_8 , HC_8CH_3 , HC_8CN . The curves related to methyl- and cyano-capped polyynes were smoothed in order to better individuate the sp -carbon features.

In the case of H-capped polyynes, the interaction with Ag colloids is equal at the two endings, as shown from the symmetrical SERS band at 2079 cm^{-1} . When the methyl-group is substituted to one hydrogen, the centre of the band slightly shifts to lower wavenumber (i.e. 2073 cm^{-1}) and induces a small broadening of the band. Instead, a cyano-group, that is much more polar, participates more than methyl-group in the collective vibrational mode and, consequently, it may cause a splitting of the band, forming a doublet. The most intense feature of cyanopolyynes is located at 2067 cm^{-1} and the secondary one at 2093 cm^{-1} . Fig.5.15a shows that, in cyanopolyynes, the collective vibrational mode is also localized on the cyano-group while, in methyl- and hydrogen-capped polyynes, it mainly involves CC bonds. The shift to lower wavenumber of the ECC band is explained considering that methyl- and cyano-capped polyynes are characterized at one end by the presence of a molecular group, which contributes in increasing the π conjugation of the chain. This leads to the frequency decrease of the Raman mode, which is also supported by the ECC peak shift observed in simulated Raman spectra of single molecule without Ag nanoparticles, depicted in Fig.5.15b. The difference in the position

of the bands between simulated and experimental spectra is due to the fact that Ag colloids are not considered in the theoretical calculations. Further computational analyses with appropriate models should be developed to understand the behaviour of experimental SERS spectra. Anyway, these results confirm that SERS is sensitive to the chain terminations with fixed length.

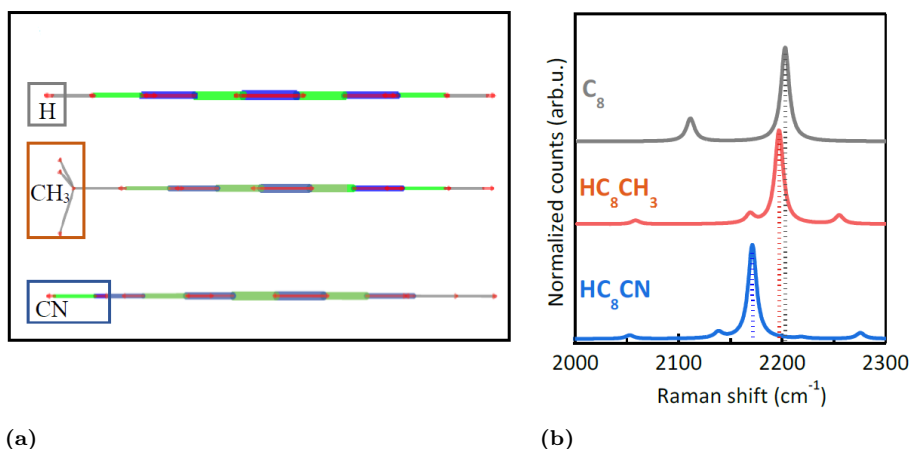


Figure 5.15: (a) Collective vibrational mode of CC bond related to (from the top): C₈, HC₈CH₃, HC₈CN. (b) Normalized simulated Raman spectra of the corresponding molecules. Data computed by PBE0/cc-pVTZ functional.

5.3.4 Stability analysis

After the characterization of polyynes in mixture and polyynes selected in basis of the size or end-group, a study related to CAWs stability as a function of their length, termination and liquid environments was performed. To do that, periodic HPLC analyses on polyynes mixtures during 30 days were carried out, leaving the samples into closed vials between two consecutive measurements. The degradation in time was estimated from the area of chromatographic peak of each polyyne after the analysis (A_t) compared to the initial area (A_0). The experimental values reported in the form of $\ln(A_t/A_0)$ and the instrumental error bar of 5% due to HPLC apparatus are showed in Fig.5.16. The decay time constants (τ) extrapolated from the linear fit of the experimental

data are provided in Table 5.3.

The data regarding the chain length effect on polyynes stability are reported in Fig.5.16a referring to hydrogen-capped polyynes. The temporal evolution is well described by a linear fit. As already known [81], longer chains are more unstable with respect to the shorter ones. In addition, increasing the chain length, the decay time constant exponentially decreases, as illustrated in the inset of Fig.5.16a.

The termination effect on polyynes stability is depicted in Fig.5.16b for the case of acetonitrile solution. Cyanopolyynes are much more unstable due to their high reactivity and oxidise first compared to hydrogen- and methyl-polyynes. Indeed, cyanopolyynes have a decay time constant of two order of magnitude lower than the other two species [81]. Methyl-capped polyynes present similar values of hydrogen-capped chains, in fact they can be preserved in liquid for longer time with respect to cyanopolyynes because of their less reactive terminating group. However, it was not possible to carry out a linear fit and extrapolate τ for methylpolyynes as in the other cases because of the evident fluctuations that can be possibly due to their low concentration.

Regarding the effect of the solvent (see Fig.5.16c), the study was conducted looking at C_8 , since it is the most concentrated type of sp-carbon chain. High polar solvent, like water, represents a high hostile environment rich of oxygen which oxidises the chains. The decay time constant of polyynes in this solvent is only of 1.8 days, so polyynes were not anymore revealed by DAD after only 10 days. Instead, the decay time constants in the case of organic solvents, where polyynes are more soluble, are two orders of magnitude higher, see Table 5.3. Acetonitrile turns out to be the most stabilizing environment, probably due to its lowest polarity and oxygen solubility with respect to ethanol and isopropanol, as previously discussed. Ethanol and isopropanol are solvents with similar χ_p , but the first seems to maintain polyynes for longer time. This may be due to the smaller quantity of oxygen dissolved in ethanol, as shown in Table 5.1.

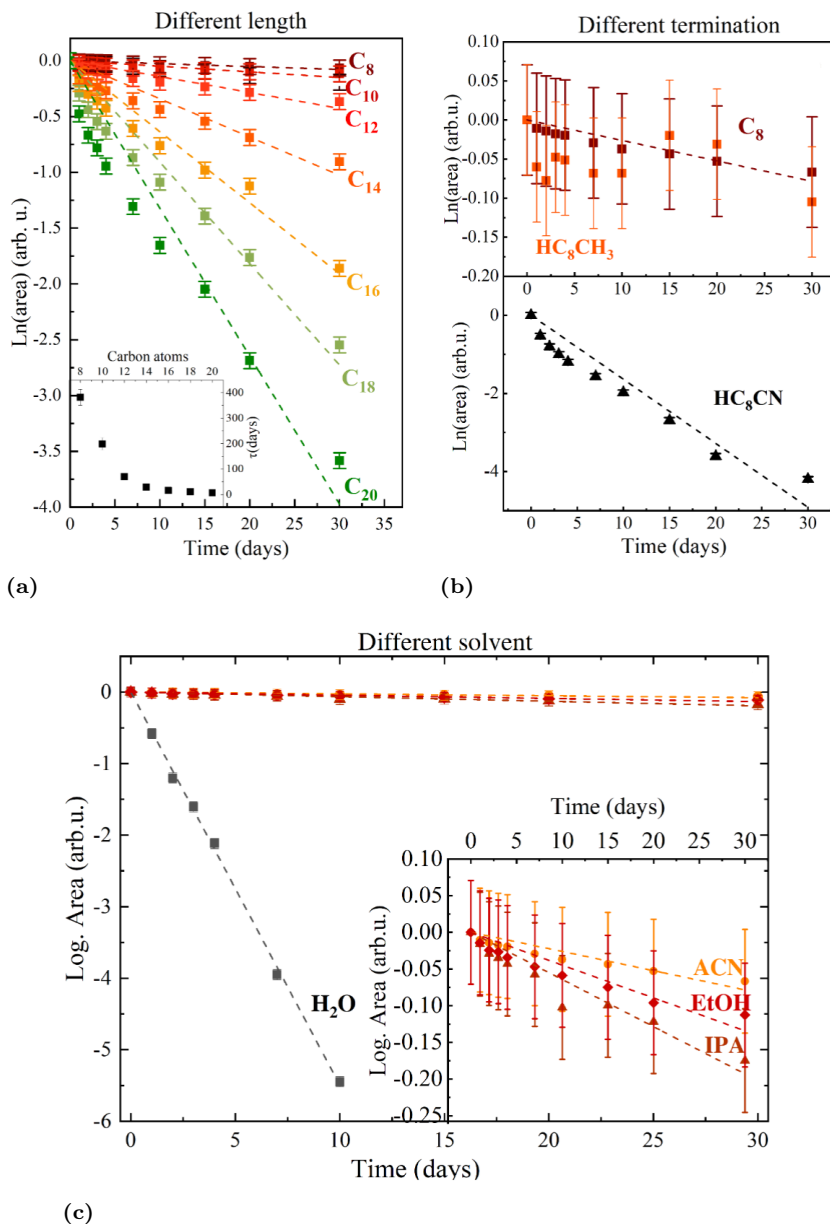


Figure 5.16: Time evolution of chromatographic peak area of polyynes, changing one characteristic at a time. (a) Chain length: from C_8 to C_{20} in acetonitrile. Inset: decay time constant (τ) for each H-polyyne. (b) Terminations: C_8 , HC_8CH_3 and HC_8CN in acetonitrile. (c) Liquid environment: water, acetonitrile, isopropanol, ethanol, looking at C_8 . Inset: Zoom on polyynes solutions in organic solvents. All the decay time constants are reported in Table 5.3.

Table 5.3: Decay time constants (τ) and corresponding R^2 , extrapolated from the fit of experimental values related to chromatographic peak area of polyynes at different length, termination and in different solvents.

Length	τ (days)	R^2
C ₈	-382.381 ± 31.578	0.93575
C ₁₀	-198.860 ± 24.259	0.86876
C ₁₂	-70.187 ± 5.949	0.93252
C ₁₄	-29.223 ± 2.206	0.94579
C ₁₆	-15.708 ± 0.837	0.97235
C ₁₈	-11.002 ± 0.600	0.97104
C ₂₀	-7.553 ± 0.464	0.96353
Termination	τ (days)	R^2
-H	-382.381 ± 31.578	0.93575
-CN	-6.105 ± 0.413	0.95606
Solvent	τ (days)	R^2
H ₂ O	-1.8191 ± 0.018	0.99929
ACN	-382.381 ± 31.578	0.93575
IPA	-155.438 ± 10.500	0.95617
EtOH	-223.464 ± 17.020	0.94487

These results give further information on polyynes stability, helping to understand and, so, to control the behaviour of these carbon nanostructures, also discussed in Section 4.1.4 in the case of polyynes solutions by SADL. As already said, sp-carbon chains synthesized in the same solvent but with different technique, i.e. SADL or PLAL, lead to a different yield of polyynes and impurities.

5.4 Summary

This chapter covered the outcomes related to polyynes production obtained from pulsed laser ablation of graphite in different solvents.

First, the technique needed to be designed and set-up, taking care of all the requirements necessary to develop the experiments of this thesis work. Then, two ways of increasing polyynes concentration were discussed: the optimization of process parameters and post-synthesis concentration methods. Moreover, the effect of the solvent on yield, termination, length, and stability of polyynes by PLAL was studied by a multi-technique characterization. SERS spectra of polyynes with

three different terminations, i.e. H-, CH₃- and CN-, show changes on the shape and position of the sp bands, remarking the sensitivity of the technique on the capping of carbon chains. In addition, the results bring out some clarifications on the mechanism of polyynes formation and underline the tuning of the polyynes termination as a function of the solvent molecular structure, as also discussed in the case of SADL. Acetonitrile was proved to be the best solvent among water, methanol, ethanol and isopropanol, in terms of polyynes yield, stability and for the different types of polyynes that can be synthesized, i.e. hydrogen-capped polyynes (C_n, n=6-22), methylpolyynes (HC_nCH₃, n=6-18) and cyanopolyynes (HC_nCN, n=6-12).

These achievements have contributed to investigate more deeply the role of solvents during PLAL and in paving the way to polyynes properties modulation by tuning the chain length and termination by PLAL.

6

Wire-based nanocomposites

This chapter describes a novel method developed for the fabrication of nanocomposites based on carbon-atom wires embedded in a polymeric matrix with the intention to prepare new polyynes-based materials, where these nanostructures are stabilized.

The first polymer taken into consideration is the poly(vinyl alcohol) (PVA). All the steps necessary to produce polyynes-based free-standing films are presented in Section 6.1. UV-Vis measurements before and after ablation of graphite in solution with different concentrations of PVA in water are reported in Section 6.2. SERS measurements on liquid and solid PVA/Ag/polyynes samples are discussed in Section 6.3, while the corresponding stability studies are showed in Section 6.4. The second polymer chosen for this work was the poly(methyl methacrylate), whose results on PMMA/Ag/polyynes solutions and nanocomposites are illustrated in Section 6.5. My personal contribution consisted in the whole experimental activity here presented and, specifically, some measurements of Section 6.5 were performed in collaboration with one Master student [180]. I also reported the novel findings related to PVA/Ag/polyynes samples in a published paper [179].

6.1 *In situ* synthesis of polyynes in PVA aqueous solution

It was demonstrated that a polymer, as poly(vinyl alcohol) (PVA), can be employed to encapsulate hydrogen-capped polyynes, stabilizing them and forming a solid functional material [95–97]. PVA is a good candidate because it is characterized by water-solubility, which allows the use of Ag colloids for SERS measurements, low cost, chemical stability and high filmability. A few studies have discussed the production of a nanocomposite by adding PVA granules to an organic solution of polyynes and metal nanoparticles [95,96]. However, the addition of the polymer after the synthesis of polyynes could prevent the complete blending between polyynes, metal nanoparticles and polymer. Furthermore, the heating process necessary to dissolve the solid polymeric pellets could affect the integrity of the chains, which are susceptible to temperature rises [78]. Conversely, if PVA is dissolved in a solvent and, then, added to the solution with CAWs, the sp-carbon chains concentration decreases, reducing the signal intensity in optical and structural characterizations. To overcome all these critical issues regarding the preparation of polyynes-based nanocomposites, a novel synthesis method was developed and here presented. The procedure consists in the ablation of a graphite solid pellet by ns-laser at 532 nm directly in an aqueous solution of PVA, so hydrogen-capped polyynes are formed *in situ*, already in the polymer, as sketched in Fig.6.1.

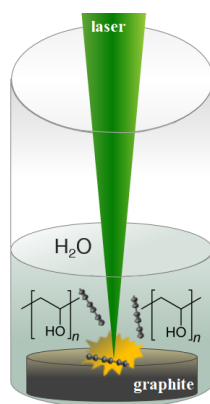


Figure 6.1: *In situ* PLAL: ablation of a graphite pellet in aqueous PVA solution.

6.1. *In situ* synthesis of polyynes in PVA aqueous solution

To investigate the role of the polymer during the ablation, solutions with different concentration of PVA in water, i.e. 0.03, 0.5, 1, 3, 10 wt.%, were prepared by dissolving PVA pellets at 373.1 K and are, herein, indicated with PVAx%, where x is the percentage of PVA. The solution with polyynes obtained after ablation is displayed in Fig.6.2 on the left and it is marked with L-x%. Then, to perform SERS analyses, an empirically estimated optimum value of Ag colloids was added to each PVA/polyynes solution for a volume ratio of 2:1, 2 for Ag colloids and 1 for PVA/polyynes solution. An example of these samples, called L-x%_Ag, is reported in the centre of Fig.6.2. Finally, the solution was drop cast and left to dry at room temperature, so a free-standing thin film, referred to as S-x%_Ag and depicted on the right in Fig.6.2, was peeled off from the substrate. All the steps followed to prepare polyynes-based nanocomposites are outlined in Table 6.1.

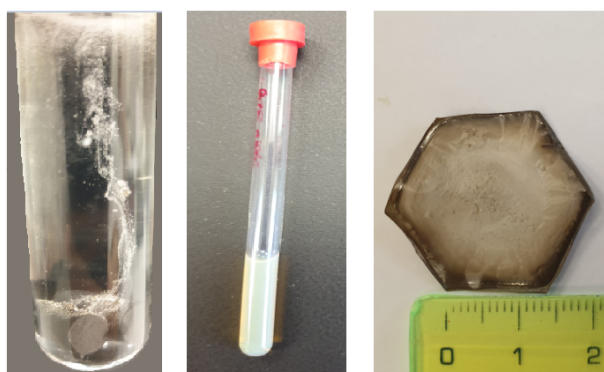


Figure 6.2: *Sample at different stages of polyynes-based nanocomposite preparation (from left): aqueous solution of polyynes and PVA right after the ablation, solution after the addition of Ag colloids, nanocomposite obtained after solvent evaporation.*

Table 6.1: Steps for the preparation of a solid material based on polyynes in a polymeric matrix (PVA).

Step	Description	Sample Name
1 st	Preparation of solvents for PLAL, i.e. PVA at different concentration in water: wt. %: $x = 0.03, 0.5, 1, 3, 10$.	PVA x %
2 nd	PLAL of graphite in solutions of PVA at different concentration in water (i.e. PVA/polyynes solution).	L- x %
3 rd	Addition of Ag colloids in a volume ratio of 2:1 with respect to PVA/polyynes solutions (i.e. Ag/PVA/polyynes solution).	L- x %_Ag
4 th	Drop casting and solvent evaporation for 24 hours at room temperature (i.e. Ag/PVA/polyynes nanocomposite).	S- x %_Ag

6.2 UV-Vis spectroscopy of PVA/polyynes solutions

UV-Vis spectroscopy was performed on PVA x % and L- x %_Ag samples, whose spectra are showed in Fig.6.3a and Fig.6.3b, respectively. PVA is transparent at visible wavelength but absorbs in UV region at 278 nm. Its absorption corresponds to the $\pi \rightarrow \pi^*$ transition of the carbonyl groups (C=O), in turn linked to the unsaturated ethylene bond (C=C) of the type $-(HC=CH)_2CO-$, characteristic of the end groups [201]. The peaks individuated in Fig.6.3b, i.e. 199, 206, 215, 225 and 251 nm, are related to hydrogen-capped polyynes long 6, 8 and 10 atoms of carbon. Longer polyynes are hardly detectable for their low concentration and for being more covered by PVA signal. With a polymer concentration in water over 0.5 wt.%, UV absorption of PVA compromises the visibility of polyynes signals. However, UV absorptions of polyynes in the aqueous solution of PVA0.03% are clearly higher than those of polyynes in water, reported in the inset of Fig.6.3b, showing that the formation of CAWs was helped by the presence of the polymer. Specifically, the peak-valley difference at 199 nm of C₆ and at 225 nm of C₈ in L-0.03% demonstrates an increase in intensity of 2.3 times compared to L-0%. PVA can, indeed, contribute to sp-carbon chains synthesis, providing carbon atoms to grow the wires and further hydrogen atoms to cap them, and by changing the liquid viscosity as discussed in the next Section.

6.3. SERS measurements of PVA/Ag/polyynes solutions and nanocomposites

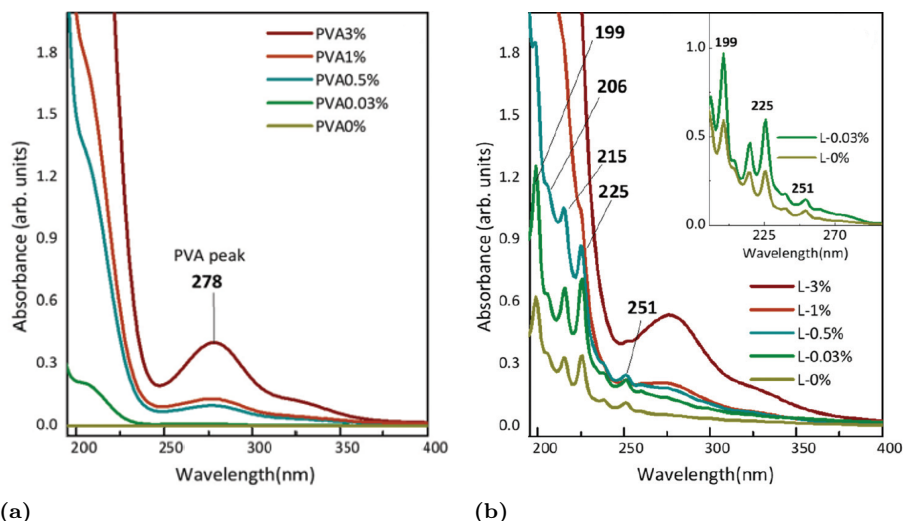


Figure 6.3: UV-Vis spectra of aqueous solution of PVA at different concentration: (a) before and (b) after the ablation of graphite. Inset: spectra of polyynes solutions with and without PVA0.03%, obtained after subtraction with the corresponding background spectra, i.e. PVA0.03% and PVA0%.

6.3 SERS measurements of PVA/Ag/polyynes solutions and nanocomposites

SERS measurements were needed to analyse all the prepared solid and liquid samples, since the UV-Vis absorption of PVA covers that of sp-carbon chains and increases in accordance with its concentration in water. Polyynes Raman fingerprint ($1800\text{-}2300\text{ cm}^{-1}$) is indeed well distinct from that of the polymer, which is related to the symmetrical stretching vibrational mode $\nu_s(\text{CH}_2)$ at about 2910 cm^{-1} . PVA, characterized by semi-crystalline structure, could also present two shoulders, at 2851 cm^{-1} and one at 2934 cm^{-1} [202]. The first is related to the weak intensity stretching mode $\nu(\text{CH})$ and the second is connected to the medium intensity asymmetrical stretching mode $\nu_a(\text{CH}_2)$ [202]. These typical bands can change in basis of the structural disorder of PVA [203]. To get qualitative information on the presence of polyynes, the same quantity of Ag colloids is added to each solution of PVA/polyynes, obtaining L-x%_Ag samples, whose SERS

spectra are reported in Fig.6.4a. The corresponding nanocomposites, i.e. S-x%_Ag, are showed in Fig.6.4b. In both graphs, SERS spectra of the samples are compared to a background signal. In liquid solutions, the background spectrum refers to that of PVA1%, whereas, in solid samples, it is related to that of solidified PVA1%. SERS spectra of liquid and solid samples, visible in Fig.6.4a and Fig.6.4b, are characterized by the presence of PVA and sp-carbon features. The band of PVA, in liquid cases, increases in intensity in accordance with the concentration of the polymer, while it is unvaried in nanocomposites, since the water is evaporated. Concerning sp-carbon chains bands, the one below 2000 cm^{-1} is broad with a unique peak almost in all the liquid and solid samples, whereas the one over 2000 cm^{-1} presents different shapes depending on the sample. In solutions, except for L-10%_Ag, the last-mentioned band has four narrow features, while, in nanocomposites, it is broad and without defined peaks. The four narrow peaks emerging from the band at higher wavenumber are associated to the presence of polyynes of different lengths. The longer the chain, the lower the wavenumber of the corresponding band is, in agreement with molecular simulations and experiments of previous works [41, 168, 204]. To establish the origin of those bands, SERS spectra of size-selected polyynes synthesized in Ag/PVA matrix should be performed, similar to what done with gold colloids in the work of An and coworkers, so adding the polymer after the synthesis and separation by HPLC of size-selected polyynes [96]. Moreover, it was observed that the highest SERS enhancement is reached in correspondence of PVA1% in both solutions and solid films. To improve the less intense SERS signal related to L-10%_Ag and, as a consequence, to increase the signal of the corresponding nanocomposite (S-10%_Ag), the ablation time in PVA10% was doubled. Nevertheless, the SERS signal is a little more intense without achieving the enhancement of the case of PVA1%, as shown in the inset of Fig.6.4a.

6.3. SERS measurements of PVA/Ag/polyyne solutions and nanocomposites

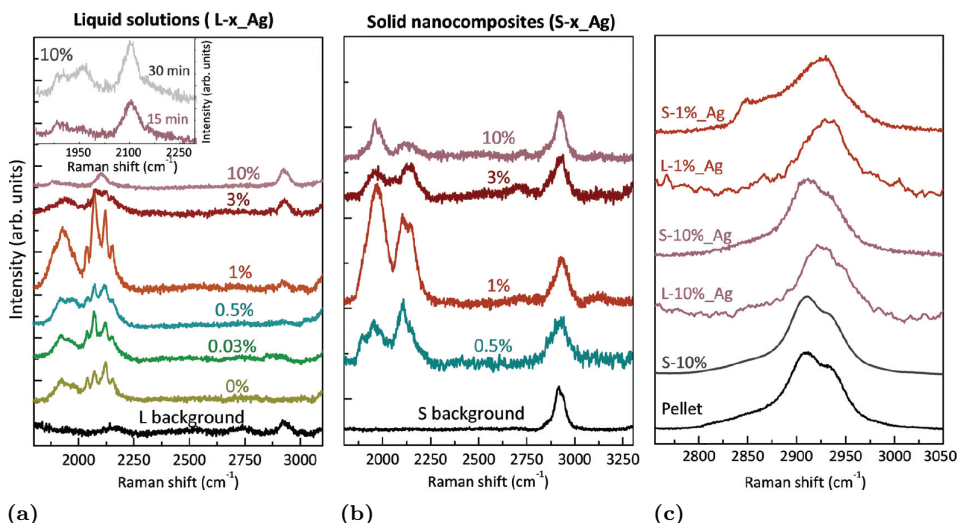


Figure 6.4: (a) SERS spectra of solutions (L-x%_Ag) at different concentrations. In black line a spectrum of liquid PVA1% before ablation (L background). Inset: SERS spectra of L10%_Ag after 15 and 30 minutes of ablation. (b) SERS spectra of free-standing films (S-x%_Ag). The measurements were taken at the centre of the samples. In black line, spectra of solidified PVA1% without polyyne and Ag colloids (S background). (c) SERS spectra limited to the region of CH-stretching mode of PVA in different phases. Excitation line for all spectra: 514.5 nm.

The features observed in SERS spectra as a function of PVA concentration highlight a non trivial role of PVA, possibly connected to the different viscosity of the solution. The viscosity of PVA1% is ~ 2.53 mPa·s at 298.1 K [205] and is similar to the viscosity of decalin at 298.1 K (considered as a mixture of cis-decalin and trans-decalin with a viscosity of 3.042 mPa·s and 1.948 mPa·s, respectively). Decalin was employed as a solvent for laser ablation in the study of Matsutani and co-workers [144], who observed the longest polyyne ever reached by PLAL, i.e. C₃₀. This significant achievement was connected to the low diffusion of polyyne in a viscous medium, which allows a larger growth of the chain before being capped by hydrogen atoms compared to the case of low viscous liquids, so obtaining longer size and higher yield. If the viscosity is too high, which can be the case of the maximum concen-

tration of PVA dissoluble in water [206], i.e. PVA10% (~ 25.91 mPa·s at 298.1 K [207]), the already formed end-capped chains have a too low mobility. This property keeps CAWs confined in the plasma region, where they may be decomposed and thermally degraded. Moreover, in more viscous media, microbubbles may persist for longer time [208,209] causing a partial shielding of the laser, thus reducing polyynes yield. Another important factor to consider is that high-concentrated PVA molecules may surround Ag nanoparticles and polyynes, hindering the direct adsorption of sp-carbon chains on silver colloids, hence giving a less intense SERS signal.

Differences in shape of sp bands of solid and liquid samples, already observed in previous studies [93,96,188], are particularly evident looking at spectra of L-1%_Ag and S-1%_Ag. In a solution, polyynes can diffuse and easily be adsorbed on Ag colloids, even if PVA is present, usually obtaining SERS measurements with detailed features. In a solid, the different chemical environments of sp-carbon chains close to silver nanoparticles are fixed, so resulting in broader bands [90]. In addition, in this case, the presence of PVA, which surrounds polyynes and Ag colloids, may limit their reciprocal interaction increasing even more the band broadness.

SERS spectra of different PVA phases are compared in Fig.6.4c focusing on CH stretching peak. Specifically, the characterized samples were: PVA pellet, solidified aqueous solution of PVA, aqueous solutions with Ag colloids and polyynes and the corresponding solid nanocomposites. This graph can help in understanding how the structure of the polymer changes in presence of Ag colloids and polyynes and so, the final degree of blending between polyynes, Ag nanoparticles and polymer once the nanocomposite is formed. First of all, the fact that PVA peak is detected in all these samples implies that the polymer does not suffer significant decomposition by laser ablation. In addition, this peak is characterized by approximately the same height in all cases with and without Ag colloids, meaning that PVA does not undergo SERS enhancement. It is known that PVA band is modified by structural disorder, and, as a consequence, shape and position at which the band is centred depend on the sample phase: $2910/2911$ cm^{-1} for

a solid pellet or cast film, 2918 cm^{-1} for an aqueous polymeric solution [203].

It seems that, in the case of films obtained from high-concentrated PVA solution as S-10%_Ag, Ag colloids and polyynes do not affect enough the original structure of the polymer during the solvent evaporation. PVA band is indeed equal in shape and position to that of the pristine pellet, even if the corresponding solution (L-10%_Ag) is characterized by a shifted band centred at 2925 cm^{-1} . Instead, in the case of S-1%_Ag, Ag colloids and polyynes may limit the capability of PVA to form ordered crystalline phases during solidification. PVA band is, in fact, shifted with respect to that of the pellet, positioning at 2928 cm^{-1} , which is close to the case of the corresponding liquid sample, i.e. 2933 cm^{-1} . If Ag colloids and polyynes are not present in the nanocomposite, the spectrum of solidified solution of PVA1% coincides to the one of the pellet.

Hence, the presence of polyynes and Ag nanoparticles in a low concentrated solution of PVA may form an intimate blend when the solid phase is formed, keeping the conformational disorder typical of a liquid solution. On the contrary, when PVA is too high concentrated, the segregation of polymer crystalline domains occurs during the solvent drying and may lead to a less effective encapsulation of polyynes, reducing the blending between all the components. This indicates the importance of employing a solution with PVA concentration in water that allows a good blending between polyynes, metal nanoparticles and polymer in the wires-based nanocomposite.

Ag/PVA/polyynes nanocomposite from PVA1% solution, i.e. S-1%_Ag, with the highest SERS enhancement was characterized by scanning electron microscopy (SEM), whose images are displayed in Fig.6.5. SEM pictures show a different colour and morphology at the centre and at the edge of the sample, confirming the coffee-ring effect visible to the naked eye as a consequence of drop casting. Indeed, Ag colloids concentrate preferentially at the extremity of the sample forming many agglomerates of nanoparticles, while, at the centre, a more homogeneous distribution and local dispersion is identified. In spite of the slight non-uniformity of silver nanoparticles distribution over

several millimetres scale, no segregation of Ag colloids and polyynes from PVA matrix was observed in S-1%_Ag, in accordance with the considerations discussed above concerning PVA CH-stretching band.

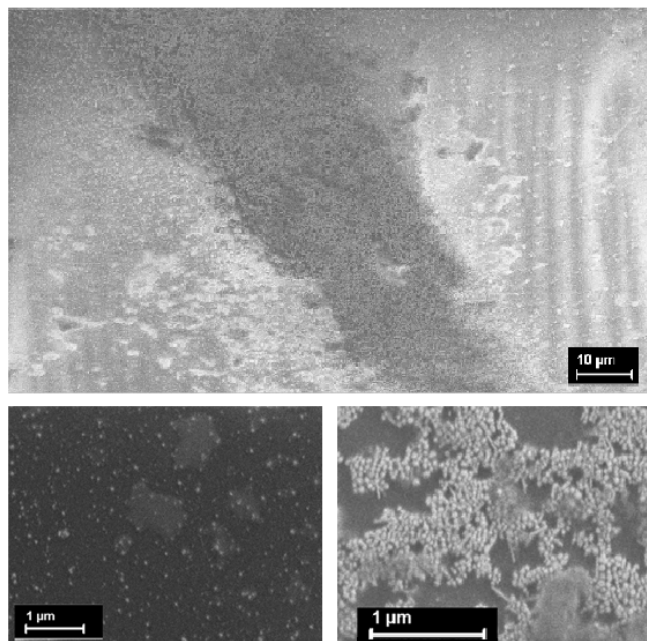


Figure 6.5: SEM images of free-standing film, i.e. S-1%_Ag (detector: SE2, accelerating voltage: 1.5 kV, working distance: 4.5 mm): (top) Detail on the border of the nanocomposite, rich of Ag nanoparticles (dark region) (magnification: 1000), (bottom-left) homogeneous region at the centre of the sample (magnification: 50000) and (bottom-right) zoom on the border of the film, where Ag nanoparticles are concentrated (magnification: 36000).

In addition to SEM pictures, SERS map analysis on free-standing thin film (S-1%_Ag) presented in Fig.6.6, allows the measurement of SERS response every 200 μm along a line from the centre to the border of the sample. Looking to all SERS spectra normalized with respect to PVA band, the sp-carbon signal decreases in intensity moving from the centre to the border, where Ag colloids are highly concentrated. In each spectrum, the total area of sp-carbon bands is normalized to PVA band. Computed ratios between the two areas are reported in the inset of Fig.6.6. This graph highlights the smaller SERS enhancement at

the border of the film compared to that in the centre. This behaviour could be explained considering that overabundant Ag nanoparticles may absorb Raman radiation or can occupy SERS "hot spot" in place of CAWs, thus reducing the overall polyynes SERS enhancement [210]. All these outcomes underline, once more, how complex the SERS effect is, since it depends on several factors, e.g. the relative concentration between silver colloids and CAWs, and the position and shape of plasmonic peak, which depend on the distribution and size of Ag nanoparticles [90].

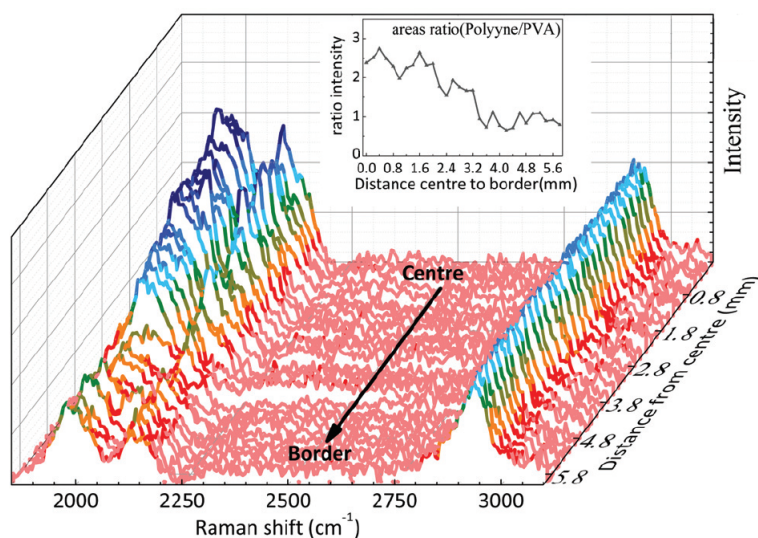


Figure 6.6: Normalized SERS spectra of free-standing film, i.e. S-1%_Ag, measured from the centre to the border. Measurements were taken with a step size of $200\mu\text{m}$ along a line (centre-border) at the excitation line of 532nm . Inset: ratio between the area of sp-carbon bands and the area of PVA peak.

6.4 Stability of PVA/Ag/polyynes solutions and nanocomposites

The stability of the encapsulated polyynes is a crucial factor for employing these nanocomposites in future applications. For this reason, SERS signals of the liquid (i.e. L-1%_Ag) and solid samples (i.e. S-1%_Ag) were carried out at different times to observe the polyynes

evolution, as depicted in Fig.6.7. SERS measurements are normalized to the peak of PVA and, in the case of nanocomposite, were performed at the centre of the sample, where it was found a morphologically homogeneous area with the higher SERS enhancement. The centre was individuated with the help of a centimetre scale applied to the sample.

In L-1%_Ag sample, the narrow peaks of the band above 2000 cm^{-1} are replaced by a broad band already after 1 week. After 3 weeks, the integrated area of sp-carbon region diminishes of 60% with respect to that of the as-prepared solution. The degradation results, anyway, lower than polyynes in aqueous solution without PVA, whose SERS spectra registered a decrease in sp area up to about 95%, as noticeable in Fig.6.8. The spectrum in the sp-carbon region is completely flat after 2 months. Considering the nanocomposite, i.e. S-1%_Ag, the integrated area of SERS polyynes bands underwent a degradation of approximately 50% after 1 week. However, after this period of time, the area decreased more slowly, i.e. only of 10% in 6 months. Indeed, the two bands of sp-carbon chains are still present after 11 months. Okada and collaborators showed a stability of 1 month for polyynes aggregated to Ag colloids in PVA [95] and An *et al.* noticed the signal of polyynes adsorbed on gold colloids in PVA up to 6 months [96]. These studies are in accordance with what obtained in our work, where the period of analysis was instead extended to 11 months.

In this thesis, polyynes in liquid media showed an improved stability when PVA is present in the solution. This could be associated to the partial inhibition of cross-linking reactions between sp-carbon chains thanks to the presence of the polymer. However, CAWs are not completely immobilized in PVA liquid phase and the interactions between the chains are not totally eliminated. In the case of solid nanocomposites, the stabilizing effect is instead more effective, since once the solution was dried, polyynes cannot move and, so, remain somehow protected and stable for a prolonged time.

6.5. PMMA/Ag/polyynes solutions and nanocomposites

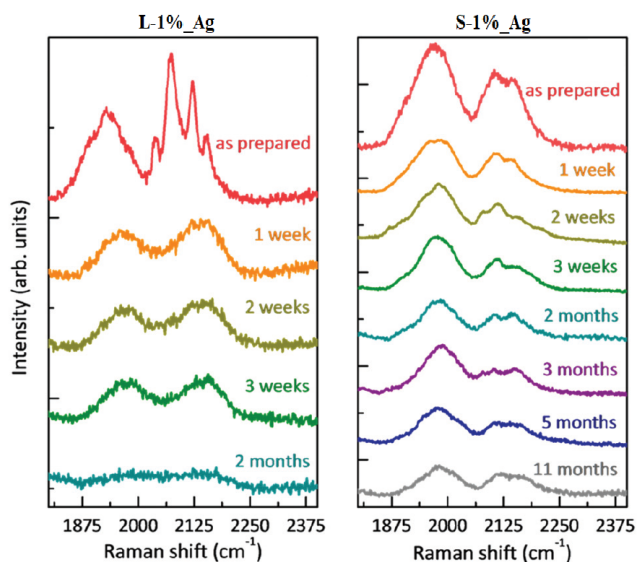


Figure 6.7: Evolution in time of SERS spectra (excitation line at 514.5 nm): (left) liquid sample (L-1%_Ag) and (right) free-standing nanocomposite (S-1%_Ag).

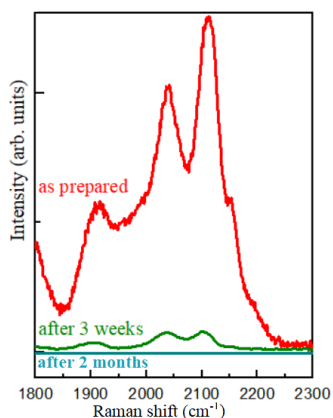


Figure 6.8: Evolution in time of SERS spectra of polyynes in aqueous solution without PVA (excitation line at 514.5 nm).

6.5 PMMA/Ag/polyynes solutions and nanocomposites

In situ synthesis method developed to produce polyynes directly in a polymeric matrix was also applied to another polymer, the poly(methyl methacrylate) (PMMA). As far as we know, these nanocomposites were

never prepared before. PMMA was selected because it is transparent, high-compatible with silver nanoparticles and insoluble in water. This last aspect allows the preparation of a water-resistant nanocomposite, which is appealing for waterproof technological applications but it prevents the use of chemically synthesized aqueous Ag colloids to perform SERS measurements. For this reason, Ag nanoparticles were produced by ablating for 5 minutes a silver solid target immersed in 2 ml of PMMA 2 wt.% in acetone by employing a laser wavelength of 532 nm and a fluence of 2 J/cm^{-1} . The synthesis of polyynes was carried out in the just mentioned SERS-active solution by ablating a graphite target for 15 minutes, keeping the same laser parameters. This liquid sample was named PMMA/Ag/polyynes solution. Then, the solution was drop cast on a silicon substrate and, after the solvent evaporation, a nanocomposite, indicated by PMMA/Ag/polyynes nanocomposite, was formed.

SERS spectra of PMMA/Ag/polyynes solution and nanocomposite are illustrated in Fig.6.9 and were normalized equalizing the two most intense CH stretching modes of acetone and PMMA, respectively. In the spectrum of the solution, the bands of polyynes are not evident neither the signals of PMMA, which are covered by CH stretching modes of acetone, among which the most intense one is at 2926 cm^{-1} , as also found in literature [211]. In the nanocomposite, polyynes bands are present together with typical CH stretching vibrational modes of PMMA, where the one at 2951 cm^{-1} is the strongest one [212]. Ag nanoparticles obtained by PLAL in a PMMA solution are characterized by the plasmonic peak depicted in the inset of Fig.6.9. It presents a tail, which covers the wavelength employed in the Raman spectrometer, i.e. 532 nm, so allowing the SERS enhancement. However, Ag nanoparticles, here synthesized by PLAL, are very low concentrated compared to chemically synthesized aqueous Ag colloids (10^{-3} M). Indeed, exploiting the tabulated data of Paramelle *et al.* related to citrate-capped silver nanoparticles in water [151], it was possible to extrapolate a concentration of Ag nanoparticles in PMMA solution of $\sim 10^{-11} \text{ M}$. Moreover, polyynes and Ag nanoparticles in polymeric solution are distributed in a volume of 2 ml, while, in the nanocomposite,

the reciprocal interaction between silver and sp-carbon chains may be more favoured because the species are localized on a substrate without the organic solvent, which is evaporated. These considerations could explain the presence of polyynes SERS signal only in the spectrum of the nanocomposite.

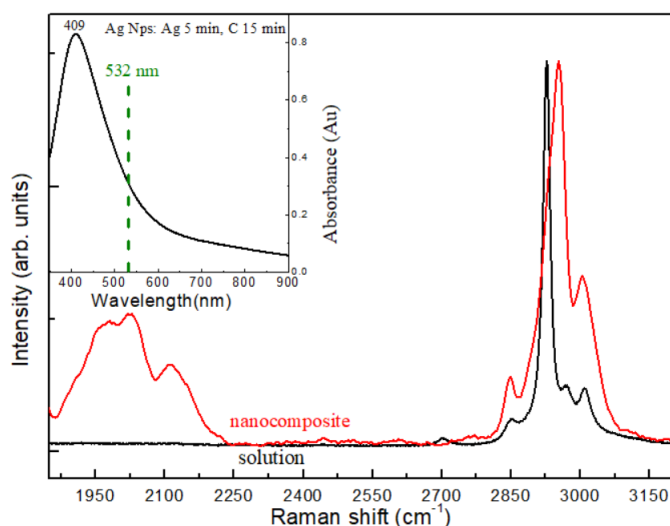


Figure 6.9: Normalized SERS spectra (excitation line at 532 nm) of PMMA/Ag/polyynes solution and nanocomposite. Inset: plasmonic peak of Ag nanoparticles at the end of silver and graphite ablations.

The polyynes stability in nanocomposites obtained from a solution of PMMA 2% wt. in acetone with silver nanoparticles was monitored for 21 weeks. Periodic SERS maps were performed near the centre of the nanocomposite, always individuated by a graduate centimetre scale applied to the sample. Measurements were carried out by means of the Raman spectrometer with diode-pumped laser at 532 nm and the automatic translator, which allows the map acquisition around the centre of the sample. In this way, spectra with the corresponding standard error could be computed and reported in Fig.6.10. The two main bands of CAWs, even if some changes in intensity and shape occur, are preserved at least for 5 months. This demonstrates a prolonged stability of polyynes when they are encapsulated in PMMA matrix, similarly to what observed in the case of PVA.

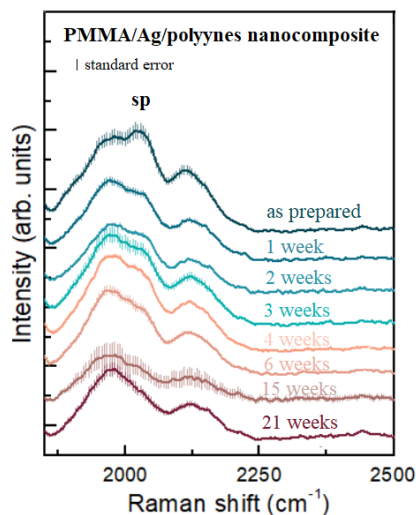
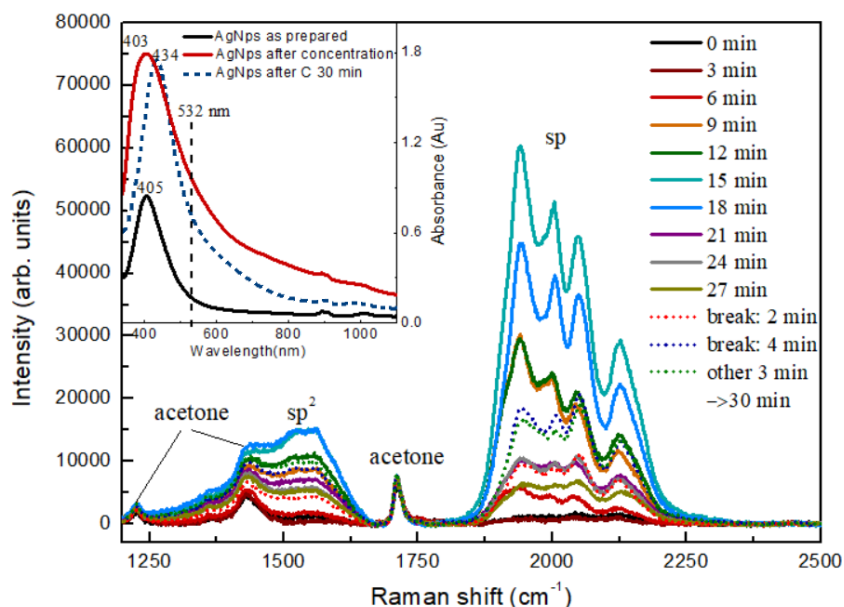


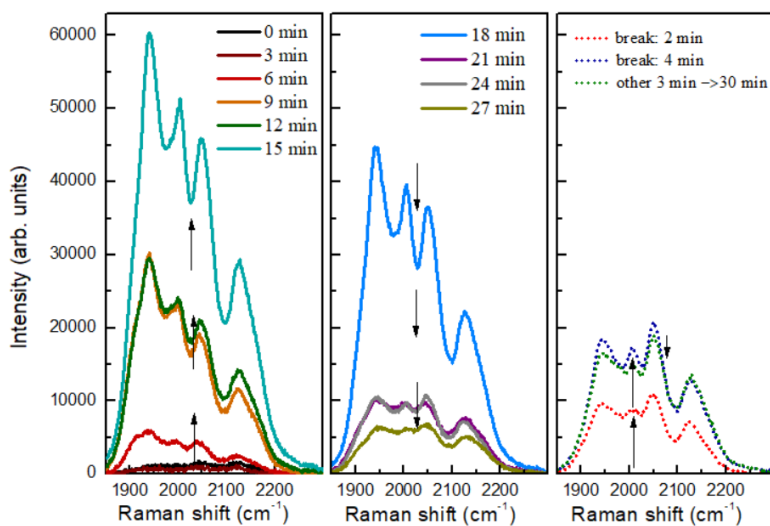
Figure 6.10: Normalized SERS spectra (excitation line at 532nm) of PMMA/Ag/polyynes nanocomposites with the corresponding standard error at different time.

Since SERS sp-carbon signals of PMMA/Ag/polyynes solution in Fig.6.9 are not present, Ag nanoparticles need to be concentrated to investigate the polyynes formation process by ablation of graphite in polymeric solution. Six ablations of silver target immersed in a solution of PMMA 2 wt.% in acetone were carried out with the same process parameters mentioned before. A total volume of 12 ml of PMMA/Ag solution was obtained and then, the solvent was left to evaporate until 2 ml of PMMA 12 wt.% in acetone were reached. UV-Vis absorption of Ag nanoparticles in PMMA solution before and after the concentration are presented in the inset of Fig.6.11a. At this point, a graphite target was inserted in the PMMA/Ag concentrated solution and the laser was turned on. *In situ* SERS measurements were conducted by means of the Raman spectrometer configured as described in Section 3.4.1. Measurements were taken every 3 minutes of ablation, stopping the laser. All the collected spectra are reported in Fig.6.11a. Besides the signals of acetone at 1224 cm^{-1} , 1432 cm^{-1} , and 1710 cm^{-1} , sp^2 and sp carbon signals start to be well defined after 6 minutes of ablation of graphite target. The sp^2 band is very broad and does not reach

during the ablation the intensity of sp signals, which are characterized by four distinct features. However, sp^2 and sp bands undergo a similar behaviour in time, increasing and then decreasing. To better follow the trend of sp-carbon chains during time, SERS spectra were limited to the sp region, as illustrated in Fig.6.11b. CAWs bands increase from 0 up to 15 minutes of ablation and then decrease between 16 and 27 minutes. After 2 and 4 minutes of break, i.e. without ablation, additional SERS measurements were performed, experiencing another increase of sp signal. Restarting to ablate for 3 minutes, the observed features point out a further decrease of the intensity. This peculiar behaviour is similar to what observed in *in situ* SERS measurements performed during SADL (see Section 4.2), namely an initial increase of sp bands intensity and, then a decrease. Possible explanations, in this case, can be associated to the degradation of polyynes due to the laser irradiation, the saturation of SERS active sites of Ag nanoparticles or to the phenomenon of metal nanoparticles resizing and reshaping by PLAL, leading to a more uniform size distribution [213]. As revealed from the dotted curved in the inset of Fig.6.11a, the plasmonic peak of Ag nanoparticles is narrower after 30 minutes of graphite ablation and the UV-Vis absorption at the Raman excitation wavelength is reduced. In this way, the SERS enhancement results less responsive. This effect was confirmed observing the increase of SERS intensity in sp bands measured after 2 and 4 minutes of ablation break. In fact, leaving to polyynes the time necessary to induce Ag nanoparticles aggregation and to diffuse in the liquid, SERS signals grow again. In addition, the further ablation of 3 minutes reshapes again silver nanoparticles and so, sp signal decreases once more. This study paves the way to understand the mechanism of formation of polyynes during laser ablation in liquid. To give further details to this investigation, *in situ* measurements should be carried out simultaneously with the ablation, without stopping the laser.



(a)



(b)

Figure 6.11: *In situ* SERS measurements (excitation line at 532 nm) performed between consecutive ablations of graphite in PMMA solution with concentrated Ag nanoparticles for a total ablation time of 30 minutes. (a) Spectra with sp^2 and sp signals marked. Inset: UV-Vis spectra of Ag nanoparticles as prepared, after concentration and after 30 minutes of graphite ablation. (b) Focus on SERS sp signals in time: increase (left), decrease (centre) and after breaks (right).

6.6 Summary

This chapter presented a novel procedure to prepare polyynes-based nanocomposites. Sp-carbon chains are synthesized by *in situ* method, which implies the laser ablation of graphite directly in a polymeric solution. The results related to nanocomposites based on two different polymeric matrices, i.e. PVA and PMMA, were here discussed.

Hydrogen-capped polyynes synthesized in aqueous solution of PVA were first analysed by means of UV-Vis spectroscopy, noticing that the presence of the polymer during the ablation helps in the formation of sp-carbon chains. Moreover, a non trivial role of PVA during PLAL emerged from SERS measurements on liquid and solid samples, obtained from different concentration of PVA in water. Specifically, the highest SERS enhancement was obtained employing a solution of PVA1% wt. in water, where the viscosity of the solution seems to be beneficial for polyynes formation. At this specific PVA concentration, a good blending between polyynes, Ag colloids and polymeric matrix can be reached and can also explain the prolonged stability of polyynes, which were detected up to 11 months.

Then, CAWs were synthesized by PLAL in a solution of Ag nanoparticles and PMMA dissolved in acetone. After solvent evaporation, Ag/PMMA/polyynes nanocomposites were obtained and investigated by SERS measurements. This was the first time, as far as we know, that this kind of nanocomposite was prepared and characterized. Polyynes SERS signals were noticed up to 5 months, showing that sp-carbon chains even in this polymeric matrix are more stable than in the case of the same nanostructures not encapsulated.

Moreover, after an adequate concentration of Ag nanoparticles synthesized by PLAL, *in situ* SERS measurements were collected during the synthesis of polyynes by laser ablation in a SERS-active PMMA solution.

All these outcomes showed that polyynes can be efficiently stabilized in a polymeric matrix and CAWs nanocomposites can be potential functional materials for new technological applications.

7

Conclusions and perspectives

This work was focused, first, on the synthesis and characterization of carbon-atom wires (CAWs) at single wire level and, then, to the preparation and study of properties of wires-based nanocomposites. These new materials respond to a two-fold aim: stabilizing sp-carbon chains and being applied in different technological fields. In this thesis, CAWs-based materials were developed carrying out the following steps: setting up the synthesis and characterization techniques, optimization of the synthesis methods, CAWs characterization in liquid solutions, stability properties investigation and preparation of solid film.

This Ph.D. activity started a new line of research for the laboratory. So, the first task was to settle up all the necessary equipment, starting from the synthesis methods, as the installation of the submerged arc discharge in liquid (SADL) and the design and implementation of pulsed laser ablation in liquid (PLAL). In addition, HPLC methods were developed to analyse and separate size- and end- selected CAWS.

Different experimental process parameters of SADL and PLAL were changed in order to reach the highest possible yield of polyynes and, in turn, to improve the characterization of size- or terminations- selected polyynes. In particular, current, time of discharge and depth at which electrodes are in contact are factors that were optimized for submerged arc discharge in water, while ablation time, solvent volume and fluence

were tested for improving the polyynes yield by pulsed laser ablation in water. This solvent is the one which requires more the optimization of the process parameters to increase the polyynes yield, since water cannot furnish carbon atoms for the chain growth during the ablation. In addition, concentration methods were employed only for aqueous solutions to further increase the quantity of polyynes post-synthesis. A well-known technique is the concentration by solid-phase extraction (SPE) cartridge, which was showed in the case of polyynes solutions by laser ablation in water. Moreover, a novel procedure to automatize the concentration, separation and collection of size-selected polyynes in water was developed during this thesis. It is entirely based on HPLC and consists of first operating the so-called batch-loading on column concentration method and, then, of starting the program to separate and collect concentrated polyynes. The efforts spent in improving the concentration of sp-carbon chains in water were intended to investigate the possibility of future mass production of CAWs-based materials with a sustainable and cost-effective solvent.

Experiments based on arc discharge and laser ablation in water and in organic solvents were carried out to study the effect of the liquid environments on polyynes properties, i.e. length, terminations, yield and stability by a multi-technique characterization.

After the optimization of process parameters and the post-synthesis concentration, arc discharge in water turns out to give the same kind of polyynes, i.e. H-polyynes up to 16 atoms of carbon, that can be obtained with organic solvents but without toxicity and flammability issues. Moreover, the most concentrated size-selected hydrogen-capped polyynes, as C₆, C₈, C₁₀, were collected and separately characterized by SERS to assign the origin of the bands in SERS spectra of polyynes mixture.

Organic solvents, as acetonitrile and isopropanol, mixed with distilled water were employed in SADL, producing hydrogen - capped polyynes up to C₁₆, methyl-capped species (HC_nCH₃, n=8-12) and cyano-capped polyynes (HC_nCN₃, n=6-18). In the case of PLAL, pure organic solvents, i.e. acetonitrile, methanol, ethanol and isopropanol, were

utilized finding a correlation between polyynes and by-products concentration, and solvent polarity. By HPLC, an extended range of CAWs, as hydrogen-capped polyynes (C_n , $n=6-22$), methylpolyynes (HC_nCH_3 , $n=6-18$) and cyanopolyynes (HC_nCN , $n=6-12$), were individuated and separated. Since some of the species were not already reported in literature, all these outcomes were supported by time-dependent density functional theory (TDDFT) simulations. The differences revealed in SERS spectra bands of selected polyynes with 8 atoms of carbon, capped by hydrogen, methyl- and cyano- group respectively, confirmed the correct identification and demonstrated the sensitivity of the SERS technique on terminations. The shift in the position of the main sp-carbon band of the experimental SERS spectra was verified by theoretical calculations of single molecules vibrational spectra. However, the shape of the band cannot be foreseen because simulations did not involve the interaction with Ag colloids.

Some considerations on the mechanism of formation of polyynes in liquid emerge from the discussion of the obtained results. First, solvents during ablation/arc discharge can contribute to the formation of sp-carbon chains by giving carbon, hydrogen atoms or entire functional groups, as cyano- or methyl- group, depending on the solvent molecular structure. Cyanopolyynes were, indeed, only found in the case of ablation/arc discharge in presence of acetonitrile. Second, the identification of HC_nCH_3 in water, whose structure is not characterized by methyl-groups, can be due to the binding of three hydrogen together with a carbon atom produced during the synthesis process.

To study the stability of polyynes solutions, different conditions were experimented. The exposure to air decomposes CAWs more quickly than the exposure to solar light and temperature at 50°C . In fact, polyynes dried on a silicon substrate degrade immediately unless Ag colloids are added to the solution before the solvent evaporation. In this way, silver nanoparticles, strongly interacting with polyynes, may change the electronic configuration or act as spacers by keeping distant the chains, so stabilizing CAWs at least for one month. Among the solvents selected in this study, acetonitrile is the one which preserves better CAWs. Moreover, longer cyano-capped polyynes are less

stable than shorter hydrogen and methyl-capped species. Acetonitrile turns out to be the best solvent compared to water, methanol, ethanol and isopropanol, not only in terms of stability but also for the polyynes yield and for the different types of chains that can be synthesized.

With the intention of studying polyynes evolution during arc discharge, *in situ* SERS measurements were conducted. The sp carbon SERS signals were observed for 40 minutes during arc discharge in aqueous solution with Ag nanoparticles previously made by SADL. The signals grow until 29 minutes and, then, decrease up to 40 minutes. This can may be due to the loss of Ag nanoparticles and/or polyynes being degraded by the continuous arcing. This study is important for understanding the mechanism of formation of polyynes during the synthesis by arc discharge in a liquid with silver nanoparticles.

After the investigation of CAWs at single wire level, the preparation and then characterization of polyynes-based materials were carried out. A novel synthesis method, which consists of ablating graphite in a polymeric solution, allows the formation of polyynes *in situ*, directly in the polymer, so avoiding the heating or the dilution step of polyynes solution. This method was applied so far to two different polymers, i.e. PVA and PMMA. Ag nanoparticles, necessary for structural SERS analysis, can either be added to the solution in the form of chemically synthesized Ag colloids (in case of PVA experiments) or be synthesized by irradiating a silver pellet in the polymeric solution before the ablation of graphite (in case of PMMA experimental work). Studies on the stability of the encapsulated CAWs and for understanding the final degree of blending between polymer, metal nanoparticles and polyynes were performed.

In the case of Ag/PVA/polyynes nanocomposites, it was noticed that PVA may help in the formation of polyynes contributing to the chain growth with carbon atoms and by changing the viscosity of the solution. Moreover, a blending between polyynes, Ag nanoparticles and polymer was achieved at low concentration of PVA in water, i.e. of around wt. 1%, and the signal of hydrogen-capped polyynes in this system was detected up to at least 11 months.

Concerning PMMA/Ag/nanocomposites, stability of sp-carbon chains has been tested for 5 months. After the concentration of Ag nanoparticles and the set-up of new Raman apparatus, *in situ* SERS measurements were performed to study the evolution of the sp-signal during the synthesis by laser ablation of graphite in a polymeric solution with Ag nanoparticles. The sp signal increases up to 15 minutes of ablation, then decreases until 27 minutes. After a break of 4 minutes, the signal increases again but, restarting the laser irradiation, the intensity of SERS bands reduces. This behaviour can be associated to the resizing and reshaping of Ag nanoparticles induced by laser ablation, which changes the plasmonic peak of Ag nanoparticles and consequently the absorption at the Raman wavelength.

The results of this thesis pave the way to several further investigations, currently mainly oriented to stabilize and concentrate sp-carbon chains. The first aim can be achieved either by ending the single wires with a bulky group during the synthesis or by finding other polymeric matrices to encapsulate unstable wires, e.g. hydrogen-capped polyynes. The improved stability observed when polyynes are immobilized in PVA and PMMA matrices and the simplicity of the synthesis method here developed are significant steps for the preparation of new CAWS-based materials. The second point to address is to reach a polyynes concentration in nanocomposites capable of improving the polymer properties by the outstanding characteristics of carbon-atom wires. Another potential follow-up of this research could involve the study of oriented CAWs in free-standing films, and mechanical and electrical measurements on the nanocomposites in view of future industrial applications.

Appendix

Theoretical simulations

Some more details on simulations, reported in this Ph.D. work and performed by other members of EspLORE team, are herein furnished. Density functional theory (DFT), which is one of the most accurate and fast method for the description of inter- and intramolecular interactions, was employed to obtain the simulated data reported in this thesis. DFT calculations are carried out on single linear chains using Gaussian09 [214]. Some examples of polyynes structural models are reported in Fig.7.1. These structures represent the optimized geometries calculated at energy ground level. Vibronic spectra were obtained by time-dependent density functional theory (TD-DFT) simulations at CAM-B3LYP/cc-pVTZ level of theory, while Raman spectra were computed by PBE0/cc-pVTZ calculations. Huang-Rys factors and vibronic spectra, based on TD-DFT simulations, were calculated by home-made program [215]. A scale factor of 0.961 was applied to the vibrational frequencies after the comparison with experimental spectra of Ref. [184]. The two mentioned functionals, e.g. CAM-B3LYP and PBE0, were selected to simulate UV-Vis and Raman spectra, respectively, depending on their accuracy to compute the two properties. Indeed, the simulated vibronic spectra obtained with CAM-B3LYP showed a very good agreement with the experimental

ones, presenting the same trend with the chain length, as shown in the paper [184], which refers to the results of Section 4.1. The PBE0 functional, instead, overestimating π -conjugation effects for longer and longer polyynes, causes a less precise description of the vibronic spectra. Conversely, the description of vibrational spectra are more reliably predicted by PBE0 instead of CAM-B3LYP/cc-pVTZ [33, 46].

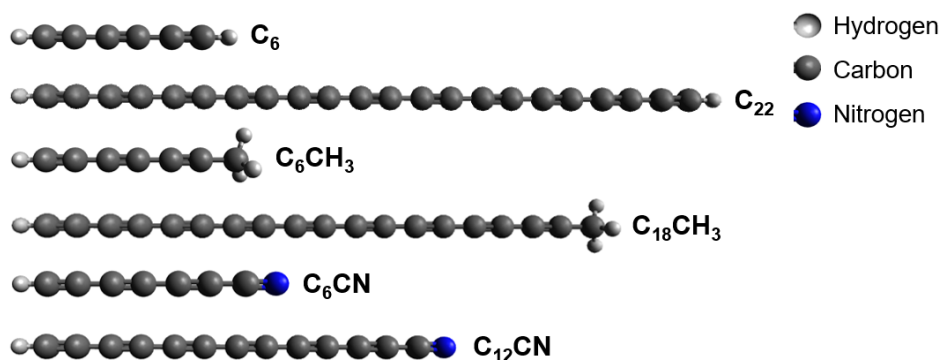


Figure 7.1: Structural models obtained from simulations at CAM-B3LYP/cc-pVTZ level of theory of some polyynes experimentally synthesized: C_6 ($BLA=0.164$), C_{22} ($BLA=0.144$), C_6CH_3 ($BLA=0.163$), $C_{18}CH_3$ ($BLA=$), C_6CN ($BLA=0.156$), $C_{12}CN$ ($BLA=0.160$).

List of Figures

1.1	Significant achievements of the synthetic carbon allotropes era.	10
1.2	Ternary diagram depending on carbon hybridization state.	10
1.3	Band structure of the two possible arrangements of CAWs: the metallic cumulene on the left and the semiconducting polyynes on the right.	12
1.4	(a) Band structure of cumulene and polyynes at different values of BLA in Å, (b) Band gap of sp-carbon chains as a function of BLA. At the top the sp-chain structure. (c) Potential energy of infinite carbon atomic wires as a function of BLA.	13
1.5	(a) Phonon dispersion branches of cumulene (left) and polyynes (right), (b) Longitudinal optical phonon branches of cumulene and polyynes with different values of BLA. The region close to $\mathbf{q}=0$ is zoomed.	15
1.6	Comparison between calculated equilibrium bond lengths of hydrogen-capped polyynes, uncapped and vinyl-capped cumulene.	17
1.7	(a) Finite carbon-atoms wires with different end-caps, i.e. hydrogen, phenyl-group, vinylidene-group and uncapped (from top to bottom), (b) the corresponding bond length in Å and (c) BLA as a function of carbon atoms of sp-chains bared or with different terminations.	18
1.8	Transfer characteristic of a cumulenic 3-Ph microcrystal bottom-gate bottom-contact FET (top) and sketch of the cross section of FET device.	21
1.9	Carbow: chemical structures of 20 polyynes (top) and distinct Raman frequencies (bottom).	22
1.10	(a) Surface-enhanced Raman spectroscopy (SERS) spectra of polyynes and Ag nanoparticles in PVA films as prepared (A), after a week (B) and a month (C). (b) time evolution of Lorentzian fitted SERS spectra of polyynes and Au nanoparticles in PVA film.	25
2.1	Sketches of four physical methods employed to synthesize carbon-atom wires	29

List of Figures

2.2	(a) Flux of electrons, carbon atoms and ions between two graphite electrodes at DC current, (b) Sketch of the physical model of the arc discharge in liquid	33
2.3	(a) Submerged arc discharge in liquid apparatus employed by Cataldo, (b) UV-Vis spectra of polyynes mixture after arc discharge in acetonitrile (at the top) and decalin (at the bottom).	35
2.4	Mechanism of formation of Ag nanoparticles.	37
2.5	(a) Schematics of the ns laser ablation, (b) ns-laser ablation steps: from the pulse penetration in liquid to the growth of nanomaterials.	39
2.6	Classification of plasmas depending on electron energy and density.	41
2.7	Set-up of the PLAL technique employed by Tsuji.	43
2.8	Scheme of the mechanism of polyynes formation.	44
2.9	Nanoparticles obtained by laser ablation of Ag in different solvents with 9 ns pulses at 1064 nm and 10 J/cm ² .	46
2.10	Sketch of Rayleigh scattering and Raman scattering (Stokes and anti-Stokes)	49
2.11	(a) Experimental Raman spectra of carbon solids and nanostructures, (b) DFT simulations of Raman lines of polyynes and cumulene.	51
2.12	(a) Experimental Raman spectra of H-capped polyynes by PLAL with “ <i>alpha</i> ” and “ <i>beta</i> ” lines and the corresponding simulated peaks, marked by “A” and “B”, (b) Atomic displacements associated to CC stretching modes of H-capped polyynes at specific frequency, obtained by DFT calculations.	52
2.13	Raman spectra of different types of polyynes and sp-sp ² moieties.	53
2.14	(a) On the left, SERS spectrum related to polyynes by SADL in methanol mixed with Ag colloids. On the right, SERS spectrum of polyynes by PLAL in ethanol deposited on a silver nanoisland film. (b) Comparison between Raman (up) and SERS (down) spectra.	54
2.15	(a) Comparison between Raman spectrum and SERS spectra at different laser wavelength, (b) Comparison between SERS spectra obtained with two different SERS enhancers: Ag colloids and Ag islands.	55
2.16	Main parts of the HPLC apparatus.	57
2.17	(a) UV-Vis spectra of hydrogen-capped polyynes at different length by PLAL in decalin, (b) UV-Vis spectra of cyanopolyynes (left) and hydrogen-capped polyynes (right).	58
3.1	Submerged arc discharge in liquid (SADL) apparatus.	66
3.2	Sketch of the compact Nd:YAG laser head with the two modules for doubling and tripling the frequency.	67
3.3	The immersion optic connected to the laser probe approaching the sample.	69
3.4	High-Performance Liquid Chromatography apparatus (HPLC).	70
4.1	Water after 15 minutes of arc discharge between two electrodes of graphite.	74
4.2	UV-Vis spectra of polyynes solutions by arc discharge in water: (a) changing the current, (b) changing the depth at which the discharge is generated and (c) changing the time of discharge.	76

-
- 4.3 UV-Vis spectra of the solutions after arc discharge in water carrying out breaks of 2 or 5 minutes every 2 or 5 minutes of arcing. 78
- 4.4 Chromatogram at 199, 225 and 251 nm to visualize the peak of C₆, C₈ and C₁₀, respectively. 79
- 4.5 Sketch of the HPLC procedure for automatizing the concentration, separation and collection of size-selected aqueous polyynes solutions. 80
- 4.6 Sections of chromatograms relative to each detected hydrogen-capped polyne, before and after the concentration. Chromatograms are observed at the wavelength at which each size-selected polyne has his maximum absorption. 81
- 4.7 Chromatograms observed at 225 nm before and after (in the inset) the collection of C₈. 82
- 4.8 Normalized UV-Vis spectra of size-selected hydrogen-capped polyynes from 6 up to 16 atoms of carbon. In black, experimental data, in red, simulated UV-Vis spectra obtained by DFT calculations. The inset shows the magnification of low intensity peaks of C₈. 83
- 4.9 (a) Absorption spectra of chemically synthesized Ag colloids (in black) and Ag colloids mixed with solution of polyynes mixture in water (in red). Dotted line (in blue) indicates the wavelength (λ) at 514.5 nm of the Raman laser employed. Inset: SEM image of Ag colloids (detector: InLens, accelerating voltage: 10 kV, magnification: 150000, working distance: 4.4 mm). (b) From the top to the bottom, SERS spectra of: polyynes mixtures in water, C₆, C₈, C₁₀. 85
- 4.10 UV-Vis spectra of polyynes mixture as prepared and after different exposures of one hour to: solar light, 323.1 K and air flow. 86
- 4.11 (a) UV-Vis spectra of polyynes mixture in time after dilution with 20% in volume of water, (b) UV-Vis spectra of polyynes mixture in time after dilution with 20% in volume of acetonitrile, (c) degradation rate of peak at 199 nm in the two cases. 87
- 4.12 UV-Vis spectra of C₈ polyynes at different ageing time: (a) sample kept in closed vial, (b) effect of a hole in the tap of the vial. 88
- 4.13 SERS spectra (excitation line: 514.5 nm) at different ageing time of polyynes mixture mixed with Ag colloids dried on a substrate. 89
- 4.14 Evolution of SERS spectra (excitation line: 785 nm) during 40 minutes of arc discharge. (a) Data normalized with respect to the signal of the fiber. Inset: Ag nanoparticles (AgNps) synthesized by arc discharge between two silver electrodes in water. (b) Smoothed and vertically shifted data after the subtraction of the spectrum at 0 minutes. 91
- 4.15 UV-Vis spectra of polyynes in solutions of: (a) water and different percentage of acetonitrile, (b) water and different percentage of isopropanol. 93
- 4.16 Simulated (dashed lines) and experimental (solid lines) normalized absorption spectra of H-capped polyynes (C_n) with n=6-18, methylpolyynes (HC_nCH₃) with n=8-12, and cyanopolyynes (HC_nCN) with n=6-10. 94

List of Figures

5.1	Design of PLAL technique.	99
5.2	PLAL apparatus under chemical hood at Nanolab.	99
5.3	UV-Vis spectra of polyynes mixtures with main UV-Vis peaks of C ₈ , C ₁₀ and C ₁₂ marked: (a) after different irradiation time of graphite pellet in distilled water, (b) after ablation of graphite pellet in 1.5 ml, 2 ml and 10 ml of distilled water.	101
5.4	Refraction effect on the focal length for the liquid ablation.	102
5.5	UV-Vis spectra of polyynes mixtures after the ablation of a graphite pellet in water at different fluences, obtained varying the energy per pulse from 10 mJ to 300 mJ and keeping fixed the spot size at 5.35 mm ²	104
5.6	DAD-absorption spectra of size-selected hydrogen-capped polyynes obtained from HPLC separation of polyynes mixtures synthesized at different fluences:(a) C ₈ ,(b) C ₁₀	104
5.7	Chromatographic peak area of C ₆ and C ₈ from each ml of eluting solvent, i.e. acetonitrile.	105
5.8	Polyynes solutions after ablation in different solvents.	106
5.9	UV-Vis spectra of filtered solutions of polyynes in acetonitrile (ACN), isopropanol (IPA), methanol (MeOH), ethanol (EtOH) and water (H ₂ O) after laser ablation (a) before background (dotted lines) subtraction and (b) after. The fitting performed on the background and on the main absorption peaks of hydrogen-capped polyynes were highlighted in the inset.	107
5.10	Polyyne concentration (mol/L) (in black) and χ_p (in red) as a function of solvent polarity.	108
5.11	HPLC analysis of polyynes solution in acetonitrile: normalized experimental (thick lines) and simulated (thin lines) UV-Vis spectra of H-polyynes (left), CH ₃ -polyynes (centre) and CN-polyynes (right).	110
5.12	HPLC analysis of polyynes solution in acetonitrile: absorbance as a function of the wavelength and time extracted from DAD coupled with HPLC, with all the types of polyynes marked.	111
5.13	HPLC chromatogram of polyynes solution in water, extracted at 225 nm, with the chromatographic peaks of C ₈ and HC ₈ CH ₃	112
5.14	Normalized experimental SERS spectra (excitation line: 532 nm) of solutions of size-selected polyynes with four triple bonds and different endcap (from the top): C ₈ , HC ₈ CH ₃ , HC ₈ CN. The curves related to methyl- and cyano-capped polyynes were smoothed in order to better individuate the sp-carbon features.	113
5.15	(a) Collective vibrational mode of CC bond related to (from the top): C ₈ , HC ₈ CH ₃ , HC ₈ CN. (b) Normalized simulated Raman spectra of the corresponding molecules. Data computed by PBE0/cc-pVTZ functional.	114
5.16	Time evolution of chromatographic peak area of polyynes, changing one characteristic at a time. (a) Chain length: from C ₈ to C ₂₀ in acetonitrile. Inset: decay time constant (τ) for each H-polyyne. (b) Terminations: C ₈ , HC ₈ CH ₃ and HC ₈ CN in acetonitrile. (c) Liquid environment: water, acetonitrile, isopropanol, ethanol, looking at C ₈ . Inset: Zoom on polyynes solutions in organic solvents.	116

-
- 6.1 *In situ* PLAL: ablation of a graphite pellet in aqueous PVA solution. . . . 120
- 6.2 Sample at different stages of polyynes-based nanocomposite preparation (from left): aqueous solution of polyynes and PVA after the ablation, solution after addition of Ag colloids, nanocomposite obtained after solvent evaporation. . 121
- 6.3 UV-Vis spectra of aqueous solution of PVA at different concentration: (a) before and (b) after the ablation of graphite. Inset: spectra of polyynes solutions with and without PVA0.03%, obtained after subtraction with the corresponding background spectra, i.e. PVA0.03% and PVA0%. 123
- 6.4 (a) SERS spectra of solutions (L-x%_Ag) at different concentrations. In black line a spectrum of liquid PVA1% before ablation (L background). Inset: SERS spectra of L10%_Ag after 15 and 30 minutes of ablation. (b) SERS spectra of free-standing films (S-x%_Ag). In black line, spectra of solidified PVA1% without polyynes and Ag colloids (S background). (c) SERS spectra limited to the region of CH-stretching mode of PVA in different phases. Excitation line for all spectra: 514.5 nm. 125
- 6.5 SEM images of free-standing film, i.e. S-1%_Ag (detector: SE2, accelerating voltage: 1.5 kV, working distance: 4.5 mm): (top) Detail on the border of the nanocomposite, rich of Ag nanoparticles (dark region) (magnification: 1000), (bottom-left) homogeneous region at the centre of the sample (magnification: 50000) and (bottom-right) zoom on the border of the film, where Ag nanoparticles are concentrated (magnification: 36000). 128
- 6.6 Normalized SERS spectra of free-standing film, i.e. S-1%_Ag, measured from the centre to the border. Measurements were taken with a step size of 200 μm along a line (centre-border) at the excitation line of 532 nm. Inset: ratio between the area of sp-carbon bands and the area of PVA peak. 129
- 6.7 Evolution in time of SERS spectra (excitation line at 514.5 nm): (left) liquid sample (L-1%_Ag) and (right) free-standing nanocomposite (S-1%_Ag). . 131
- 6.8 Evolution in time of SERS spectra of polyynes in aqueous solution without PVA (excitation line at 514.5 nm). 131
- 6.9 Normalized SERS spectra (excitation line at 532 nm) of PMMA/Ag/polyynes solution and nanocomposite. Inset: plasmonic peak of Ag nanoparticles at the end of silver and graphite ablations. 133
- 6.10 Normalized SERS spectra (excitation line at 532 nm) of PMMA/Ag/polyynes nanocomposites at different time. 134
- 6.11 *In situ* SERS measurements (excitation line at 532 nm) performed between consecutive ablations of graphite in PMMA solution with concentrated Ag nanoparticles for a total ablation time of 30 minutes. (a) Spectra with sp² and sp signals marked. Inset: UV-Vis spectra of Ag nanoparticles as prepared, after concentration and after 30 minutes of graphite ablation. (b) Focus on SERS sp signals in time: increase (left), decrease (centre) and after breaks (right). 136

List of Figures

- 7.1 Structural models obtained from simulations of the longest and shortest hydrogen-capped polyynes, methyl-capped polyynes and cyano-capped polyynes experimentally synthesized. 146

List of Tables

2.1	Characteristics of different discharges types.	30
2.2	Species produced by SADL.	36
3.1	Properties of the solvents selected for the experimental work.	64
4.1	Temperature measured by a thermocouple, before and after arc discharge at different arcing and break times.	78
5.1	Polarity (p), Ostwald coefficient (l), polyynes concentration (c) data. . . .	109
5.2	Chromatographic and UV-Vis data on polyynes synthesized in acetonitrile.	110
5.3	Decay time constants (τ) and corresponding R^2	117
6.1	Steps for the preparation of a solid material based on polyynes in a polymeric matrix (PVA).	122

Bibliography

- [1] S Tennant. IV. on the nature of the diamond. *Philosophical transactions of the Royal Society of London*, 87:123–7, 1797.
- [2] D R Askeland, P P Phulé, W J Wright, and D K Bhattacharya. *The science and engineering of materials*. Pacific Grove and Calif. : Brooks/Cole-Thomson Learning, 4th edition, 2003.
- [3] C Glaser. *Ber. Dtsch. Chem. Ges.*, 2:422–4, 1869.
- [4] A Baeyer. *Ber. Dtsch. Chem. Ges.*, 18:2269–81, 1885.
- [5] V V Vil'yams, V S Smimov, and V P Gol'mov. Concerning the nature of a crystalline matter from essential oil of lachnophyllum gossypinum. *Zh. Obsch. Khim*, 5:1195–204, 1935.
- [6] M Anchel. Identification of an antibiotic polyacetylene from clitocybe diatreta as a suberamic acid enediyne. *J. Am. Chem. Soc.*, 75:4621–2, 1953.
- [7] J D Bu'Lock. Acetylenic compounds as natural products. *Quarterly Reviews and Chemical Society*, 10:371–94, 1956.
- [8] G Nakaminami. The structures of natural acetylenic compounds and their biogenesis. *J. Soc. Org. Synth. Chem.*, 21:751–65, 1963.
- [9] A L K Shi Shun and R R Tykwinski. Synthesis of naturally occurring polyynes. *Angew Chem Int Ed Engl*, 45(7):1034–1057, 2006.
- [10] A E Goresy. Eine neue kohlenstoff-modifikation aus dem nördlinger ries. *Naturwissenschaften*, 56:493–4, 1969.
- [11] A El Goresy and G Donnay. *Science*, 161:363, 1968.
- [12] R Eastmond, TR Johnson, and DRM Walton. Sylation as a protective method for terminal alkynes in oxidative couplings. *Tetrahedron*, 28:4601–16, 1972.

Bibliography

- [13] A G Whittaker and P L Kintner. Carbon: Observations on the new allotropic form. *Science*, 165(3893):589–91, 1969.
- [14] A G Whittaker. *Science*, 200:763, 1978.
- [15] Y P Kudryavtsev, A M Sladkov, V I Kasatochkin, and V V Korshak. Inventors certificate no. 107, Dec. 7 and 1971 and priority date Nov. 4 and 1960.
- [16] P P K Smith. Carbon in carbonaceous chondrites: carbyne or graphite? *Nature*, 291:15–6, 1981.
- [17] P P K Smith and P R Buseck. Carbon in the allende meteorite: evidence for poorly graphitized carbon rather than carbyne. In New York, Oxford, and Pergamon Press, editors, *Lunar and Planetary Science Conference 12th*, pages 1167–75, 1982.
- [18] P P K Smith and P R Buseck. Carbyne forms of carbon: do they exist? *Science*, 216(4549):984–6, 1982.
- [19] P P K Smith and P R Buseck. *Science*, 229:486, 1985.
- [20] A G Whittaker. Carbyne forms of carbon: evidence for their existence. *Science*, 229:485, 1985.
- [21] J Jansta and FP Dousek. Some aspects of existence of elementary carbon with sp-hybridized bonds. *Carbon*, 18(6):433–7, 1980.
- [22] R J Lagow and et al. Synthesis of linear acetylenic carbon: The "sp" carbon allotrope. *Science*, 267(5196):362–7, 1995.
- [23] A G Whittaker, E J Watts, R S Lewis, and E Anders. Carbynes: Carriers of primordial noble gases in meteorites. *Science*, 209(4464):1512–4, 1980.
- [24] W Duley and D. Williams. Interstellar polyynes from the disruption of carbon grains. *Monthly Notices of the Royal Astronomical Society*, 211:97–103, 1984.
- [25] J August, H W Kroto, and N Trinajstic. Interstellar polyynes and related species. *Astrophysics and Space Science*, 128:411–9, 1986.
- [26] H W Kroto, J R Heath, S C O'Brien, R F Curl, and R E Smalley. C₆₀: Buckminsterfullerene. *Nature*, 318:162–3, 1985.
- [27] A Hirsch. The era of carbon allotropes. *Nature Materials*, 9, 2010.
- [28] S Iijima. Helical microtubules of graphitic carbon. *Nature*, 354(6348):56–8, 1991.
- [29] K S Novoselov, A K Geim, S V Morozov, D J Y Zhang, S V Dubonos, I V Grigorieva, and A A Firsov. Electric field effect in atomically thin carbon films. *Science*, 306(5696):666–9, 2004.
- [30] R H Baughman and H Eckhardt. Structure-property predictions for new planar forms of carbon: Layered phases containing sp² and sp atoms. *J. Chem. Phys.*, 87:6687, 1987.
- [31] A L Ivanovskii. Graphynes and graphdynes. *Progress in Solid State Chemistry*, 41(1):1–19, 2013.
- [32] Carbon allotropes https://www.chemistry.nat.fau.eu/sfb953_old/research-program/#collapse_0.

- [33] CS Casari, M Tommasini, RR Tykwinski, and A Milani. Carbon-atom wires: 1-D systems with tunable properties. *Nanoscale*, 8:4414–35, 2016.
- [34] CS Casari and A Milani. Carbyne: from the elusive allotrope to stable carbon atom wires. *MRS Comm.*, 8(2):207–19, 2018.
- [35] S Tongay, R T Senger, S Dag, and S Ciraci. Ab-initio electron transport calculations of carbon based string structures. *Phys Rev Lett.*, 93(13), 2004.
- [36] M Tommasini, D Fazzi, A Milani, M Del Zoppo, C Castiglioni, and G Zerbi. Effective hamiltonian for p electrons in linear carbon chains. *Chem Phys Lett*, 450:86–90, 2007.
- [37] Peierls and RE. *Quantum theory of solids*. Clarendon Press, 1996.
- [38] A Karpfen. Ab initio studies on polymers. I. The linear infinite polyynes. *J. Phys. Chem.*, Solid State Phys. 12:3227, 1979.
- [39] A Milani, M Tommasini, D Fazzi, C Castiglioni, M Del Zoppo, and G Zerbi. First-principles calculation of the peierls distortion in an infinite linear carbon chain: the contribution of Raman spectroscopy. *J. Raman Spectrosc.*, 39:164–8, 2008.
- [40] A Milani, M Tommasini, M Del Zoppo, C Castiglioni, and G Zerbi. Carbon nanowires: Phonon and π -electron confinement. *Phys Rev B*, 74:153418, 2006.
- [41] C Castiglioni, M Tommasini, and G Zerbi. Raman spectroscopy of polyconjugated molecules and materials: confinement effect in one and two dimensions. *Phil. Trans. R. Soc. Lond. A*, 362:2425–59, 2004.
- [42] N W Ashcroft and N. D. Mermin. *Solid State Physics*. Saunders, 1976.
- [43] F Innocenti, A Milani, and Chiara Castiglioni. Can Raman spectroscopy detect cumulenic structures of linear carbon chains? *J. Raman Spectrosc.*, 41:226–36, 2010.
- [44] S Yang and M Kertesz. Linear cn clusters: Are they acetylenic or cumulenic? *Phys. Chem. A*, 112:146–51, 2008.
- [45] C-P Chou, W-F Li, and H A Witek. *Vibrational Spectroscopy of Linear Carbon Chains*. World Scientific, 2011.
- [46] A Milani, M Tommasini, V Russo, A Li Bassi, A Lucotti, and F Cataldo et al. Raman spectroscopy as a tool to investigate the structure and electronic properties of carbon-atom wires. *Belst. J. of Nano.*, 6:480–91, 2015.
- [47] J A Januszewski, D Wendinger, C D Methfessel, F Hampel, and Rik R. Tykwinski. Synthesis and structure of tetraarylcumulenes: Characterization of bond-length alternation versus molecule length. *Angew. Chem. Int. Ed.*, 52:1817–21, 2013.
- [48] J A Januszewski and R R Tykwinski. Synthesis and properties of long [n] cumulenes ($n \leq 5$). *Chem. Soc. Rev. and*, 43:3184, 2014.
- [49] C Castiglioni, J T Lopez Navarrete, and G Zerbi. A simple interpretation of the vibrational spectra of undoped and doped and photoexcited polyacetylene amplitude mode theory in the gf formalism. *Solid State Communications*, 65(7):625–30, 1988.

Bibliography

- [50] M Del Zoppo, C Castiglioni, P Zuliani, and G Zerbi. *Handbook of Conductive Polymers*. Dekker, 1998.
- [51] M Del Zoppo, C Castiglioni, M Tommasini, P Mondini, C Magnoni, and G Zerbi. Intramolecular charge delocalization and nonlinear optical properties from vibrational spectroscopy. *Synthetic Metals* 102 (1999), 102:1582–83, 1999.
- [52] G Zerbi. page 487–537. Wiley: Chichester, 2007.
- [53] H Tabata, M Fujii, S Hayashi, T Doi, and T Wakabayashi. Raman and surface-enhanced Raman scattering of a series of size-separated polyynes. *Carbon*, 44:3168–76, 2006.
- [54] H Tabata, M Fujii, and Shinji Hayashi. Laser ablation of diamond particles suspended in ethanol: Effective formation of long polyynes. *Carbon*, 44:522–9, 2006.
- [55] PB Sorokin, H Lee, LY Antipina, AK Singh, and BI Yakobson. Calcium-decorated carbyne networks as hydrogen storage media. *Nano Lett.*, (11):2660–5, 2011.
- [56] M Liu, VI Artyukhov, H Lee, Fangbo Xu, and BI Yakobson. Carbyne from first principles: Chain of C atoms and a nanorod or a nanorope. *ACS Nano*, 7(11):10075–82, 2013.
- [57] I E Castelli, P Silvestrini, and N Manini. Mechanical properties of carbynes investigated by ab initio total-energy calculations. *Phys Rev B*, 85:214110, 2012.
- [58] V I Artyukhov, M Liu, and B I Yakobson. Mechanically induced metal-insulator transition in carbyne. *Nano Letters*, 14(8):4224–9, 2014.
- [59] R Landauer. Spatial variation of currents and fields due to localized scatterers in metallic conduction. *IBM J. Res. Dev.*, 1:223–231, 157.
- [60] N D Lang and Ph Avouris. Oscillatory conductance of carbon-atom wires. *Phys Rev Lett.*, 81(16):3515–8, 1998.
- [61] X Tu, H Wang, Z Shen, Y Wang, S Sanvito, and S Hou. Cu-metalated carbyne acting as a promising molecular wire. *J. Chem. Phys.*, 145:244702, 2016.
- [62] Z Zanolli, G Onida, , and JC Charlier. Quantum spin transport in carbon chains. *ACS Nano*, 4(9):5174–80, 2010.
- [63] Y Zhu, H Bai, and Y Huang. Electronic property modulation of onedimensional extended graphdiyne nanowires from a first-principle crystal orbital view. *Chem. Open*, 5(78):78–87, 2016.
- [64] M Wang and S Lin. Ballistic thermal transport in carbyne and cumulene with micron-scale spectral acoustic phonon mean free path. *Sci. Rep.*, 5(18122), 2015.
- [65] L Ravagnan, P Piseri, M Bruzzi, S Miglio, G Bongiorno, and A Baserga et al. Influence of cumulenic chains on the vibrational and electronic properties of sp-sp² amorphous carbon. *Physical Review Letters*, 98:216103, 2007.
- [66] C Wang, A S Batsanov, M R Bryce, S Martín, R J Nichols, S J Higgins, V M García-Suárez, , and C J Lambert. Oligoyne single molecule wires. *J. Am. Chem. Soc.*, 131(43):15647–54, 2009.

- [67] P Moreno-García, M Gulcur, D Z Manrique, T Pope, W Hong, V Kaliginedi, C Huang, and et al. Single-molecule conductance of functionalized oligoynes: Length dependence and junction evolution. *J. Am. Chem. Soc.*, 135(53):12228–40, 2013.
- [68] M Gulcur, P Moreno-García, X Zhao, M Baghernejad, A S Batsanov, W Hong, M R Bryce, and T Wandlowski. The synthesis of functionalised diaryltetraynes and their transport properties in single-molecule junctions. *J Chemistry: a European journal.*, 20(16):4653–4660, 2014.
- [69] S Ballmann, W Hieringer, D Secker, Q Zheng, J A Gladysz, A Görling, and H B Weber. Molecular wires in single-molecule junctions: Charge transport and vibrational excitations. *J ChemPhysChem*, 11(10):2256–2260, 2010.
- [70] O Cretu, A R Botello Mendez, I M Janowska, C Pham-Huu, J-C Charlier, and Florian Banhart. Electrical transport measured in atomic carbon chains. *Nano Lett.*, 13(8):3487–93, 2013.
- [71] A La Torre, A Botello-Mendez, W. Baaziz, J-C Charlier, and F Banhart1. Strain-induced metal–semiconductor transition observed in atomic carbon chains. *Nature Comm.*, 6:6636, 2015.
- [72] T D Yuzvinsky, W Mickelson, S Aloni, G E Begtrup, A Kis, and A Zettl. Shrinking a carbon nanotube. *Nano Lett.*, 6(12):2718–22, 2006.
- [73] A D Scaccabarozzi, A Milani, S Peggiani, S Pecorario, B Sun, and R R Tykwinski et al. A field-effect transistor based on cumulenic sp-carbon atomic wires. *J. Phys. Chem. Lett.*, 11:19704, 2020.
- [74] F Hu, C Zeng, R Long, Y Miao, Lu Wei, Q Xu, and et al. Supermultiplexed optical imaging and barcoding with engineered polyynes. *Nature Materials*, 15:194–200, 2018.
- [75] F Cataldo. Polyynes production in a solvent-submerged electric arc between graphite electrodes. III. Chemical reactivity and stability toward air and ozone and and light. *Fullerenes and Nanotubes and Carbon Nanostructures*, 12(3):619–31, 2004.
- [76] F Cataldo. Stability of polyynes in air and their degradation by ozonolysis. *Polymer degradation stability*, 91(2):317–323, 2006.
- [77] W Cui, T Saito, P Ayala, T Pichler, and L Shi. Oxidation stability of confined linear carbon chains and carbon nanotubes and and graphene nanoribbons as 1D nanocarbons. *Nanoscale*, 11(32):15253–15258, 2019.
- [78] CS Casari, A Li Bassi, L Ravagnan, F Siviero, C Lenardi, and P Piseri et al. Chemical and thermal stability of carbyne-like structures in cluster-assembled carbon films. *Physical Review B*, 69:075422–7, 2004.
- [79] F Cataldo. Synthesis of polyynes in a submerged electric arc in organic solvents. *Carbon*, 42(1):129–42, 2004.
- [80] F Cataldo, G Strazzulla, and S Iglesias-Groth. UV photolysis of polyynes at = 254 nm and at > 222 nm. *International Journal of Astrobiology*, 7(2):107–116, 2008.

Bibliography

- [81] F Cataldo. Storage stability of polyynes and cyanopolyynes in solution and the effect of ammonia or hydrochloric acid. *FN CN*, 15:155–66, 2007.
- [82] D Nishide, H Dohi, T Wakabayashi, E Nishibori, S Aoyagi, and M Ishida et al. Single-wall carbon nanotubes encaging linear chain C₁₀H₂ polyyne molecules inside. *Chemical Physics Letters*, 428:356–60, 2006.
- [83] L Shi, P Rohringer, K Suenaga, Y Niimi, J Kotakoski, and JC Meyer. Confined linear carbon chains as a route to bulk carbyne. *Nature Mat.*, 15:634–9, 2016.
- [84] Y Zhang, J Zhao, Y Fang, Y Liu, and X Zhao. Preparation of long linear carbon chain inside multi-walled carbon nanotubes by cooling enhanced hydrogen arc discharge method. *Nanoscale*, 10:17824–33, 2018.
- [85] LD Movsisyan, M Franz, F Hampel, AL Thompson, RR Tykwinski, and HL Anderson. Polyyne rotaxanes: Stabilization by encapsulation. *Journal of the American Chemical Society*, 138:136676, 2016.
- [86] LG Bettini, F Della Foglia, P Piseri, and P Milani. Interfacial properties of a carbyne-rich nanostructured carbon thin film in ionic liquid. *Nanotechnology*, 27(115403):1–6, 2016.
- [87] L Ravagnan, F Siviero, C Lenardi, P Piseri, E Barborini, and P Milani. Cluster beam deposition and in situ characterization of carbyne-rich carbon films. *Phys Rev Lett.*, 89:28–31, 2002.
- [88] R Rivelino, RB dos Santos, and F de Brito Mota. Conformational effects on structure and electron states and Raman scattering properties of linear carbon chains terminated by graphene-like pieces. *J. Phys. Chem. C*, 114:16367–72, 2010.
- [89] RR Tykwinski, W Chalifoux, S Eisler, A Lucotti, M Tommasini, D Fazzi, M Del Zoppo, and G Zerbi. Toward carbyne: Synthesis and stability of really long polyynes. *Pure Appl. Chem.*, 82(4):891–904, 2010.
- [90] A Milani, A Lucotti, V Russo, M Tommasini, F Cataldo, and A Li Bassi et al. Charge transfer and vibrational structure of sp-hybridized carbon atomic wires probed by surface enhanced Raman spectroscopy. *J. Phys. Chem. C*, 115:12836–43, 2011.
- [91] F Cataldo, O Ursini, A Milani, and CS Casari. One-pot synthesis and characterization of polyynes end-capped by biphenyl groups (a,u-biphenylpolyynes). *Carbon*, 126:232–40, 2017.
- [92] A Milani, M Tommasini, V Barbieri, A Lucotti, V Russo, F Cataldo, and et al. Semiconductor-to-metal transition in carbon-atom wires driven by sp² conjugated end groups. *J. Phys. Chem.*, 121:10562–70, 2017.
- [93] CS Casari, V Russo, A Li Bassi, CE Bottani, F Cataldo, A Lucotti, and et al. Stabilization of linear carbon structures in a solid Ag nanoparticle assembly. *App. Phys. Lett.*, 90(013111):1–3, 2007.
- [94] R Matsutani, F Ozaki, R Yamamoto, Y Okada T Sanada, and K Kojima. Preparation of polyynes up to C₂₂H₂ by liquid-phase laser ablation and their immobilization into SiO₂ gel. *Carbon*, 47:1659–63, 2009.

- [95] S Okada, M Fujii, and S Hayashi. Immobilization of polyynes adsorbed on Ag nanoparticle aggregates into poly(vinyl alcohol) films. *Carbon*, 49:4704–9, 2011.
- [96] K An, G Wei, G Qi, L Sheng, L Yu, W Ren, and et al. Stability improvement of C₈H₂ and C₁₀H₂ embedded in poly(vinylalcohol) films with adsorption on gold nanoparticles. *Chemical Physics Letters*, 637:71–6, 2015.
- [97] R Sata, H Suzuki, N Ueno, Y. Morisawa, M. Hatanaka, and T. Wakabayashi. UV-polarizing linear polyynes molecules aligned in PVA. *Chinese journal of chemical physics*, 32(2):175–181, 2019.
- [98] C Jin, H Lan, L Peng, K Suenaga, and S Iijima. Deriving carbon atomic chains from graphene. *Physical review letters*, 102(20):205501, 2009.
- [99] W Chodkiewicz. Synthesis of acetylenic compounds. *Ann. Chim.*, 2:819, 1957. (Paris).
- [100] S Szafert and JA Gladysz. Carbon in one dimension: Structural analysis of the higher conjugated polyynes. *Chem. Rev.*, 103(11):4175–206, 2003.
- [101] W A Chalifoux and R R Tykwinski. Synthesis of extended polyynes: Toward carbyne. *Comptes Rendus Chimie*, 12(3):341–358, 2009.
- [102] M Jevric and M B Nielsen. Synthetic strategies for oligoynes. *Asian Journal of Organic Chemistry*, 4(4):286–295, 2015.
- [103] G Schermann, T Grösser, F Hampel, and A Hirsch. Dicyanopolyynes: A homologous series of end-capped linear sp carbon. *Chemistry—A European Journal*, 3(7):1105–1112, 1997.
- [104] T Gbittner, F Hampel, J-P Gisselbrecht, and A Hirsch. End-cap stabilized oligoynes: model compounds for the linear sp carbon allotrope carbyne. *Chemistry—A European Journal*, 8(2):408–432, 2002.
- [105] Y P Kudryavtsev, S E Evsyukov, M B Guseva, V G Babaev, and V V Khvostov. Carbyne—the third allotropic form of carbon. *Russian chemical bulletin*, 42(3):399–413, 1993.
- [106] Y P Kudryavtsev and S E Evsyukov. The formation of diamond from carbynoid material at ambient pressure. *Diamond related materials*, 6(12):1743–1746, 1997.
- [107] D Wendinger and R R Tykwinski. Odd [n] cumulenes (n= 3 and 5 and 7 and 9): synthesis and characterization and reactivity. *Accounts of chemical research*, 50(6):1468–1479, 2017.
- [108] P Milani and S Iannotta. *Cluster beam synthesis of nanostructured materials*. Springer Science Business Media, 2012.
- [109] CS Casari, CS Giannuzzi, and V Russo. Carbon-atom wires produced by nanosecond pulsed laser deposition in a background gas. *Carbon*, 104:190–5, 2016.
- [110] F Cataldo. Simple generation and detection of polyynes in an arc discharge between graphite electrodes submerged in various solvents. *Carbon*, 41:2653–89, 2003.
- [111] M Tsuji, T Tsuji, S Kuboyama, T Tsujimoto S Yoon, Y Korai, and et al. Formation of hydrogen-capped polyynes by laser ablation of graphite particles suspended in solution. *Chem. Phys. Lett.*, 355(1-2):101–8, 2002.

Bibliography

- [112] J-S Chang. Physics and chemistry of plasma pollution control technology. *J Plasma Sources Science Technology*, 17(4):045004, 2008.
- [113] K Bekki, T Yamamoto, and K Sawa. Breaking arc in dielectric liquids. In *Electrical Contacts-1996. Proceedings of the Forty-Second IEEE Holm Conference on Electrical Contacts. Joint with the 18th International Conference on Electrical Contacts*, pages 252–261. IEEE.
- [114] H D Carter and A N Campbell. Electric discharges in liquids. Part I-the arc discharge in water. *Transactions of the Faraday Society*, 28:479–496, 1932.
- [115] H Lange, M Sioda, A Huczko, Y Q Zhu, H W Kroto, and D R M Walton. Nanocarbon production by arc discharge in water. *Carbon*, 41(8):1617–1623, 2003.
- [116] G Xing, S Jia, and Z Shi and. The production of carbon nano-materials by arc discharge under water or liquid nitrogen. *New Carbon Materials*, 22(4):337–341, 2007.
- [117] N Arora and N N Sharma. Arc discharge synthesis of carbon nanotubes: Comprehensive review. *Diamond and Related Materials*, 50:135–150, 2014.
- [118] H O L Li, J Kang, K Urashima, and N Saito. Comparison between the mechanism of liquid plasma discharge process in water and organic solution. *Inst. Electrostat. Jpn*, 37(1):22–27, 2013.
- [119] M Tsuji, S Kuboyama, T Matsuzaki, and T Tsuji. Formation of hydrogen-capped polyynes by laser ablation of C60 particles suspended in solution. *Carbon*, 41(11):2141–8, 2003.
- [120] F Cataldo. *Polyynes:synthesis and properties and applications*. CRS Press, 2005.
- [121] F Cataldo. Polyynes and cyanopolyynes synthesis from the submerged electric arc: about the role played by the electrodes and solvents in polyynes formation. *Tetrahedron*, 60:4265–74, 2004.
- [122] F Cataldo. Polyynes production in a solvent-submerged electric arc between graphite electrodes II. Analysis by liquid chromatography. *Fullerenes and Nanotubes and Carbon Nanostructures*, 12(3):619–31, 2004.
- [123] F Cataldo. Polyynes production in a solvent-submerged electric arc between graphite electrodes. I. Synthesis and spectroscopy. *Fullerenes Nanotubes and Carbon Nanostructures*, 12:603–617, 2004.
- [124] F Cataldo. Soot and other products formation from the submerged carbon arc in halogenated solvents. *Fullerenes and Nanotubes and Carbon Nanostructures*, 13(3):239–257, 2005.
- [125] Y Wu, Y Zhang, T Zhu, H Li, Y Liu, and X Zhao. Effects of precursor molecules on polyne formation by arc discharge between two copper electrodes. *Chem. Phys. Lett.*, 730:64–9, 2019.
- [126] H Li, Y Wu, Y Zhang, T Zhu, T Maruyama, and Y Liu et al. Submerged carbon arc in deionized water: A green route for scalable preparation of gas containing polyynes. *Chemical Physics*, 535(110804), 2020.

- [127] D-C Tien, L-C Chen, N Van Thai, and S Ashraf. Study of Ag and Au nanoparticles synthesized by arc discharge in deionized water. *Journal of nanomaterials*, 2010, 2010.
- [128] K-H Tseng, Y-C Chen, and J-J Shyue. Continuous synthesis of colloidal silver nanoparticles by electrochemical discharge in aqueous solutions. *Journal of Nanoparticle Research*, 13(5):1865–1872, 2011.
- [129] A Kanitz, M-R Kalus, E L Gurevich, A Ostendorf, S Barcikowski, and D Amans. Review on experimental and theoretical investigations of the early stage and femtoseconds to microseconds processes during laser ablation in liquid-phase for the synthesis of colloidal nanoparticles. *Plasma Sources Sci. Technol.*, 28:103001–35, 2019.
- [130] V Amendola and M Meneghetti. What controls the composition and the structure of nanomaterials generated by laser ablation in liquid solution? *Phys.Chem. Chem. Phys.*, 15:3027–46, 2013.
- [131] A Couairon and A Mysyrowicz. Femtosecond filamentation in transparent media. *Physics Reports*, 441(2):47–189, 2007.
- [132] C Momma, BN Chichkov, N N Boris, S Nolte, F von Alvensleben, A Tünnermann, H Welling, and B Wellegehausen. Short-pulse laser ablation of solid targets. *Optics Communications*, 129(1):134–142, 1996.
- [133] T Sakka, K Saito, and Y H Ogata. Emission spectra of the species ablated from a solid target submerged in liquid: vibrational temperature of C₂ molecules in water-confined geometry. *J Applied surface science*, 197:246–250, 2002.
- [134] R Matsutani, K Inoue, N Wada, and K Kojima. Wavelength dependence of polyynes preparation by liquid-phase laser ablation using pellet targets. *Chem. Commun.*, 47:5840–42, 2011.
- [135] G Compagnini, V Mita, RS Cataliotti, L D’Urso, and O Puglisi. Short polyynes chains produced by pulsed laser ablation of graphite in water. *Carbon*, 45:2445–2458, 2007.
- [136] S K Shin and S M Park. Preparation of polyynes by the laser ablation of graphite in water and organic solvents. *Bull. Korean Chem. Soc.*, 33(2):597–601, 2012.
- [137] G Compagnini, V Mita, L D’Urso, RS Cataliotti, and O Puglisi. Spectroscopic study of polyynes obtained by laser ablation in liquids. *J. Raman Spectrosc.*, 39:177–81, 2008.
- [138] G Forte, L D’Urso, E Fazio, S Patanè, F Neri, O Puglisi, and G Compagnini. The effects of liquid environments on the optical properties of linear carbon chains prepared by laser ablation generated plasmas. *Applied Surface Science*, 272:76–81, 2013.
- [139] R Matsutani, T Kakimoto, H Tanaka, and K Kojima. Preparation of polyynes by liquid-phase laser ablation using different irradiation target materials and solvents. *Carbon*, 49:77–81, 2011.

Bibliography

- [140] R Matsutani, T Kakimoto, K Wada, T Sanada, H Tanaka, and K Kojima et al. Preparation of long-chain polyynes C₁₈H₂ and C₂₀H₂ by laser ablation of pellets of graphite and perylene derivative in liquid phase. *Carbon*, 46:1091–109, 2008.
- [141] H Tabata, M Fujii, and S Hayashi. Laser ablation of diamond nanoparticles suspended in solvent: synthesis of polyynes. *Chemical Physics Letters*, 395:138–42, 2004.
- [142] H Tabata, M Fujii, and S Hayashi. Synthesis of polyynes by laser ablation of diamond nanoparticles suspended in solution. *The European Physical Journal D*, 34:223–225, 2005.
- [143] K Inoue, R Matsutani, T Sanada, and K Kojima. Preparation of long-chain polyynes of C₂₄H₂ and C₂₆H₂ by liquid-phase laser ablation in decalin. *Carbon*, 48:4197–214, 2010.
- [144] R Matsutani, K Inoue, T Sanada, N Wada, and K Kojima. Preparation of long-chain polyynes of C₂₈H₂ and C₃₀H₂ by liquid-phase laser ablation. *Journal of Photochemistry and Photobiology A: Chemistry*, 240:1–4, 2012.
- [145] T Wakabayashi, M Saikawa, Y Wada, and T Minematsu. Isotope scrambling in the formation of cyanopolyynes by laser ablation of carbon particles in liquid acetonitrile. *Carbon*, 50:47–56, 2012.
- [146] Y Wada, K Koma, Y Ohnishi, Y Sasaki, and T Wakabayashi. Photoinduced reaction of methylpolyynes H(CC)_nCH₃ (n = 5–7) and polyynes H(CC)₅H with I₂ molecules. *Eur. Phys. J. D*, 66(322), 2012.
- [147] A Ramadhan, M Wesolowski, T Wakabayashi, H Shiromaru, T Fujino, T Kodama, and et al. Synthesis of hydrogen- and methyl-capped long-chain polyynes by intense ultrashort laser pulse irradiation of toluene. *Carbon*, 118:680–85, 2017.
- [148] Y Taguchi, H Endo, Y Abe, J Matsumoto, T Wakabayashi, and T Kodama et al. Polyynes formation by graphite laser ablation in argon and propane mixed gases. *Carbon*, 94:124–8, 2015.
- [149] Y Taguchi, H Endo, T Kodama, Y Achiba, H. Shiromaru, and T Wakabayashi et al. Polyynes formation by ns and fs laser induced breakdown in hydrocarbon gas flow. *Carbon*, 115:169–74, 2017.
- [150] Y Herbani, Irmaniar, R S Nasution, F Mujtahid, and S Masse. Pulse laser ablation of Au and Ag and Cu metal targets in liquid for nanoparticle production. *Journal of Physics: Conference Series*, 985:012005, 2018.
- [151] D Paramelle, A Sadovoy, S Gorelik, P Free, J Hobley, and D G Fernig. A rapid method to estimate the concentration of citrate capped silver nanoparticles from UV-visible light spectra. *The Analyst*, 139(19):4855, 2014.
- [152] W W M Shukri, H Bakhtiar, and N Bidin. Synthesis and characterization of gold-silver nanoparticles in deionized water by pulsed laser ablation (PLAL) technique at different laser parameter. *International Journal of Nanoscience*, 2018.
- [153] K Chaudhari, T Ahuja, V Murugesan, V SubRamanian, M A Ganayee, T Thundat, and T Pradeep. Appearance of SERS activity in single silver nanoparticles by laser-induced reshaping. *Nanoscale*, 11(1):321–330, 2019.

- [154] I Pavliček, P Gawel, D R Kohn, Z Majzik, Y Xiong, G Meyer, H L Anderson, and L Gross. Polyynes formation via skeletal rearrangement induced by atomic manipulation. *Nature chemistry*, 10(8):853–858, 2018.
- [155] U Szczepaniak, K Ozaki, K Tanaka, Y Ohnishi, Y Wada, J-C Guillemin, C Crépin, R Kołos, Y Morisawa, H Suzuki, and T Wakabayashi. Phosphorescence excitation mapping and vibrational spectroscopy of HC9N and HC11N cyanopolynes in organic solvents. *Journal of Molecular Structure*, 1214:128201, 2020.
- [156] Fr Shindo, Y Bénilan, P Chaquin, J-C Guillemin, A Jolly, and Fr Raulin. IR spectrum of C₈H₂: integrated band intensities and some observational implications. *J Journal of Molecular Spectroscopy*, 210(2):191–195, 2001.
- [157] WA Chalifoux and RR Tykwinski. Synthesis of polyynes to model the sp-carbon allotrope carbyne. *Nature Chemistry*, 2:967–71, 2010.
- [158] G Grasso, L D’Urso, E Messina, F Cataldo, O Puglisi, and G Spoto et al. A mass spectrometry and surface enhanced Raman spectroscopy study of the interaction between linear carbon chains and noble metals. *Carbon*, 47:2611–9, 2009.
- [159] A A Zaidi, A Hu, M J Wesolowski, X Fu, J H Sanderson, Y Zhou, and et al. Time of flight mass spectrometry of polyynes formation in the irradiation of liquid alkanes with femtosecond laser pulses. *Carbon*, 48(9):2517–2520, 2010.
- [160] M J Wesolowski, S Kuzmin, B Moores, B Wales, R Karimi, and A A Zaidi et al. Polyynes synthesis and amorphous carbon nano-particle formation by femtosecond irradiation of benzene. *Carbon*, 49:625–30, 2011.
- [161] K S Krishnan C V Raman. A new type of secondary radiation. *Nature*, 121(3048):501–502, 1928.
- [162] P Brüesch. *Phonons: Theory and Experiments II: Experiments and Interpretation of Experimental Results*, volume 65. Springer Science Business Media, 2012.
- [163] C C Moura. Raman spectroscopy and coherent anti-stokes Raman scattering imaging: prospective tools for monitoring skeletal cells and skeletal regeneration. 13(118):20160182, 2016.
- [164] C S Casari. Carbon atomic wires: From stars to nanotechnology. *Istituto Lombardo-Accademia di Scienze e Lettere-Rendiconti di Scienze*, 2012.
- [165] A Lucotti. *PhD Thesis*. Thesis, 2005.
- [166] A Champion and P Kambhampati. Surface-enhanced Raman scattering. *Chemical society reviews*, 27(4):241–250, 1998.
- [167] J R Lombardi, R L Birke, T Lu, and J Xu. Charge-transfer theory of surface enhanced Raman spectroscopy: Herzberg–teller contributions. *The Journal of chemical physics*, 84(8):4174–4180, 1986.
- [168] A Lucotti, M Tommasini, M Del Zoppo, C Castiglioni, G Zerbi, F Cataldo, and et al. Raman and SERS investigation of isolated sp carbon chains. *Chem. Phys. Lett.*, (417):78–82, 2006.

Bibliography

- [169] H Tabata, M Fujii, and S Hayashi. Surface-enhanced Raman scattering from polyynes solutions. *Chemical physics letters*, 420(1-3):166–170, 2006.
- [170] K Hanamura, M Fujii, T Wakabayashi, and S Hayashi. Surface-enhanced Raman scattering of size-selected polyynes (C₈H₂) adsorbed on silver colloidal nanoparticles. *Chem. Phys. Lett.*, 503:118–23, 2011.
- [171] A M Krstulovic and P R Brown. *Reversed-Phase High-Performance Liquid Chromatography*. 1982.
- [172] <https://microbenotes.com/high-performance-liquid-chromatography-hplc/>.
- [173] A E Gillam and E S Stern. *An introduction to electronic absorption spectroscopy in organic chemistry*. Arnold, 1955.
- [174] Explore and erc consolidator grant and politecnico di milano: <https://www.esplora.polimi.it/>.
- [175] S Peggiani, P Marabotti, R A Lotti, A Facibeni, P Serafini, A Milani, V Russo, A Li Bassi, and C S Casari. Solvent-dependent termination and size and stability in polyynes synthesis by laser ablation in liquids. *Phys. Chem. Chem. Phys.*, 22:26312–21, 2020.
- [176] A Senis. *Synthesis of Carbon Atom Wires through Arc Discharge in Water*. Thesis, 2018.
- [177] G Cerrato. *Synthesis of polyynes through arc discharge in selected organic solvents*. Thesis, 2019.
- [178] R A Lotti. *sp-Carbon chains by Pulsed Laser Ablation in Liquid: Synthesis and Stability*. Thesis, 2019.
- [179] S Peggiani, A Facibeni, A Milani, C Castiglioni, V Russo, A Li Bassi, and C S Casari. *In situ* synthesis of polyynes in a polymer matrix by pulsed laser ablation in liquid. *Materials Advances*, 1(8):2547–3074, 2020.
- [180] S Sala. *Linear sp carbon chains-polymer nanocomposites by Pulsed Laser Ablation in Liquid*. Thesis, 2020.
- [181] I M Smallwood. *Handbook of organic solvent properties*. 1996.
- [182] PC Lee and DJ Meisel. Adsorption and surface-enhanced Raman of dyes on silver and gold sols'. *J. Phys. Chem.*, 86:3391–95, 1982.
- [183] P Hoffmann, B Dutoit, and RP Salathe. Comparison of mechanically drawn and protection layer chemically etched optical fiber tips. *Ultramicroscopy*, 61:165–70, 1995.
- [184] S Peggiani, A Senis, A Facibeni, A Milani, P Serafini, G Cerrato, A Lucotti, M Tommsini, D Fazzi, C Castiglioni, V Russo, A Li Bassi, and C S Casari. Size-selected polyynes synthesised by submerged arc discharge in water. *Chemical Physics Letters*, 740:137054–61, 2020.
- [185] S Heeg, L Shi, L V Poulidakos, T Pichler, and L Novotny. Carbon nanotube chirality determines properties of encapsulated linear carbon chain. *Nano Letters*, 18(9):5426–5431, 2018.

- [186] F Shindo, Y Benilan, JC Guillemin, P Chaquin, A Jolly, and F Raulin. Ultraviolet and infrared spectrum of C₆H₂ revisited and vapor pressure curve in titan's atmosphere. *Planetary and Space Science*, 51:9–17, 2003.
- [187] Y Li, K An, L Sheng, L Yu, W Ren, and X Zhao. Surface-enhanced Raman scattering investigations of C₂nH₂(n = 4–6) in as-prepared and dried Ag colloid. *Chem. Phys. Lett.*, 631–2:12–5, 2015.
- [188] A Milani, V Barbieri, A Facibeni, V Russo, A Li Bassi, A Lucotti, and et al. Structure modulated charge transfer in carbon atomic wires. *Scientific Reports*, 9(1):1648, 2019.
- [189] G R R Bebahani, P Hogan, and W E Waghorne. Ostwald concentration coefficients of acetonitrile in aqueous mixed solvents: A new and rapid method for measuring the solubilities of volatile solutes. *J. Chem. Eng. Data*, 47:1290–2, 2002.
- [190] A Lucotti, M Casella, and M Tommasini. *Surface-Enhanced Multipurpose Nanosensing with Microneedle-Shaped Fiber Optics*, book section 8, pages 283–305. Pan Stanford, Boca Raton and FL, 2015.
- [191] Y E Park, S K Shin, and S M Park. The physical effects on the formation of polyynes by laser ablation. *Chemical Physics Letters*, 568:112–116, 2013.
- [192] A Menéndez-Manjón, P Wagener, and S Barcikowski. Transfer-matrix method for efficient ablation by pulsed laser ablation and nanoparticle generation in liquids. *J. Phys. Chem. C*, 115(12):5108–14, 2011.
- [193] B C Stuart, M D Feit, S Herman, A M Rubenchik, B W Shore, and M D Perry. Nanosecond-to-femtosecond laser-induced breakdown in dielectrics. *Physical Review B*, 53(4):1749–1761, 1996. PRB.
- [194] K Sasaki, T Wakasaki, and K Kadota. Observation of continuum optical emission from laser-ablation carbon plumes. *Applied surface science*, 197:197–201, 2002.
- [195] N M Bulgakova, A B Evtushenko, Y G Shukhov, S I Kudryashov, and A V Bulgakov. Role of laser-induced plasma in ultradeep drilling of materials by nanosecond laser pulses. *Applied Surface Science*, 257(24):10876–10882, 2011.
- [196] S Zhu, Y F Lu, M H Hong, and X Y Chen. Laser ablation of solid substrates in water and ambient air. *Journal of Applied Physics*, 89(4):2400–2403, 2001.
- [197] J A Dean. *Lange's handbook of chemistry*. R. R. Donnelley Sons Company., fifteenth edition, 1999.
- [198] C B Kretschmer, J Nowakowsici, and A R Wiebe. Solubility of oxygen and nitrogen in organic solvents from -25° to 50°C. *Industrial and Engineering Chemistry*, 38(5):506–9, 1946.
- [199] S A Shchukarev and T A Tolmacheva. Solubility of oxygen in ethanol-water mixtures. *Zhurnal Strukturnoi Khimii*, 9(1):21–8, 1968.
- [200] A Lucotti, CS Casari, M Tommasini, A Li Bassi, D Fazzi, V Russo, and et al. sp carbon chain interaction with silver nanoparticles probed by surface enhanced Raman scattering. *Chem Phys Lett*, 478:45–50, 2009.

Bibliography

- [201] W H Eisa and A A Shabaka. Ag seeds mediated growth of Au nanoparticles within PVA matrix: An eco-friendly catalyst for degradation of 4-nitrophenol. *Reactive Functional Polymers*, 73:1510–1516, 2013.
- [202] T F Cooney, L Wang, SK Sharma, R W Gauldie, and A J Montana. Raman spectral study of solid and dissolved poly(vinyl alcohol) and ethylene-vinyl alcohol copolymer. *Journal of Polymer Science B*, 32:1163–74, 1994.
- [203] YA Badr, M Abd El-Kader, and RM Khafagy. Raman spectroscopic study of CdS and PVA composite films. *Journal of Applied Polymer Science*, 92:1984–92, 2004.
- [204] M Tommasini, D Fazzi, A Milani, M Del Zoppo, C Castiglioni, and G Zerbi. Intramolecular vibrational force fields for linear carbon chains through an adaptative linear scaling scheme. *J. Phys. Chem. A*, 111:11645–11651, 2007.
- [205] M Mohsen-Nia and H Modarress. Viscometric study of aqueous poly(vinyl alcohol) (PVA)solutions as a binder in adhesive formulations. *J. Adhesion Sci. Technol*, 20(1):1273–80, 2006.
- [206] M Perfetti, N Gallucci, I Russo Krauss, A Radulescu, S Pasini, and O Holderer et al. Revealing the aggregation mechanism and structure and and internal dynamics of poly(vinyl alcohol) microgel prepared through liquidliquid phase separation. *Macromolecules*, 53(3):852–61, 2020.
- [207] Y Wang and YL Hsieh. Immobilization of lipase enzyme in polyvinyl alcohol (PVA) nanofibrous membranes. *Journal of Membrane Science*, 309:73–81, 2008.
- [208] M-R Kalus, N Bärsch, R Streubel, E Gökce, S Barcikowski, and B Gökcea. How persistent microbubbles shield nanoparticle productivity in laser synthesis of colloids - quantification of their volume and dwell dynamics and and gas composition. *Physical Chemistry Chemical Physics*, 19:7112–23, 2017.
- [209] T Hupfeld, G Laurens, S Merabia, S Barcikowski, B Gökce, and D Amans. Dynamics of laser-induced cavitation bubbles at a solid–liquid interface in high viscosity and high capillary number regimes. *Journal of Applied Physics*, 127(4):044306, 2020.
- [210] Q He, A Zhao, L Li, H Sun, D Wang, and H Guo. Fabrication of Fe₃O₄@SiO₂@Ag magnetic-plasmonic nanospindles as highly efficient SERS active substrates for label-free detection of pesticides. *New Journal of Chemistry*, 41(4):1582–90, 2017.
- [211] P Cossee and J H Schachtschneider. Vibrational analysis of acetone and acetaldehyde and and formaldehyde. *The Journal of Chemical Physics*, 44(1):97–111, 1966.
- [212] H Willis, V Zichy, and P J Hendra. The laser-Raman and infra-red spectra of poly(methyl methacrylate). *Polymer*, 10:737–746, 1969.
- [213] M Fernández, J del Val, M Boutinguiza, A Riveiro, R Comesaña, F Lusquinos, and J Pou. Synthesis and resizing of silver nanoparticles by laser ablation in liquids. *Lasers in Manufacturing Conference 2017*, 2017.
- [214] M J Frisch, G W Trucks, H B Schlegel, G E Scuseria, M A Robb, J R Cheeseman, G Scalmani, V Barone, B Mennucci, G A Petersson, H Nakatsuji, M Caricato,

- X Li, H P Hratchian, A F Izmaylov, J Bloino, G Zheng, J L Sonnenberg, M Hada, M Ehara, K Toyota, R Fukuda, J Hasegawa, M Ishida, T Nakajima, Y Honda, O Kitao, H Nakai, T Vreven, J A Montgomery, Jr, J E Peralta, F Ogliaro, M Bearpark, J J Heyd, E Brothers, K N Kudin, V N Staroverov, R Kobayashi, J Normand, K Raghavachari, A Rendell, J C Burant, S S Iyengar, J Tomasi, M Cossi, N Rega, J M Millam, M Klene, J E Knox, J B Cross, V Bakken, C Adamo, J Jaramillo, R Gomperts, R E Stratmann, O Yazyev, A J Austin, R Cammi, C Pomelli, J W Ochterski, R L Martin, K Morokuma, V G Zakrzewski, G A Voth, P Salvador, J J Dannenberg, S Dapprich, A D Daniels, Ö Farkas, J B Foresman, J V Ortiz, J Cioslowski, and D J Fox. Gaussian 09, 2009.
- [215] WL Yang, G Yang, S Abbate, A Lucotti, M Tommasini, C Villani, and et al. Chiral peropyrene: Synthesis and structure and and properties. *Journal of the American Chemical Society*, 139:13102–9, 2017.